Dissertation zur Erlangung des Doktorgrades
der Fakultät für Chemie und Pharmazie
der Ludwig-Maximilians-Universität München

Loss of the SNARE protein Sec22p selectively represses caesium accumulation in yeast and plants

STEPHAN JOHANN DRÄXL

aus

Bad Tölz, Deutschland

2012

Erklärung

Diese Dissertation wurde im Sinne von § 7 der Promotionsordnung vom

28. November 2011 von Herrn PD Dr. Anton R. Schäffner betreut.

Eidesstattliche Versicherung

Diese Dissertation wurde eigenständig und ohne unerlaubte Hilfe erarbeitet.

München, ...

.....

(STEPHAN DRÄXL)

Dissertation eingereicht am 21.09.2012

1. Gutachterin / 1. Gutachter: PD Dr. Anton Rudolf Schäffner

2. Gutachterin / 2. Gutachter: Prof. Dr. Karl-Peter Hopfner

Mündliche Prüfung am 14.12.2012

Summary

The rare alkali ion caesium (Cs^+) is assimilated by eukaryotes, even though it is not an essential nutrient. It poses an environmental concern through the anthropogenic release of its radioisotopes, ^{134}Cs and ^{137}Cs. Bioavailability and long half-lives favour its uptake and accumulation in plants, via which radiocaesium can be introduced to the food chain. Cs^+ ions are taken up via potassium-(K^+)-related pathways due to the biophysical similarity of these cations. This makes it difficult to solely manipulate Cs^+ accumulation in plants without disturbing the homeostasis of essential ions at the same time.

This work shows that the soluble N-ethylmaleimide sensitive factor attachment receptor (SNARE) Sec22p, previously described as a member of the protein sorting machinery, specifically affects Cs^+ accumulation in yeast by regulating the selectivity of vacuolar deposition. A similar phenotype became apparent for a homologous plant protein, SEC22. The loss of *Saccharomyces cerevisiae* Sec22p reduces Cs^+ uptake by more than half, while at the same time leaving essential cations undisturbed. Mathematical modelling of wild-type and mutant Cs^+ uptake kinetics proposes that *sec22Δ* is defective in vacuolar compartmentalisation of Cs^+, which is proven by biochemical fractionation. Morphological alterations were not produced by the loss of Sec22p, only a Cs^+-dependent vacuolar fragmentation can be observed. These results indicate a so far undescribed function of Sec22p in assuring a non-selective ion deposition to the vacuole, which is necessary in ion detoxification, while its loss induces discrimination against vacuolar Cs^+ deposition. A developmentally controlled loss-of-function mutant of the orthologous gene *SEC22* (*At1g11890*) in *A. thaliana* displays a similar phenotype, having specifically reduced Cs^+ enrichment without detrimental growth defects, thereby translating the yeast findings to a multicellular context. Furthermore, a functional complementation of the yeast mutant Cs^+ phenotype by the plant gene transcript was possible. Selective reduction of Cs^+ accumulation in plants by loss of a single gene product represents a new route to limit radiocaesium input to the food chain without disturbing basic plant nutrition and growth.

See also: Dräxl et al., *Caesium accumulation in yeast and plants is selectively repressed by loss of the SNARE Sec22p/SEC22*, Nat Commu, 2013 (accepted). This publication contains major parts of this thesis plus additional data including revised yeast growth conditions and Cs^+ accumulation in the yeast mutants *trk1Δ/trk2Δ* and *ena1-4Δ*.

Contents:

Abbreviations

aa	Amino acid
bp	Base pair
cDNA	Complementary DNA
CCPM	Corrected counts per minute
ci	Curie
CTAB	Cetyltrimethylammonium bromide
ddH_2O	Double distilled water
dNTP	Deoxynucleotide-5'-triphosphate
DTT	Dithiothreitol
EDTA	Ehylene diamine tetra-acetic acid
x g	(times) earth gravity
ΔH	Enthalpy
kb	Kilo base pair
min	Minute
NASC	Nottingham Arabidopsis Stock Center
OE	Overexpression
PCR	Polymerase chain reaction
rpm	Revolutions per minute
RT-PCR	Reverse Transcription PCR
SD	Standard deviation
TAE	Tris-Acetate-EDTA
w/v	Weight per volume

Figures, Tables and Appendices.

Figures

Figures (continued)

Tables

Tables (continued)

1 INTRODUCTION - caesium accumulation in eukaryotes

Traces of anthropogenically produced radioactive caesium (Cs) isotopes in agricultural products have to be counteracted to prevent the enrichment of potentially hazardous elements in the food chain. Traditional measures are supplemented with molecular biological strategies to reduce the amount of Cs accumulating in plants. The chemical characteristics of the cation Cs^+, especially in comparison with essential alkali metal ions like potassium (K^+), impact on its uptake by plants as well as on the applicability of countermeasures against its enrichment.

1.1 Caesium – Chemical characteristics

Cs is an alkali metal of Group I of the periodic system of elements. It was discovered in 1861 by Kirchhoff and Bunsen, has an atomic number of 55, a density of 1.90 g / cm^3 and a melting point of 28.4 °C (Davis, 1963). The availability of Cs^+ salts in nature is limited ($7x10^{-4}$ % of the earth crust, 0.002 ppm in water), as its maximum concentration in soil is 25 µg / g and an average soil concentration is estimated at 0.3 µg / g (White et al., 2010). A geological reservoir containing elevated amounts of Cs^+ is the aluminium silicate pollucite, found mainly in the USA (Beger and Buerger, 1967).

Cs has a chemical relevance as reducing agent, but due to its low abundance it is rarely used as such. Medical and scientific applications including Cs ions or its isotopes are described in secondary ion mass spectrometry (Aberth and Burlingame, 1984) or chemoradiation (Wong et al., 1999).

Among the alkali metal ions Cs^+, K^+ and rubidium (Rb^+) ions have comparable physico-chemical characteristics (Tab. 1). A molecule with related features is ammonium (NH_4^+) having a single positive charge and a hydrated ionic radius of 0.331 nm.

Ionic radii and hydration energy are important attributes for ion metabolism, since they determine an ion as substrate for proteins. Accordingly, Cs^+ and Rb^+ accumulation is tightly connected to K^+ homeostasis, even though their biochemical significance is converse. K^+ is an essential nutrient (Ariño et al., 2010), while Cs^+ is not known to be essential for any eukaryote, even though a number of microorganisms were found to incorporate traces of this ion (Avery, 1995, 1996). No biological function for Cs^+ was discovered for fungi, plants and mammals (Hampton et al., 2005; Tataruch and Kiersdorf, 2003) and it is considered as toxic (Avery, 1995).

Alkali metal	Cs	K	Rb	Na	Li
Atomic radius (nm) [a]	0.267	0.220	0.235	0.180	0.145
Ionic radius (nm) [a]	0.186	0.149	0.163	0.117	0.94
Hydrated ionic radius (nm) [a]	0.329	0.331	0.329	0.358	0.382
Hydration energy ΔH (kJ/mol) [b]	- 275	- 325	- 300	- 400	- 510
Toxicity yeast < 80 mM [c]	+	-	-	-	+
Toxicity plants	+	-	-	-	+
	(> 350 µM)[d]			(> 100 mM)[e]	(> 50 mM)[f]

Table1: Alkali metals of Group I of the periodic system of elements.
They share chemical characteristics in that they are reactive, light metals that can be reduced to monovalent cations. The radii of atoms, ions and the hydrated ionic status are given. Furthermore, known limits of toxicity for baker's yeast (*Saccharomyces cerevisiae*) and diverse plants are shown. In case of yeast, toxicity was determined at a threshold of 80 mM Cs^+ salt in media. Note the difference in toxicity between Cs^+ and the related K^+ or Rb^+. [a](Volkov et al., 1997), [b](Hille, 1978), [c](Perkins and Gadd, 1993a), [d](Hampton et al., 2004), [e](Rubio et al., 1995), [f](Wallace et al., 1977).

1.2 Cs radioisotopes – sources and ecological relevance

There are 39 instable Cs isotopes (Holden, 1987). Their major sources are by-products of the nuclear fission process in nuclear power plants (NPPs) and of nuclear weapons tests (Marovic et al., 2008; Petruska et al., 1955). The most abundant isotopes are ^{134}Cs and ^{137}Cs with a high fission yield and a long half-life (Unterweger et al., 1992). Their decay to a stable nuclide produces beta and gamma radiation with high energy (Tab. 2).

Isotope	^{134}Cs	^{137}Cs
$t_{½}$ (years)	2.07	30.17
Decay	100 % β → Ba-134 (0.16 MeV);	92 % β → Ba-137m (0.51 MeV);
	0.0003 % e^- capture	8 % β → Ba-137 (1.18 MeV)
	→ Xe-134 (1.23 MeV)	

Table 2: Characteristics of the most important Cs isotopes.
Decay schemes are indicated. Both isotopes decay via Barium isotope Ba-134. Eight % of ^{137}Cs decays to Ba-137. Only a minor portion of ^{134}Cs decays to Xe-134 via electron capture. Ba-137m denotes metastable Ba-137. Ba isotopes further decay emitting γ radiation.

The most notorious releases of radiocaesium in the last 40 years occurred at the Chernobyl accident (1986), with amounts of soil contamination of 30 Bq / cm^3 in Ukraine and a high level of contamination over Europe (Michel and Voigt, 2006; UNSCEAR, 2000), and at the Fukushima Daiichi NPP meltdown, caused by a natural disaster in 2011 (Yasunari et al., 2011). In both cases, a mixture of radioactive elements was released to the atmosphere and fallout was distributed as gas or aerosol particles, which were partially deposited to the ground.

As indicated in Fig. 1, in the case of Fukushima, critical amounts of ^{137}Cs deposition to soil were estimated in the regions close to the reactor site (Yasunari et al., 2011). Cs isotopes are considered as relevant soil contaminants in long term estimations, due to their long half lifes and their low mobility in upper soil layers (Cline and Hungate, 1960; Filipović-Vinceković et al., 2005; Schimmack and Bunzl, 1992; Schimmack et al., 2004). Most deposed Cs^+ will not reach soil layers deeper than 7 cm. The accordingly high availability of the alkali ion to plant roots marks the soil uptake via roots as an important pathway for radiocaesium inclusion in the food chain (Alexakhin et al., 1993; Alexakhin et al., 2007; Avery, 1996; Prister et al., 1992). Less than 3 % of soil-bound Cs^+ is considered bioavailable for plants, but this amount is sufficient to demand restriction of crop production on these areas (Lasat et al., 1997). The detrimental effects on agriculture and stock farming after soil deposition may culminate in land use restriction as it was introduced after the Fukushima incident, e.g. for tea and cauliflower, according to the informations of the International Atomic Energy Agency (IAEA) (http://www.iaea.org).

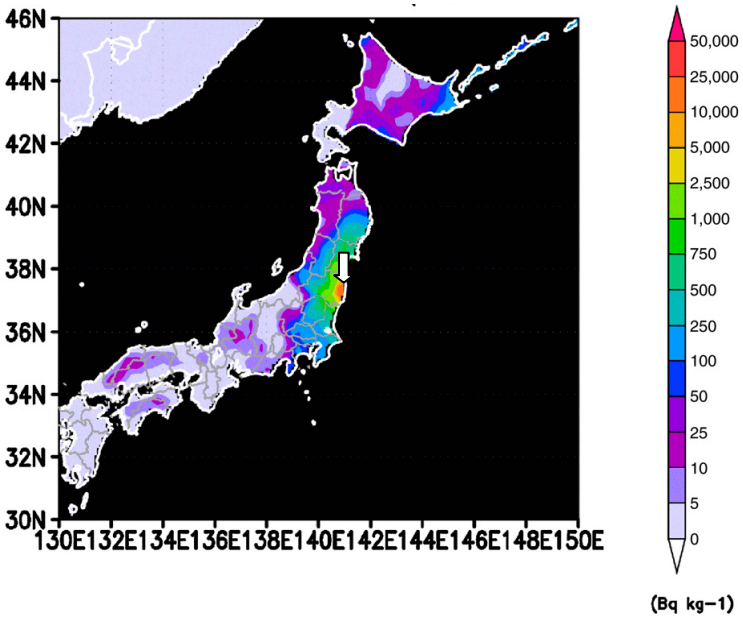

Figure 1. Soil concentration of ^{137}Cs on the Japanese mainland estimated after 2012.
After deposition of ^{137}Cs by the Fukushima Daiichi NPP (white arrow) incident, the soil concentration was estimated by computer simulation (modified from Yasunari et al. 2011). The wide spread contamination with estimated soil concentrations of above 1 kBq (green) becomes apparent. The figure is reprinted with kind permission by the author.

Once introduced to a plant organism, Cs^+ was found to accumulate in all plant organs, including seed and fruit bodies (Carini, 2001; Middleton, 1959; Ould-Dada et al., 2006; Witherspoon and Brown, 1965). The combination of high availability in soil, long half-life and efficient uptake via the plant root marks the detrimental role of Cs^+ in ecology. Plants represent a sink for radioactive Cs and a source for it to enter the food chain (White et al., 2010). In conclusion, reducing the uptake of Cs^+ via plant roots would also reduce the inclusion of the Cs radioisotopes in the food chain.

1.3 Countermeasures against Cs^+ uptake by plants

A number of strategies to limit root uptake of radiocaesium were developed and tested (Howard et al., 2005; Nisbet, 1993; Nisbet et al., 1993; Valcke and Cremers, 1994; Vandenhove et al., 2005; Vidal et al., 2001). Stripping contaminated soil layers or mixing them with deeper layers could deplete or dilute the absolute Cs^+ availability for biota (Vidal et al., 2001). Increase in pH could reduce the bioavailability of Cs^+, and fertilization with increased concentrations of K^+ and NH_4^+ could out-compete Cs^+ (Avery, 1995; Valcke and Cremers, 1994). Nevertheless, these tactics are cost-intensive and may not be easily applicable on any location.

Selection or genetic modification of crop plants is an alternative or synergistic complement to these measures. Two strategies are pursued: bioremediation and the “safer” crop strategy (White et al., 2010). The first approach utilizes organisms, preferably fungi and plants that enrich a high amount of Cs^+, in order to deplete the soil from its contaminant. The requirements for such organisms are high tolerance against the toxic Cs^+, fast growth and the possibility for an easy removal after one round of “cleaning” (Entry et al., 1996; Jacob et al., 2001; Lasat et al., 1997). Such a strategy is limited by the time-intensive approach and the necessary disposal of radionuclide-enriched remediating organisms. The second possibility and probably the most relevant in future is to genetically engineer or select plants that accumulate significantly lower amounts of Cs^+. Accordingly, the plants would be ready for food production even on contaminated ground and were therefore termed “safer crop” (White and Broadley, 2000). Possible strategies to reach this goal would be an alteration of membrane permeability through site-directed mutagenesis of Cs^+ transporting proteins and / or to search for other mechanisms that control the specificity of Cs^+ accumulation and that can be manipulated without affecting the essential ion homeostasis. If e.g. the closely related K^+ was affected, the fitness and yield of the plants would be reduced.

It could be shown that the trait of Cs^+ enrichment in plants depends not only on inter-species differences (e.g. influenced by morphology), but it also varies within plant families and even between local accessions of the same species (Broadley et al., 1999; Payne et al., 2004; Gerstmann and Schimmack, 2006; Putyatin et al., 2006; Kanter et al., 2010). The enrichment of Cs^+ and organ transfer factors were assessed in such different plants as marine algae (Styron et al., 1976), the model Brassicaceae *Arabidopsis thaliana* (Broadley et al., 2001; Hampton et al., 2005; Kanter et al., 2010), crop plants (wheat, rye, maize, barley) (Gerstmann and Schimmack, 2006; Prister et al., 1992; Schneider et al., 2008) and fruits of various trees (Carini, 2001, 2009; Linkov et al., 2006). These studies showed that Cs^+ accumulation is a heritable trait in plants and thus is controlled by their genetic setup.

Single genes and their gene products may be identified as potential targets for modulating Cs^+ enrichment with the aim to generate discrimination between Cs^+ and the essential K^+ (and other essential ions), and to potentially breed a safer crop. Cs^+ root uptake has been intensively studied in plants and until now, components of this machinery were the only discussed targets for manipulating Cs^+ uptake (White et al., 2010).

1.4 Cs^+ enrichment depends on K^+ transport systems

Due to the chemical similarities of K^+ and Cs^+ the non-essential Cs^+ takes the role of a hitch-hiker of root uptake mechanisms for K^+ (Hampton et al., 2005; White and Broadley, 2000). Highly regulated K^+-permeating systems are abundant to maintain an optimum K^+ content in the cytoplasm, as K^+ is essential for pH control, membrane potential maintenance, cell turgor regulation, compensation for negative charges and enzyme functionality (Ariño et al., 2010; Avery, 1995; Okorokov et al., 1983; Rhodes et al., 1986; Rodriguez-Navarro, 2000; Walker et al., 1996). The rate of uptake for Cs^+ and K^+ was found to be comparable *in planta* (Collander, 1941), indicating the use of similar uptake mechanisms. This was supported by microbiological data from *E. coli*, *Rhodococcus sp.*, *Chlorella spp.* and a diversity of fungi, which accumulate Cs^+ and whose K^+ transport systems were proven or suggested as entry route (Avery, 1995; Avery et al., 1993; Bakken and Olsen, 1990; Bossemeyer et al., 1989; Dighton et al., 1991; Tomioka et al., 1992, 1994). Further indication of similar uptake mechanisms was provided by the fact that Cs^+ and K^+ show mutual competition and inhibition in a diversity of organisms (Adelman and French, 1978; Armstrong and Rothstein, 1967; Avery, 1995; Borst-Pauwels, 1981; Isenberg, 1976). Two general transport routes for cationic nutrients exist when passing from root cortex towards the central cylinder and into the vascular system of the plant: a) circumventing the plasmamembrane of the cortical cells by travelling with the apoplastic stream, which leads to the endodermis in most plants, where a further apoplastic path is blocked by the casparian strip, or b) entering and / or leaving the cortical cells via ion transport systems and follow a transcellular or even a symplatic route via cell connecting plasmodesmata (Bresinsky et al., 2008). In most plants, Cs^+ was proposed to mainly take the symplastic route (White et al., 2010). K^+ influx or efflux processes are mediated either by transporters, which can catalyse the permeation of ions against their electrochemical or concentration gradient, or channels, through which ions flow according to the gradient. Transporters either act as symporters, which mediate a co-transport of two ions, or as antiporters / exchangers, by which two different ions are exchanged (White et al., 2010).

In the unicellular baker's yeast (*Saccharomyces cerevisiae*), a two-system uptake for K^+ via transporters was described, which also applies for plants (Borst-Pauwels, 1981; Epstein, 1972; Schachtmann, 2000):

High-affinity systems (maximum enzyme activity at low external ion concentrations) are separated from low-affinity systems. The known K^+ translocation systems in the model plant *Arabidopsis thaliana* and their possible significance in Cs^+ transport are summed up in Tab. 3 (White et al., 2010; Zhu and Smolders, 2000). High-affinity Cs^+ uptake has been attributed to **H**igh-**a**ffinity K^+ transporters / K^+ **u**ptake **p**ermeases (HAK/KUP) (Sheahan et al., 1993; Rubio et al., 2008). They are proton / cation symporters and have an important role for Cs^+ uptake when the external cation concentration is low (Qi et al., 2008). High external Cs^+ concentrations are unlikely to occur in nature. Yet, assuming physiological conditions after a Cs^+ deposition in the soil (high external K^+, contaminated by a low Cs^+ concentration) low-affinity uptake of Cs^+ is important. This was found to be mediated mainly through **v**oltage **i**nsensitive **c**ation **c**hannels (VICCs) like the CNGC (**c**yclic **n**ucleotide **g**ated **c**hannel) family (Lacombe et al., 2001; Leng et al., 2002). Cs^+ permeability in this case can be high, but is counteracted by competition with the abundant K^+. Further inward rectifying channels are the K^+ **i**nward **r**ectifying **c**hannel (KIRC), e.g. AKT1, which is inhibited by increasing concentrations of external Cs^+, and the **H**yperpolarization **a**ctivated / **D**epolarization **a**ctivated **c**ation **c**hannel (HACC / DACC) systems, which have a still unclear role in cation permeation. In addition to these proteins, a high-affinity cation K^+/H^+ symporter HKT1 plays a role, since it was found to catalyse permeation of Cs^+ (Schachtman and Schroeder, 1994; Zhu and Smolders, 2000). Efflux may be mediated via the K^+ selective / **N**on-selective **o**utward **r**ectifiying **c**hannels (KORCs / NORCs) (White et al., 2004), which are active at high cytosolic Ca^{2+} concentrations.

Overall Cs^+ and K^+ accumulation was found to be not perfectly correlated in plants, which may be due to a utilization of different uptake proteins for the two cations under certain growth conditions (Broadley and White, 2012). However, little distinction between the ions can be expected in a cell with a fully functional set of ion transport proteins (White et al., 2010). It was discussed that an elevated ratio of the partially selective KIRC channels against non selective VICC channels may diminish Cs^+ uptake (Broadley and White, 2012), but the abundance and redundancy of cation channel proteins compromises such an approach. It can be manifested that most transport systems with affinity for K^+ also transport Cs^+, and therefore are targets for reducing the cellular uptake of Cs^+, e.g. by mutation. Yet, this approach is problematic, because the loss of these systems either causes pleiotropic effects, as essential cation homeostasis and signalling cascades would be affected, or the impact may be lost due to redundancy (Alemán et al., 2011; Bertl et al., 1997; Hampton et al., 2004; Leidi et al., 2010; Nieves-Cordones et al., 2010; Pardo et al., 2006; White and Broadley, 2000). Therefore, the manipulation of Cs^+ accumulation via root plasma membrane proteins involved in ion / K^+ homeostasis alone did not pose an effective countermeasure thus far.

Transport system	Type of Transport	Proteins (number of proteins; relevant examples)	Cs^+ permeability P(Cs)/P(K)	Reference
KUP/HAK	K^+/H^+ symporter, inward, high-affinity	6 ; AtHAK5	Yes (ratio nd)	(White and Broadley 2000; Qi et al. 2008; Rubio et al. 2008)
KIRC	Channel, inward, voltage sensitive, low-affinity	7 "Shaker"-like; AtAKT1, AtKAT1, AtKC1	0.07 – 0.43	(Broadley et al. 2001; Nakamura and Gaber 2009)
VICC	Channel, inward, voltage insensitive, low-affinity	20 CNGCs 20 AtGLRs (Gutamate receptors)	1.00	(Demidchik et al., 2002; Davenport, 2002; Kaplan et al., 2007)
HACC/DACC	K^+/H^+ symporter; inward; low-affinity	7 Annexins	~ 0.85	(Demidchik et al., 2002; White and Broadley 2000; White et al. 2002)
KORC/NORC	Channel, outward, voltage-sensitive, low-affinity	2 "Shaker"-like; AtSKOR	0.12-0.31	(Gaymard et al. 1998)

Table 3: *A. thaliana* K^+ transport proteins of the root cell plasma membrane with their putative relevance for Cs^+ transport.
Channel and transporter classes are indicated with a short description of their transport process and an overview of the abundance of the according protein family, as well as an indication of putative Cs+ permeability. *nd* = not determined. The table refers to White et al. (2010).

In the unicellular system of baker's yeast (*Saccharomyces cerevisiae*), the number of cation transport systems, plasma membrane-bound or intracellular, is smaller and most of the proteins are annotated and characterized (Fig. 2). However, Cs^+ accumulation is still not fully understood in this organism. Similar to the plant system, yeast depends on a highly regulated K^+ concentration in the cytosol (Ariño et al., 2010). The complete set of known K^+ transport systems of yeast are represented in Tab. 4. The main inward transporters for K^+ (Cs^+) under physiological conditions are the high-affinity Trk1p and the low-affinity Trk2p (Fig. 2) (Bertl et al., 2003; Madrid et al., 1998; Ramos et al., 1994; Rodriguez-Navarro and Ramos, 1984). If both are lost, K^+ transport is drastically reduced and severe damages to the cell survival are reported (Rodriguez-Navarro, 2000). Other inward directed systems (Pho38 and NSC1) cannot fully substitute for a loss of Trk1/2p. Accordingly, the uptake of Cs^+ has to be considered as linked to the Trk1/2p system. The selectivity of these transporters is considered to be low at physiological conditions, but it can be modulated by altering external factors, e.g. the concentration ratios of the present ions and the surrounding pH (Armstrong and Rothstein, 1964, 1967; Haro and Rodriguez-Navarro, 2002). At low pH conditions, Cs^+ acts as a non-competitive inhibitor for K^+ uptake, while at higher pH it becomes a competitive inhibitor (Armstrong and Rothstein, 1967; Borst-Pauwels, 1981). Up to 80 % of intracellular K^+ can be replaced by Cs^+ in cells undergoing K^+ starvation, of which 60 - 90 % will be deposited to the vacuole, which is the major cytosolic ion- and pH-control compartment (Ariño et al., 2010; Klionsky et al., 1990; Perkins et al., 1993a; Scott et al., 1996). This effective compartmentalisation is probably mediated by the ion exchangers Vnx1p and Nhx1p (Cagnac et al., 2007; Cagnac et al., 2010; Nass and Rao, 1998) (Fig. 2 and Tab. 4). In case of Cs^+ the compartmentalisation may be of special importance due to its reported toxicity (Avery, 1995).

Efflux of monovalent cations to the surrounding is catalysed mainly by Tok1p, a voltage-sensitive channel (Loukin and Saimi, 2002; Roller et al., 2005) and Nha1p, a less selective cation/proton antiporter (Rodriguez-Navarro, 2000; Rodriguez-Navarro et al., 1994). The P-type ATPases Ena1p and Ena2p are mostly responsible for Na^+ export, but are also activated by changes in K^+ concentration and may therefore be relevant for K^+ / Cs^+ efflux (Banuelos and Rodriguez-Navarro, 1998; Benito et al., 1997; Garciadeblas et al., 1993; Haro et al., 1991). Further intracellular K^+ distribution is executed by the Golgi localized Kha1p (Ramirez et al., 1998). No Cs^+ / K^+ discrimination was found for these systems and the significance of the efflux transporters for regulating Cs^+ accumulation remains unclear thus far.

Manipulation of Cs^+ uptake via modulation of a single ion transport protein in yeast is confronted with the same problems as in the plant system. Alteration of Cs^+ uptake might be feasible by changing the characteristics of single proteins towards a higher discrimination between the cations. The Trk1/2p system is the most relevant for Cs^+ uptake, but it is essential for regular K^+ homeostasis. Therefore, manipulation of plasma membrane Cs^+ uptake would necessarily need to enhance the selectivity of these systems. Plasma membrane efflux, most probably mediated by Tok1, Ena1/2 and Nha1 is both, non selective and redundant. Thus, a targeted manipulation of those systems would need to result in an increased Cs^+ outward flow, while conserving a normal permeability for essential ions.

Still, there are indications that in yeast a differentiation between K^+ and Cs^+ may be achieved at the level of intracellular ion distribution and storage, since the selective toxicity of Cs^+, but not K^+ and Rb^+ per se demonstrates a necessity to distinguish between essential and potentially harmful cations.

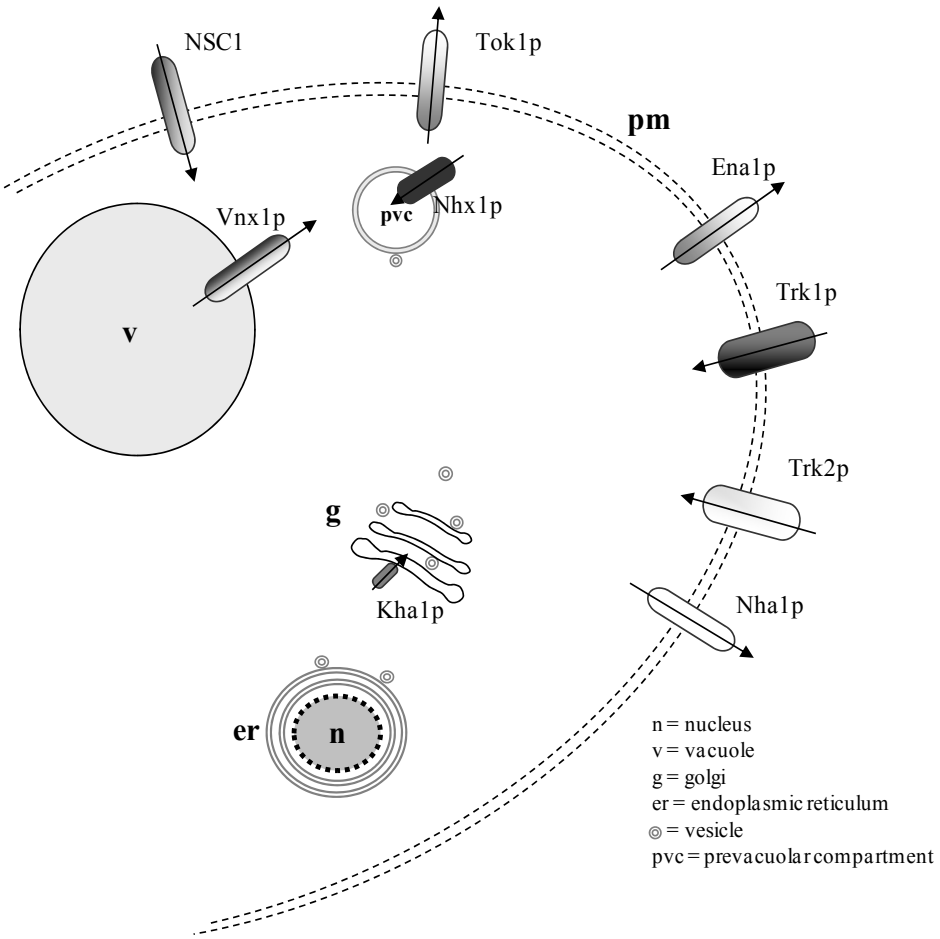

Fig. 2. Overview of known plasma membrane and intracellular alkali metal cation transporters and channels of *S. cerevisiae* with possible Cs^+ transport ability.
The trivial names of the proteins are given, together with their localization. The direction of described K^+ flux (and putative Cs^+ flux) is indicated by arrows. This figure is supplemented by the information in Tab. 4.

Transporter	Localization (membrane)	Ion transport system	Ion selectivity	Reference
Trk1	PM	K^+ (inward)	no	(Rodriguez-Navarro and Ramos, 1984)
Trk2	PM	K^+ (inward)	no	(Rodriguez-Navarro and Ramos, 1984)
Pho89	PM	Na^+ (P_i)/H^+ symport (inward)	no	(Martinez and Persson, 1998)
NSC1 (not proven)	PM	K^+ (inward) proposed	nd	(Bihler et al., 1998)
Tok1	PM	K^+ (outward)	nd	(Ketchum et al., 1995)
Ena1/2	PM	Na^+ ATPase (outward)	no	(Haro et al., 1991; Banuelos and Rodriguez-Navarro, 1998)
Nha1	PM	Na^+/H^+ antiporter (outward)	no	(Roller et al., 2005)
Mdm38	M	K^+/H^+ antiport (inward)	nd	(Nowikovsky et al., 2007)
Kha1	G	K^+/H^+ antiport (inward)	no	(Ramirez et al., 1998)
Nhx1	LE	Na^+ and K^+/H^+ antiport (inward)	no	(Nass and Rao, 1998)
Vnx1	V	Na^+ and K^+/H^+ antiport (inward)	nd	(Cagnac et al., 2007)
Vcx1 (putative)	V	K^+ and Ca^{2+}/H^+ antiport (inward)	nd	(Cagnac et al., 2010)

Table 4: Cation transporters in yeast with substrate and specificity.
All described alkali metal ion transporting proteins, their putative localization and the possible substrates are indicated. PM = plasma membrane, M = mitochondrion, G = Golgi, LE = late endosome and V = vacuole; P_i = inorganic phosphate; nd = not determined. See Fig. 2 for comparison.

1.5 Cs^+ affecting processes help to identify new targets for manipulating the Cs^+ accumulation independent of the plasma membrane uptake

There are indications that in fungi and in plants Cs^+ and K^+ uptake was not as tightly correlated as expected for a non-discriminating situation (Broadley and White, 2012; Kanter et al., 2010; Yoshida and Muramatsu, 1998). This may be linked to the Cs^+ toxicity, which is found in yeast and in plants already at low concentrations, while K^+, but also Rb^+ are considered as non toxic at elevated concentrations (Tab. 1) (Avery, 1995; Camacho and Rodriguez-Navarro, 1981Hampton et al., 2004; Perkins and Gadd, 1993a; Sheahan et al., 1993). It was proposed that Cs^+ might be mis-integrated in K^+-dependent enzymes and proteins, causing defects in their activity (Avery, 1995; Hampton et al., 2004). The detrimental effects of Cs^+ are diverse (Arpin et al., 1972; Ghosh et al., 1991, 1993; Sahr et al., 2005) and the comprehensive studies of Hampton and colleagues (2004) showed that the toxicity is not mainly due to competition with K^+ at the plasma membrane.

Cs^+ is not able to replace K^+ in all its essential functions. Along with this, the efficient intracellular deposition of Cs^+ to the vacuole can be interpreted as a targeted detoxification, while keeping the concentration of essential ions (K^+) in the cytosol at an optimum (Ariño et al., 2010; Avery, 1995). This indicates discrimination between the alkali metals according to the effects they cause inside the cell. Proteins related to the detoxification of cations may therefore be valuable targets for altering Cs^+ accumulation without being tightly connected to the maintenance of essential cation concentrations inside the cell. These proteins may be completely independent of the plasma membrane ion uptake *per se*, but they might well involve ion transport systems or regulatory components to affect detoxification. They may be ion-discriminating themselves or could be targets for an effective manipulation towards increased ion specificity. It was shown in some cases that plant-to-yeast substitution with members of a detoxifying intracellular ion homeostasis mechanism was possible (Gaxiola et al., 1999; Kinclová-Zimmermannová et al., 2004), indicating that a characterization of such proteins can be established in the unicellular model and may then be translated to the multicellular system.

A list of putative target proteins was suggested by a genome-wide mutant screen for genes with effect on Cs^+, but not Strontium (Sr^{2+}) accumulation, which did not reveal the anticipated K^+ transport systems to be important (Heuck et al., 2010). Instead, vacuolar integrity as well as vesicle mediated protein trafficking were found to have crucial roles in this regard, both of which could participate e.g. in the regulation of Cs^+ transport or compartmentalisation. As this investigation was the first genome-wide analysis of mutants in yeast affecting Cs^+ accumulation, it was used as the basis for a characterization of a loss-of-function mutant with regard to Cs^+ / K^+ selectivity.

1.6 Aim of this work

Genetic approaches to limit plant uptake of Cs^+ ions would provide a chance to develop highly effective counterstrategies against the accumulation of radioactive Cs in crop plants without the necessity of expensive soil removal. Earlier studies concentrated on cation transporters of the plasma membrane, but a targeted manipulation of Cs^+ accumulation without disturbing the homeostasis of essential ions is problematic, as these systems are either vitally important and hard to manipulate or they would have little effect at physiological conditions due to redundancy. A protein that can be manipulated to induce Cs^+ over K^+ discrimination at the uptake or during intracellular ion regulation without causing pleiotropic effects was to be identified.

This project aimed at describing the role of a single candidate protein, which was found to reduce Cs^+ accumulation in a genome wide yeast mutant screen (Heuck et al., 2010), which was shown in this work to leave K^+ and other cations unaltered, and to transfer the observations to the model plant system *Arabidopsis thaliana*.

The following objectives were approached:

- Identification of Cs^+ specificity in a *S. cerevisiae* loss-of-function mutant.
- The according mutant must be fully viable without displaying detrimental pleiotropic effects.
- The affected cellular process should be investigated.
- The candidate gene must be conserved in plants so that an according loss-of-function mutant in *A. thaliana* should be characterized for ion discrimination and viability.

2 RESULTS

2.1 *Saccharomyces cerevisiae* Sec22p is a putative Cs^{+} regulating protein

2.1.1 Selection of Sec22p from a yeast mutant library screen

Genome-wide analysis of yeast Cs^{+} uptake has been evaluated in a haploid loss-of-function mutant collection. 4862 *S. cerevisiae* mutant strains had been screened for significant alterations in the amount of Cs^{+} or Sr^{2+} enriched after 13 h tracer (^{134}Cs and ^{80}Sr) incubation (Heuck et al., 2010). In total 72 strains (approximately 1.6 %) , each representing a distinct gene deletion, were extracted that had significantly reduced Cs^{+} content, while Sr^{2+} was not affected (Tab. 5). The screen had also found a number of Cs^{+} hyper-accumulating strains, but the focus was put on a reduction of Cs^{+} since the interest of this investigation was to identify a single gene or a functional pathway for the development of a safer, i.e. Cs^{+}-limiting crop breeding strategy.

z-score	Strains
- 6.58 ← - 3.43	YDL185W, YKL080W, YEL051W, YOR332W, YKL119C, YCL007C, YBR127C, YHR060W, YOR331C, YPL234C, YEL027W, YGR105W, YKL118W, YNL084C, YHR026W, YOL162W, YMR054W, YKL135C, YPL259C, YER151C, YNL297C, YDL192W, YLR169W, YPL195W, YKL081W, YOR109W, YBR101C, YDR027C, YLR170C, **YLR268W**, YLR171W, YNL296W, YPR029C, YKL136W, YJL154C, YJL024C
- 3.43 ← - 2.50	YHR012W, YNL183C, YHL023C, YEL042W, YBL007C, YOR171C, YNL143C, YJL094C, YDR207C, YOL006C, YBR201W, YGR261C, YDR200C, YPR024W, YKL211C, YDR203W, YNR041C, YCR077C, YJR059W, YIL044C, YBL072C, YIL146C, YHL031C, YOL067C, YNL234W, YLL040C, YLL038C, YDL001W, YLR391W, YKL212W, YMR010W, YPL071C, YFL033C, YNL177C, YJR102C, YDR129C

Table 5. Yeast haploid mutants with significantly reduced Cs^{+} accumulation, but no Sr^{2+} phenotype.
The information was collected from Heuck and colleagues (2010). Data is sorted by increasing z-scores. z-scores below -2.5 were considered as a significant reduction in Cs^{+} content. *YLR268W* (= *Sec22*) is highlighted in red (z-score = -3.68). When σ_{wt} is the standard deviation of wild type, a z – score was determined as:

$$\text{z-score} = \frac{c_{\text{mutant}} - c_{wt}}{\sigma_{wt}}.$$

Gene Ontology enrichment analysis, of the ***S**accharomyces cerevisiae* **G**enome **D**atabase (SGD, http://www.yeastgenome.org/cgi-bin/GO/goSlimMapper.pl, applying Fisher's exact test) demonstrated an overrepresented role of two categories: vacuole-associated processes (composed of H^{+}-V-ATPase subunits and assembly components; p ≤ 0.001) and vesicle mediated transport / protein sorting (p ≤ 0.001), while ion transport was underrepresented (1 of 72). No plasma membrane components, e.g. channels were included. Fig. 3 indicates the functional diversity of the selected mutants with reduced Cs^{+} phenotype.

a

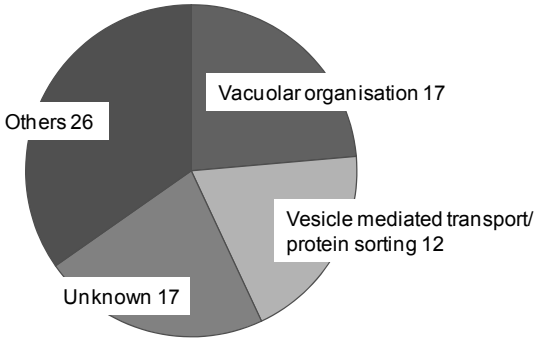

b

ORF; (GO term); identity (%)	
YDL185W (VO) 62%	*YNL297C* (VT) 19%
YKL080W (VO) 34%	*YPL195W* (VT) 28%
YEL051W (VO) 52%	*YDR027C* (VO) 22%
YOR332W (VO) 33%	*YLR170C* (VT) 51%
YKL119C (VO) 26%	***YLR268W* (VT) 40%**
YBR127C (VO) 76%	*YPR029C* (VT) 33%
YHR060W (VO) 30%	*YJL154C* (VO) 32%
YPL234C (VO) 57%	*YJL024C* (VT) 30%
YEL027W (VO) 59%	*YHR012W* (VO) 41%
YGR105W (VO) 29%	*YGR261C* (VT) 23%
YNL084C (VT) 27%	*YDR200C* (VO) 25%
YHR026W (VO) 56%	*YIL044C* (VT) 52%
YMR054W (VO) 33%	*YHL031C* (VT) 26%
YKL135C (VT) 41%	*YJR102C* (VO) 27%
YPL259C (VT) 46%	

Figure 3. Candidate selection after Gene Ontology analysis and BLAST search vs. *Arabidopsis thaliana*.
(a)Functional classification of the putative candidates for further analysis of Cs^+ accumulation. In total 72 mutants and the according Open Reading Frames (ORFs) were extracted from the selection presented in Table 5. Gene Ontology (GO) categorization in vacuolar organization (VO) or vesicle trafficking (VT) was overrepresented. Unknown protein functions could not be categorized, while "Others" compiles functional classes only represented once within the 72. (b) Similarities according to BLAST analyses are indicated by the percent of identical amino acids against a *A. thaliana* protein database. *YLR268W* (*Sec22*) is highlighted in red. Overall identity for Sec22p to At1g11890 was 36 %, maximum identity = 40 %, with a coverage of 91 %, e = $2*10^{-37}$.

Three putative candidates had been tested also for a K^+ phenotype, but showed no significant effect on K^+: *vps35*Δ (*yjl154c*Δ), *aps3*Δ (*yjl024c*Δ) and *apl4*Δ (*ypr029c*Δ). However, those mutants displayed pleiotropic effects as growth and viability either in full nutrient conditions or in the experimental setup in nutrient-depleted buffer was reduced (Fig. 4a, d, e). Additionally, other candidates associated with functions essential for vacuolar integrity were excluded since they showed abnormal pH sensitivity and lower vitality under the experimental conditions, as indicated also by literature for diverse components of the vacuolar membrane (Graham et al., 2003; Nelson and Nelson, 1990). Therefore this functional category did not offer valuable candidates for detailed characterization of ion selectivity. Accordingly, the selection of a candidate was focused on the vesicle transport related mutants with reduced Cs^+ content while preserving wild type-like growth and development.

YLR268W (= *Sec22)* was chosen as no severe growth phenotype has been reported for the yeast mutant *sec22*Δ (Liu and Barlowe, 2002). A slightly increased cell size was described for temperature sensitive mutant alleles (Jorgensen et al., 2002), but the average cell volume of *sec22*Δ confirmed a wild type-like development when grown at 28 °C in full nutrient media (YPD, pH = 6.5) (Fig. 4c).

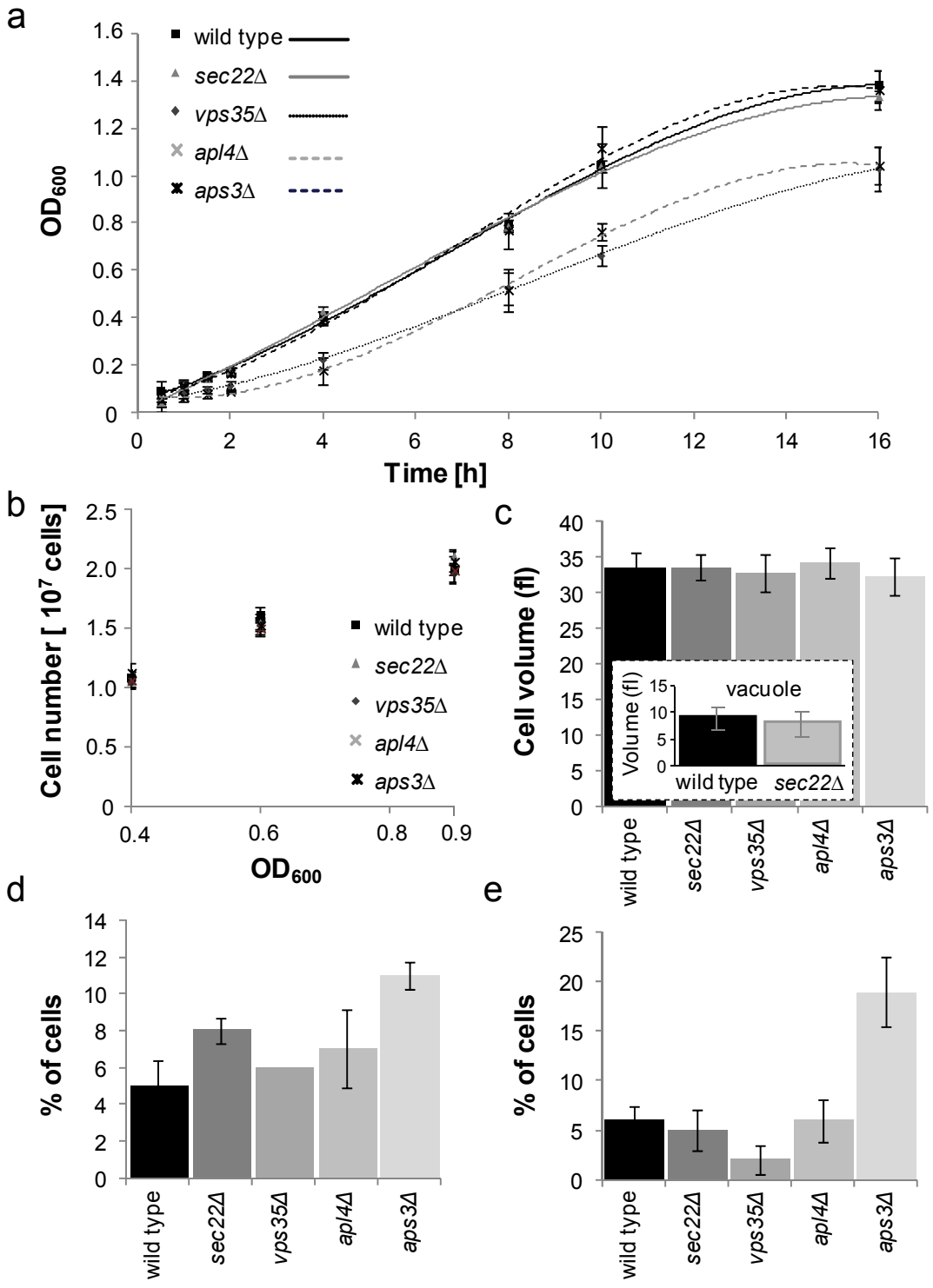

Figure 4. Growth and viability test for mutants with selectively reduced Cs^+ accumulation and *sec22*Δ.
Haploid mutants for *Vps35* (*YJL154C*), *Aps3* (*YJL024C*), *Apl4* (*YPR029C*) and *Sec22* were analysed. (a) Growth rate in YPAD medium based on OD measurement (n = 3). (b) Cell numbers per OD_{600} unit at t = 9 h (n = 5). (c) Cell volume at t = 9 h (n = 5, an average of 30 cells was taken into account per analysis). Insert: vacuolar volume of wild type and *sec22*Δ. Cell volumes are 34 ± 2.5 fl (WT) and 34.9 ± 5.8 fl (*sec22Δ*); vacuolar volumes are 8.8 ± 2.1 fl and 7.7 ± 2.1 fl. (d) Negative vital staining of 100 cells after 13 h incubation in YPAD medium (n = 3). (e) Negative vital staining of 100 cells after incubation for 13 h in assay buffer (n = 3).

The main functional role of Sec22p, the gene product of *YLR268W*, has been described. It is a soluble N-ethylmaleimide sensitive factor receptor (SNARE) including two conserved functional domains (Longin and Synaptobrevin) and a transmembrane region (Chatre et al., 2005; Liu and Barlowe, 2002; Mancias and Goldberg, 2007; Sacher et al., 1997) (Fig. 5). SNAREs mediate the fusion of vesicles in the process of protein sorting and secretion by building transient complexes with other SNAREs (3 target-(t)-SNAREs interact with 1 vesicle-(v)-SNARE) and they approximate opposing biomembranes to catalyse the fusion event (Bassham and Blatt, 2008). Sec22p is a v-SNARE of the Longin subfamily (Filipini et al., 2001). Proteins with homology to Sec22p are found throughout different kingdoms (Fig. 6). *A. thaliana* also carries a putative orthologue, At1g11890.1. This genetic model organism constitutes a potent system for analysing Cs^+ uptake via plant roots (Kanter et al., 2010). Identity between the yeast and the plant homologous proteins was 36 % with all described functional domains being conserved (Fig. 5). At1g11890.1 will be named *A. thaliana* SEC22 henceforth. A T-DNA insertion line for the according gene *At1g11890 (A. thaliana SEC22)* was available (Alonso and Strepanova, 2003; Scholl et al., 2000) and interest was further substantiated as this gene was included in a Quantitative Trait Locus (QTL) identified for the trait Cs^+ uptake via the *A. thaliana* root (Kanter et al., 2010).

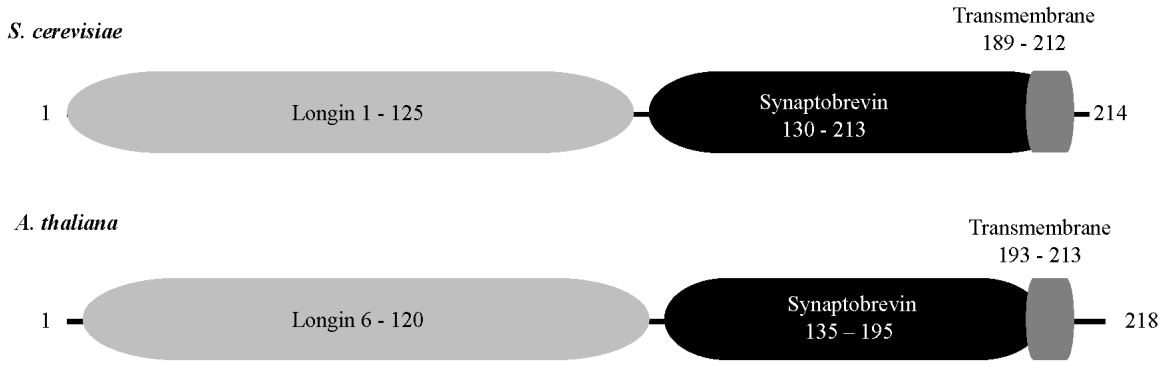

Figure 5. The domain structure of the yeast protein Sec22p (YLR268W) and the *A. thaliana* functional orthologue At1g11890.1.
A schematic representation of yeast Sec22p and *A. thaliana* SEC22 is shown, focussing on the sequence of domains from N- to C-terminus. Domains were located using sequence comparison with the integrative Interpro database (http://www.ebi.ac.uk/interpro/) for *S. cerevisiae* and Prosite (http://prosite.expasy.org/) / Pfam (http://pfam.sanger.ac.uk/) for *A. thaliana*. Longin domain, the Synaptobrevin (or SNARE) domain and the putative transmembrane region are indicated.

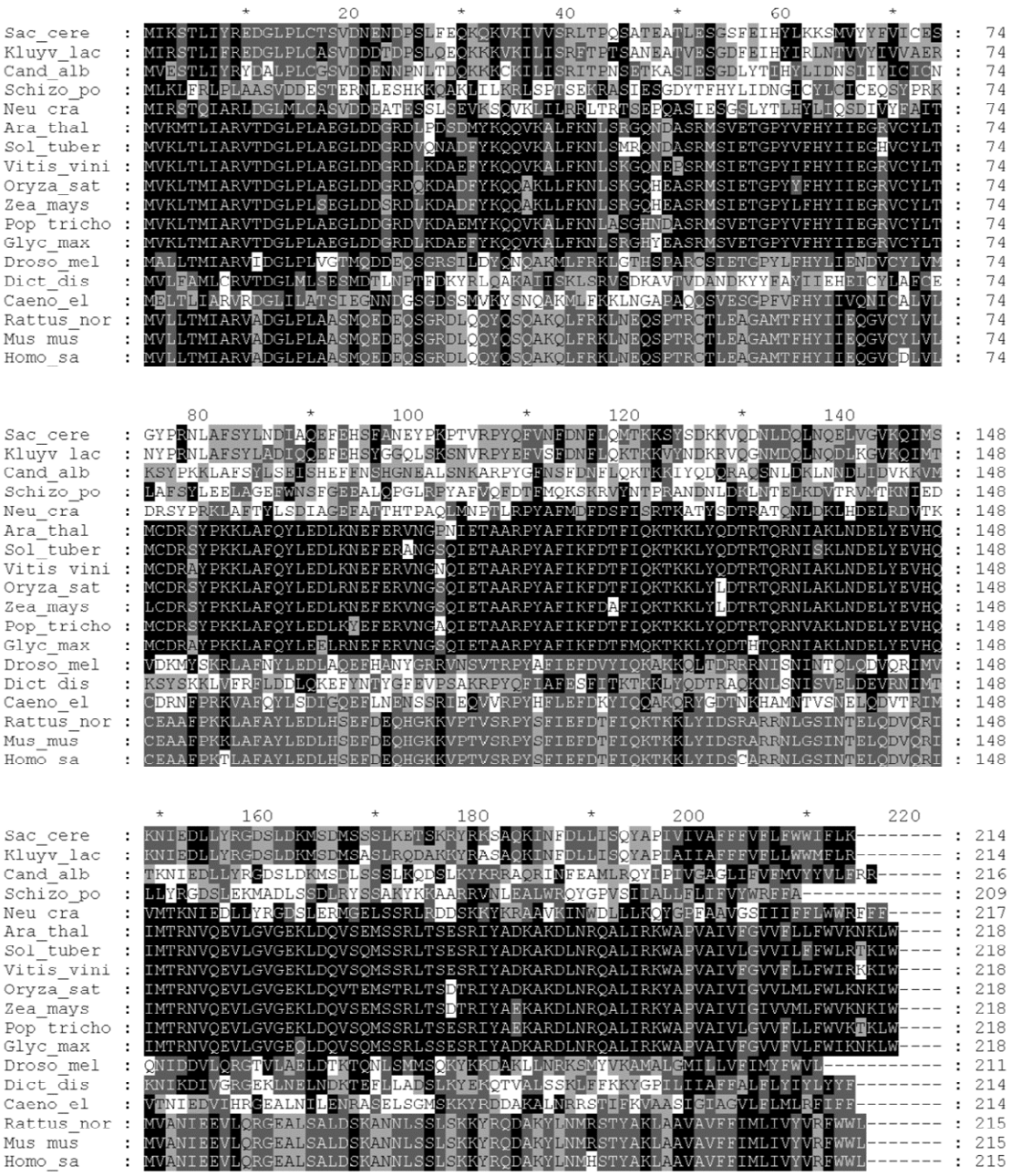

Figure 6. **Alignment of *S. cerevisiae* Sec22p and homologous proteins from selected organisms.**
A gapped alignment with a p-value threshold of ≤ 0.01 is shown. Presentation of the alignment was done using GeneDoc (www.psc.edu/biomed/genedoc) (Nicholas et al., 1997). Following settings were used: Quantify mode, 4 level shading according to residue identity. Shading key is as follows: black = conserved amino acid, dark grey ≥ 80 % conservation, light grey ≥ 60 % conservation and no shading = non conserved residue, dependend on the input sequences. Following proteins (Uniprot ID) were aligned: *S. cerevisiae* P22214; *Schizosaccharomyces pombe* Q9Y7L0; *Kluyveromyces lactis* Q6CJA0; *Candida albicans* C4YLL5; *Neurospora crassa* Q871Q9; *A. thaliana* Q94AU2; *Solanum tuberosum* Q307X8; *Vitis vinifera* A5AZI9; *Oryza sativa* B8B3Q3; *Zea mays* B6TMY9; *Populus trichocarpa* B9N7F9; *Glycine max* C6TGR3; *Drosophila melanogaster* Q77434; *Dictyostelium discoideum* Q55CRO; *Caenorabditis elegans* Q94241; *Rattus norvegicus* Q4KM74; *Mus musculus* O08547; *Homo sapiens* Q75396. *S. cerevisiae* and *A. thaliana* share 36 % identity.

2.1.2 Cs^+ accumulation is specifically reduced in *S. cerevisiae sec22*Δ

^{134}Cs tracer uptake studies in yeast were applied to confirm and further specify the phenotype of *sec22*Δ in ion homeostasis. Expression analysis by RT-PCR approved the loss of the *Sec22* transcript (Fig. 7, compare lanes 3 and 5).

The Cs^+ accumulation assay was done after a 13 h incubation phase in K^+ limitation and in the presence of 50 µM CsCl in addition to the radioactive tracer. *sec22*Δ accumulates less than 50 % of Cs^+ compared to the wild type, whereas the K^+-analog Rb^+, which was also tested in a tracer experiment, reached wild-type levels (Fig. 8a). Intracellular concentrations were calculated (Raw datasets are included in *Appendices A + B*). A complemented strain containing the vector construct pYEP352::*Sec22* for *Sec22* expression under its native promoter (1kb upstream) was tested to proof that no secondary gene loss was responsible for the phenotype. Expression was confirmed (Fig. 7; lane 7). The complemented strain accumulated Cs^+ in wild type-like manner, suppressing the mutant phenotype (Fig. 8a).

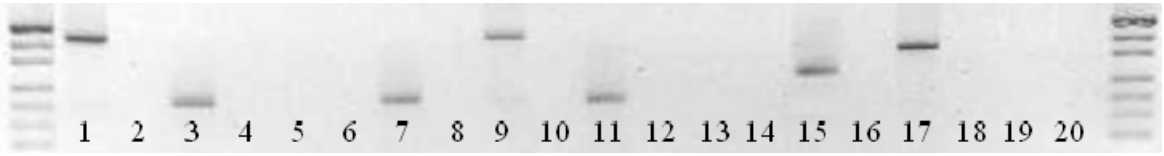

Lane	Template	Amplicon	RT	Lane	Template	Amplicon	RT
1	BY4741 (WT)	*Actin-1*	+	11	BY4741 (WT)	*Sec22*	+
2	BY4741 (WT)	*Actin-1*	-	12	BY4741 (WT)	*Sec22*	-
3	BY4741 (WT)	*Sec22*	+	13	*sec22Δ*	*At1g11890*	+
4	BY4741 (WT)	*Sec22*	-	14	*sec22Δ*	*At1g11890*	-
5	*sec22Δ*	*Sec22*	+	15	*sec22Δ::AtSEC22*	*At1g11890*	+
6	*sec22Δ*	*Sec22*	-	16	*sec22Δ ::AtSEC22*	*At1g11890*	-
7	*sec22Δ::Sec22*	*Sec22*	+	17	*sec22Δ ::AtSEC22*	*Actin-1*	+ (+ D)
8	*sec22Δ::Sec22*	*Sec22*	-	18	*sec22Δ ::AtSEC22*	*Actin-1*	- (+ D)
9	*sec22Δ*	*Actin-1*	+	19	*sec22Δ ::AtSEC22*	*At1g11890*	+ (+ D)
10	*sec22Δ*	*Actin-1*	-	20	*sec22Δ ::AtSEC22*	*At1g11890*	- (+ D)

Figure 7. RT-PCR expression analyses for *S. cerevisiae* in different yeast strains.
RT-PCR was performed to test the expression in mutant yeast strains and transformed yeast. Numbers indicate the lane. *Sec22* expression is lost in *sec22*Δ, but present in the complemented line (*sec22*Δ*::Sec22*). *SEC22* from *A. thaliana* (*AtSEC22*) could be expressed in the yeast *sec22*Δ background (*sec22*Δ*::AtSEC22*). Wild-type controls and negative controls (without Reverse Transcriptase = -RT) were added. As systemic control, the constitutively expressed (house-keeping) *Actin-1* (*YFL039C*) of *S. cerevisiae* was included. Amplicon expected sizes are *Actin-1*: 421 bp, *Sec22*: 112 bp; *At1g11890*: 256 bp. All tests were done at least in duplicate. Doxycycline addition (to abolish pCM189 driven expression of *A. thaliana SEC22* in the yeast mutant background) is indicated (+ D). One % TAE Agarose gel is shown. pUC19/MspI DNA ladder markers (Fermentas) were used. 11 and 12 are identical to 3 and 4.

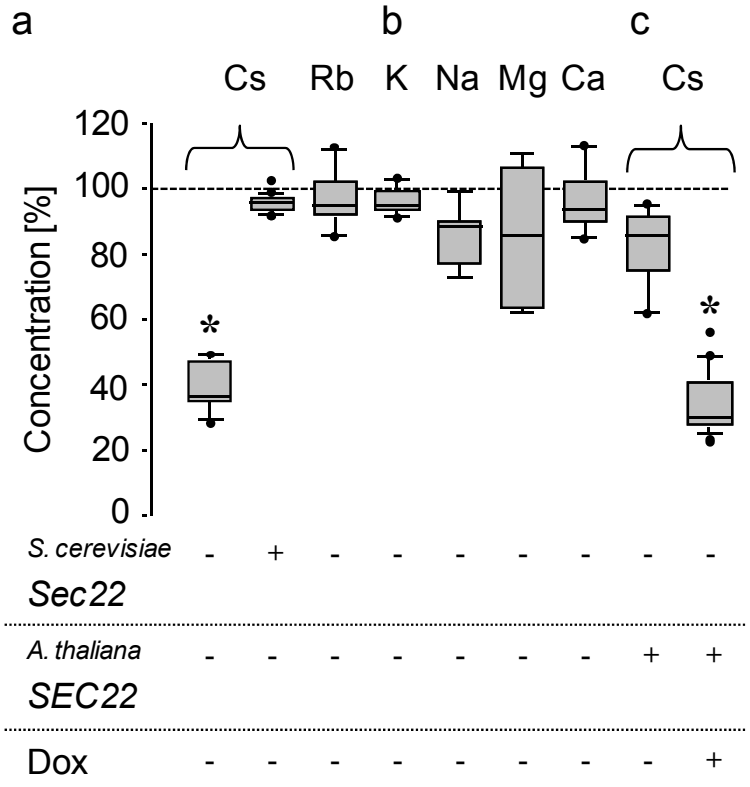

Figure 8. Cs^+-specific cation phenotype of yeast *sec22Δ*. Tracer quantification (a, c) and mass spectrometry (b), were used to determine the intracellular cation concentration. Concentration (%) per total volume in comparison to wild-type control. (a) Cs^+ and Rb^+ uptake assay for the *sec22Δ* and a complemented strain (*sec22Δ::Sec22,* second lane). The wild-type (WT) reference BY4741 contained 2.4 ± 0.1 mM Cs^+ (3.8 ± 0.2 mM Rb^+). (b) K^+, Na^+, Ca^{2+} and Mg^{2+} concentrations under assay conditions. Wild-type levels were 158.9 mM K^+, 38.4 mM Na^+, 10.0 mM Mg^{2+} and 0.5 mM Ca^{2+}, respectively. (c) Complementation of *sec22Δ* Cs^+ uptake deficiency by *A. thaliana SEC22* expressed under the control of a doxycycline-repressible promoter. Outliers are shown as black dots; asterisks indicate significant variation from wild type (t-test against 0; $p \leq 0{,}001$; $n \geq 6$). Presence / absence of *S. cerevisiae Sec22*/*A. thaliana SEC22* expression are indicated as +/-. Doxycycline addition: Dox +.

Importantly, the concentration of other cations (K^+, Na^+, Ca^{2+}, Mg^{2+}) remained unaltered when cells were grown under uptake assay conditions, as measured by atomic emission spectrography (Fig. 8b). This same was true for cells grown on full medium (Tab. 6, *Appendix C*).

Cs^+ was found to be toxic for yeast at relatively low concentrations (≥ 50 mM is the median inhibitory concentration (Perkins and Gadd, 1993a)). Surprisingly, *sec22*Δ displayed a slightly increased sensitivity against Cs^+ at 50 mM, as well as against lithium (Li^+) at normally non-toxic concentrations (Fig. 9) (Perkins and Gadd, 1993b).

Ion	K^+	Na^+	Ca^{2+}
c(Cs^+) wild type (mM)	239 ± 25	111 ± 10	1.8 ± 0.2
c(Cs^+) *sec22*Δ (mM)	230 ± 8	109 ± 6	1.5 ± 0.3

Table 6. **Cation concentrations after 13 h of standard nutrient and growth conditions (YPAD).**
The data is complementary to the concentrations presented in Fig. 9b. Absolute values for *sec22*Δ and wild type concentrations are shown. No significant differences between *sec22Δ* and wild-type were found. $n \geq 4$.

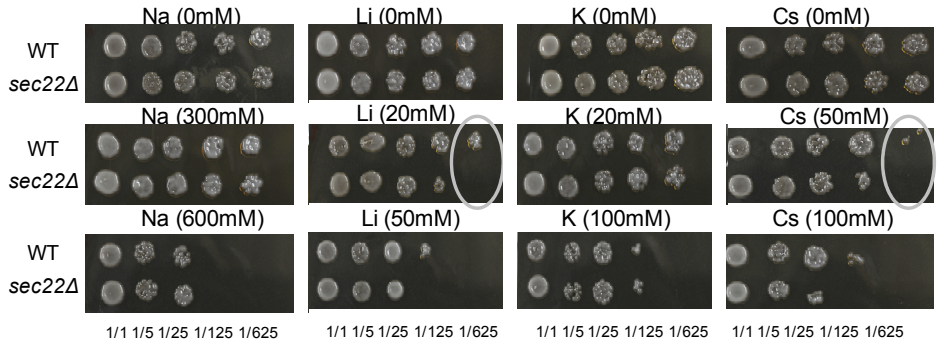

Figure 9. **Cation toxicity test of wild-type and *sec22Δ* yeast.**
Dilution series at different concentrations of ions in YPAD solid media were replica-plated from plates without additional ions. Plates were grown for 2 d at 30 °C. Grey circles indicate dilutions in which *sec22Δ* shows higher sensitivity than wild type (WT). Sensitivity against Na^+, Li^+, K^+ and Cs^+ was tested.

An overexpression strain for *Sec22*, under a doxycycline-repressible promoter, was created in the mutant background by transformation of *sec22*Δ with pCM189::*Sec22* (*Sec22* under a doxycycline repressible constitutive promoter). This strain accumulated an increased amount of Cs^+ (Fig. 10ab, *Appendix A*) and displayed a high sensitivity against Cs^+ (Fig. 10c). The cells had a decreased viability, as shown by vital staining under Cs^+ assay conditions (Tab. 7). This strain was not tested for discrimination against K^+. Accordingly, it remains unclear whether the reduced viability is due to a disturbance in ion homeostasis of other cellular functions.No further experiments were planned with this overexpression strain due to its increased mortality under experimental conditions.

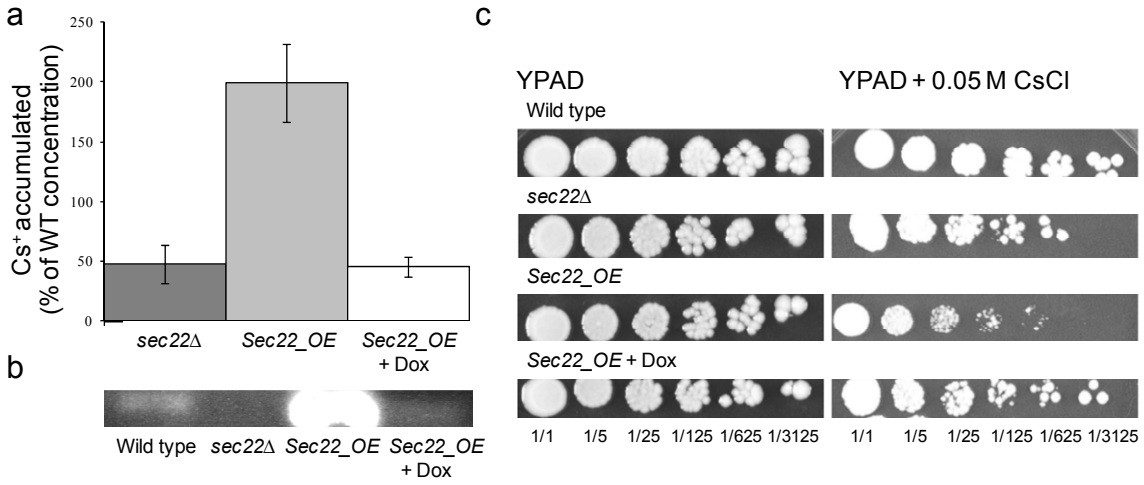

Figure 10. **Cs^+ accumulation in *Sec22* overexpression strain is increased.**
A strain overexpressing *Sec22* was analysed for Cs^+ accumulation and toxicity. (a) Cs^+ accumulation was calculated using tracer quantification. WT level was set to 100 % (= 2.4 mM intracellular Cs^+). Dark grey: *sec22Δ*, light grey: *Sec22* overexpression strain (Sec22_OE); white: treatment with doxycycline (+ Dox). (b) RT – PCR on cDNA with *Sec22* specific primers. No expression was detected for the mutant and for *Sec22_OE* treated with Dox, while expression was found in the transformed strain without Dox treatment. (c) Toxicity analysis of *Sec22*_OE. A dilution series is shown of YPAD – Agar grown yeast strains as indicated, without (left) or with (right) 50 mM CsCl in the solid medium.

Strain	Wild-type	*sec22*Δ	*sec22*Δ*::Sec22*	*Sec22*_OE
Non viable (%)	3.94 ± 1.44	3.14 ± 1.26	4.19 ± 2.09	22.12 ± 5.53*

Table 7. Estimation of the viability of yeast strains used in this study.
FM4-64 vital staining was used to monitor viability. Only seemingly intact cells (not mechanically disrupted) were taken into account. Therefore, the real number of negative staining (= non viable) may be underestimated. n = 100. Two independent measurements were done.* = significantly different from wild type (t-test against 0; $p \leq 0.0001$). The tested condition was 50 µM CsCl supplied to assay buffer.

2.1.3 Cs^+ accumulation kinetics reveals a two-phase enrichment with different saturating concentrations of wild type and *sec22*Δ

A diversity of factors might influence the Cs^+ accumulation of a cell. Ion uptake may be described as a function of external concentration, pH or as a function of time (Armstrong and Rothstein, 1964, 1967). The *sec22*Δ phenotype was investigated in more detail by recording the alteration of Cs^+ concentration with time in high resolution in the tracer assay set-up. Wild-type cells describe accumulation kinetics with distinct phases under these high-affinity conditions (50 µM CsCl external, K^+ depleted). The uptake is divided in two phases: An initial enrichment phase until approximately 2 - 3 h is sectioned from the second enrichment phase by a short (~ 1 h) delay. This two phase uptake ends in a rapid saturation (at around 8 h and an intracellular concentration of approximately 2.4 mM), as indicated before by Heuck and co-workers (2010) (Fig. 11a, data points). Raw data is included in *Appendix D*.

A two-phased uptake kinetics was not described thus far for K^+ (Armstrong and Rothstein, 1964, 1967; Cabrera et al., 2012; Rodriguez-Navarro and Ramos, 1984). Different processes may therefore be involved in the accumulation of Cs^+ and K^+. It was important to interprete the uptake kinetics in a systematic way, as alterations in the trajectory of the accumulation could help to identify unique cellular processes in Cs^+ enrichment.

The kinetics of *sec22*Δ Cs^+ uptake was similar to wild type in the two phase structure, but the transgression from delay phase to the second uptake stage was slightly slower. Yet, a steady-state was reached also at approximately 8 h, similar to wild type but with a lower mean intracellular concentration of 0.9 mM (Fig. 11b, data points). Accordingly, the phenotype of *sec22*Δ does not depend on a slow ion uptake alone, but there is a lower maximum intracellular concentration.

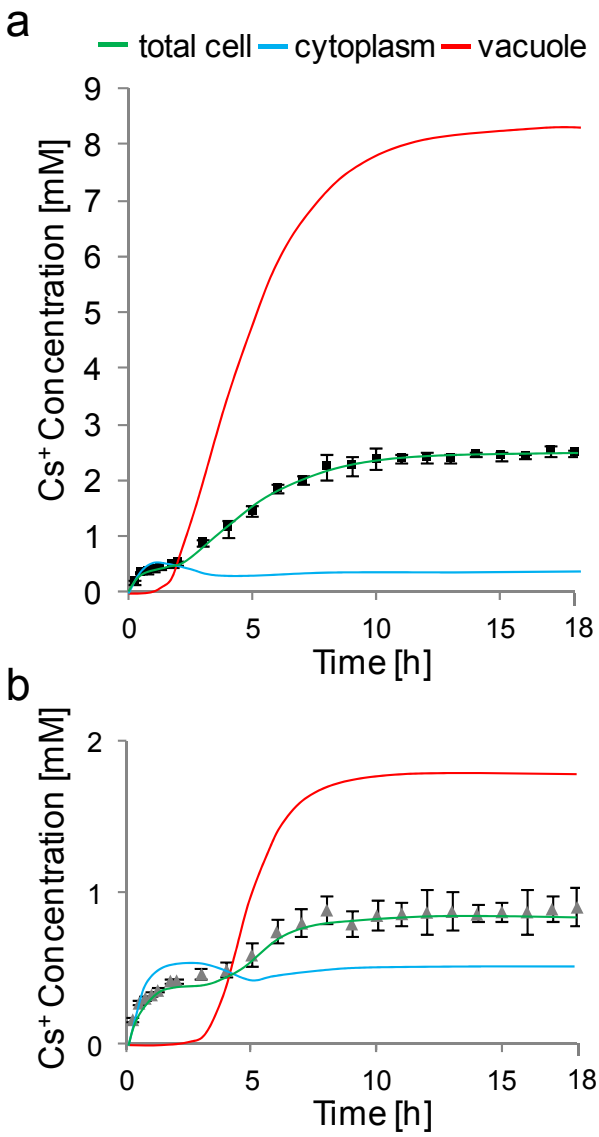

Figure 11. Cs^+ accumulation in wild-type and *sec22Δ* yeast.
Kinetics were recorded at assay conditions (50 µm external CsCl in 100 µl assay buffer). Data points with standard-deviations show the experimentally determined intracellular concentrations (n ≥ 5). (a) presents wild-type kinetics, (b) *sec22*Δ kinetics. Care for the different y -axis scale in (a) and (b). Continuous lines represent the predictions from mathematical modelling: the total intracellular concentration (green), as well as the cytoplasmic (blue) and vacuolar (red) concentrations are depicted. Note the different scales of the y-axis.

Due to the long incubation times of the assay conditions, a depletion of the external buffer Cs^+ concentration had to be estimated. At 13 h, the buffer in wild-type setup was reduced to 33 µM and for the mutant there was accordingly less reduction (from 50 to 44 µM). Since this depletion of external concentration was not to be considered negligible, a modification in the experimental setup was tested to exclude that the saturation phase was an artifact of the reduced external supply. Identical kinetics for both strains was recorded under modified assay conditions, containing 200 µM CsCl in a doubled buffer volume (i.e. 8 times higher amount of external Cs^+). Maximum buffer depletion from 200 µM to 188 µM in wild type was calculated in this case. In this quasi-stable system, the different phases were still occurring, even though the average intracellular concentration was increased (~ 1.4 times) (Fig. 12; Raw data in *Appendix E*). Importantly, the major differences between wild-type and mutant accumulation were conserved (steady state concentrations (13 h) wild-type roughly 3.4 mM, *sec22*Δ roughly 2.0 mM), confirming the acceptability of the results acquired at 50 µM conditions.

Taken together, *sec22*Δ has a significantly lower Cs^+ accumulation as these cells saturate at lower intracellular Cs^+ concentrations. Both conditions (low and increased external CsCl, representing high and low-affinity conditions for Cs^+ uptake) could be used to assess the difference between the strains.

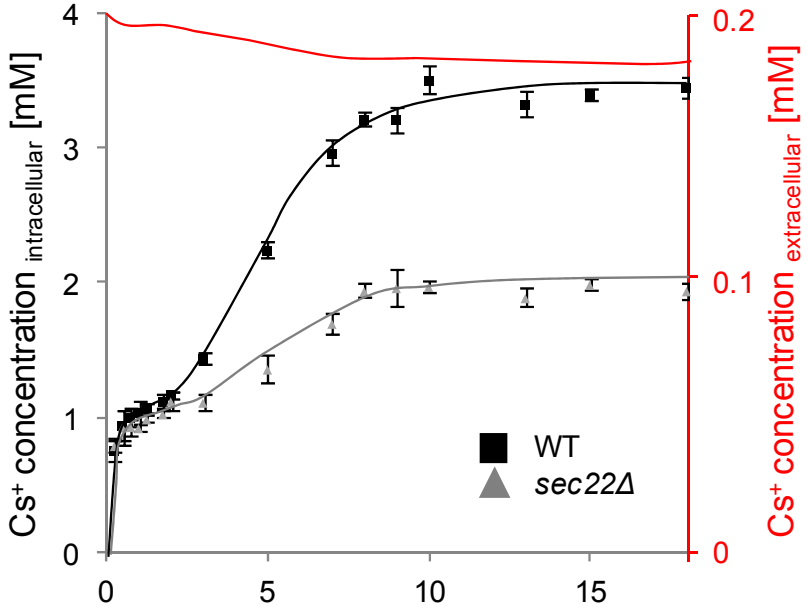

Figure 12. Uptake kinetics of wild-type and *sec22Δ S. cerevisiae* with 200 µM external Cs^+.
^{134}Cs tracer uptake kinetics was recorded at 200 µM external Cs^+ in 200 µl assay buffer. Experimental data is shown as data points. The change of Cs^+ concentration in the buffer of wild type (taking up more Cs^+ as the mutant) is shown as red curve to demonstrate the maximum depletion of buffer concentration in this setup. The phases of Cs^+ accumulation are similar compared to the 50 µM experiment (Fig. 11a, b). n ≥ 6.

2.1.4 Morphological analysis of *sec22*Δ

Since there are indications for a crucial role of the vacuole in Cs^+ accumulation, which in turn could affect the kinetics and the maximum intracellular Cs^+ concentration, the morphology of *sec22*Δ's vacuoles was tested by recording their volumes and the ratio of vacuolar to total cell volume. Vital staining for the vacuole revealed no significant differences in the volume of vacuoles between the strains, and the ratio was also not altered (Figs. 5 and 13). In assay conditions, the average cell volume was 33.8 ± 2.6 fl (wild type) and 34.9 ± 5.8 fl (*sec22Δ*), while vacuolar volumes were 8.8 ± 2.1 fl and 7.7 ± 2.1 fl for wild type and *sec22*Δ, respectively. These values are in agreement with literature (Ariño et al., 2010; Wiemken and Durr, 1974). Enrichment of Cs^+ in the cell wall or other intracellular structures was not expected in relevant amounts (Avery, 1995).

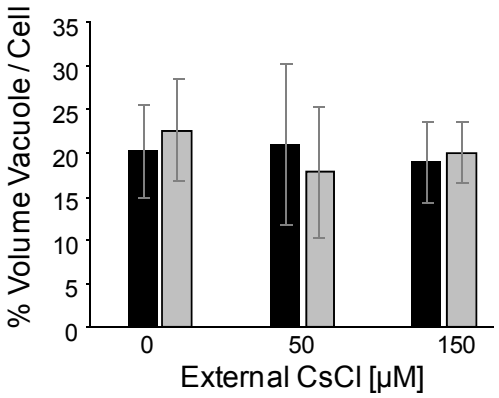

Figure 13. The ratio of vacuolar to cell volume is identical in wild type and *sec22*Δ.
The volume of vacuoles was calculated using vital staining and the result was correlated with the volume of the same cell. n = 50. Cells were incubated in assay buffer with different external Cs^+ concentrations. Black bars: wild type, grey bars: *sec22*Δ. No significant differences between the strains or the treatments were found (t-test against 0; $p \leq 1.0$).

2.1.5 Mathematical modelling proposes a compromised vacuolar deposition of Cs^+ in *sec22*Δ

An interpretation of the kinetics data in regard to Cs^+ uptake and intracellular distribution could help to understand Cs^+ accumulation in general and to find out what leads to a lower Cs^+ concentration in *sec22*Δ. The unique characteristics of the Cs^+ high-affinity accumulation kinetics of wild type suggested the development of an *ab initio* mathematical compartment model for Cs^+ fluxes in the yeast system, which reconstructs the kinetics experiment. The strategy was to first create a minimal model, which includes a solution for the intracellular distribution of the ion and to record the parameter values (= point estimates) that allow a statistically verified fit of the wild-type kinetics. *sec22*Δ kinetics are estimated by the same model and the significant differences between the parameters should inform about the possible or necessary alterations between the two fits. Further refinements of the model were then included.

This model was developed by Prof. Dr. Johannes Müller (Center for Mathematical Sciences, Technical University Munich), Dr. Weibo Li (Research Unit Medical Radiation Physics and Diagnostics, Helmholtz Zentrum München (HMGU)) and Dr. Burkhard Hense (Institute of Biomathematics and Biometry, HMGU) in cooperation with Dr. Schäffner and the author.

A) Model structure for Cs^+ fluxes based on linear kinetics.
The minimal model was built for three compartments (Fig. 14):

a) the extracellular buffer (i.e. the test tube) with volume V_1 and a Cs^+ concentration of c,
b) the cytoplasm of N cells with each single cell having a volume V_2 and a Cs^+ concentration of x, and, as intrinsic part of the cytoplasm,
c) the vacuole, with volume V_3 and concentration y.

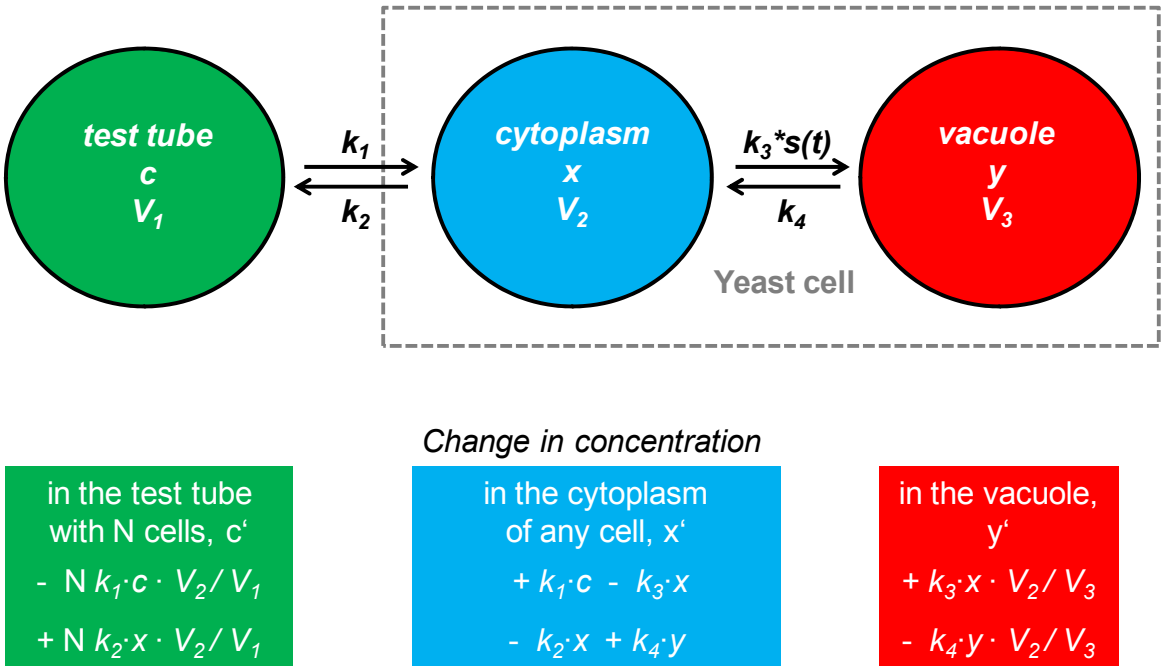

Figure 14. Scheme of the compartment model.
Four fluxes formulated based on linear reaction kinetics are adding to the changes of the Cs^+ concentration in the cytoplasm. The corresponding changes in the external medium and in the vacuole are described accordingly.

In high-affinity conditions (50 µM external concentration; no competition with K^+), linear enzyme reactions for Cs^+ transport were assumed. The model was defined only by the volume of the compartments and the starting condition (50 µM in test tube, 0 µM in cytoplasm and 0 µM in the vacuole). The vacuole was selected as intracellular sink for Cs^+ (defined by its volume), since this was in accordance with reported intracellular targeting for Cs^+, while other compartments were identified as negligible in this regard (Avery, 1995). As the model does not include the characteristics of single ion transporting proteins, the identification of the vacuole as intracellular structure is not relevant for the final modeling result – it could be any intracellular structure with a certain volume.

The translocation of Cs^+ to the cytoplasm via the plasma membrane was characterized by an influx from the test tube (with rate constant k_1) and a reflux from the cytoplasm (rate constant k_2). Each flux was defined by a linear dependency from the concentration in the corresponding compartment (e.g. the test tube loses Cs^+ to the cytoplasm as $-k1c$, but regains Cs^+ from the cytoplasm as $+k_2x$). Therefore, the concentrations of all compartments became dependent on each other (Fig. 14). As the concentration of Cs^+ within the three compartments (the test tube as one unit, but also for a single cell) was to be determined, it was necessary to correct for the total amount (N) of cells. With this, an invariance of the rate constants with respect to change of the test tube volume V_1 or the number of cells N was achieved.

In addition, the differences in volume had to be taken into account when the transfer of molar masses between compartments of different volumes was assumed, so that volume correction factors were included (i.e. the product of rate constant, concentration and volume of the compartment of exchange were divided by the volume of the respective compartment, e.g. the flux from the test tube to the cytoplasm was defined as – N $k_1 c\ V_2/V_1$). In this model structure, the cytoplasm was used as the center and corrections were applied for the test tube and the vacuole. The model equations were:

$$c' = N\frac{V_2}{V_1}\left(-k_1 c + k_2 x\right)$$
$$x' = k_1 c - k_2 x - k_3 x + k_4 y$$
$$y' = \frac{V_2}{V_3}\left(k_3 x - k_4 y\right).$$

In a first refinement of the model structure, the biphasic behavior of the kinetics – the short uptake delay at around 3 h (Fig. 11) was respected by including a Hill function

$$s(t) = t^n / (thresh^n + t^n),$$

which allows the introduction of a time dependent activation of a single process (in this model the flux to the vacuole), which is defined by a threshold (*thresh*) and the slope of the activation after the delay, *n*.

The equations describing the basic fluxes to and from the distinct compartments could then be described as:

$$c' = N\frac{V_2}{V_1}\left(-k_1 c + k_2 x\right)$$
$$x' = k_1 c - k_2 x - k_3 s(t) x + k_4 y$$
$$y' = \frac{V_2}{V_3}\left(k_3 s(t) x - k_4 y\right)$$
$$s(t) = t^n / (thresh^n + t^n).$$

In the experiment, the measured concentration was the unity of both, cytoplasm and the vacuole. Thus, the total concentration *tot* was defined as:

$$tot = \frac{V_2 x + V_3 y}{V_2 + V_3}.$$

Material and Methods chapter 4.4.1 describes the detailed development of the differential equations that describe the time dependence of *tot*, which were used to estimate the parameters for the kinetic prediction. In this process, a simplification in form of a dimension reduction was implied, i.e. the reduction of a three dimensional model to one dimension. This re-parametrisation set the rate constants of vacuolar in- and effluxes in relation and was defined as follows:

$k_3 = \Gamma\tau,\ k_4 = \Gamma(1-\tau),$

$\Gamma = k_3 + k_4.$

τ describes the equilibrium (asymptotic) ratio between x and y in the steady state phase (after 8 h, compare Fig. 12, where $s(t) \rightarrow 1$ and $k_3 x = k_4 y$). Γ represents the time scale at which this ratio is assumed. The model further included the information that vacuolar deposition is large, which points towards a fast flux to this compartment, once the Hill function delay was overcome ($s(t) \rightarrow 1$ and $t \rightarrow \infty$). This was integrated by stating that Γ was large. At the end, the system of ordinary differential equations described the Cs^+ accumulation in yeast as:

$$c(t) = c_0 - N\frac{V_2 + V_3}{V_1}tot(t)$$

$$x(t) = \frac{(V_2 + V_3)(1-\tau)}{V_3\tau\, s(t) + V_2(1-\tau)}tot(t)$$

$$y(t) = \frac{(V_2 + V_3)\tau\, s(t)}{V_3\tau\, s(t) + V_2(1-\tau)}tot(t).$$

B) Parameter estimation.

Two different sets of experiments were analysed, with wild type and *sec22*Δ in each case. They correlate to the data presented in 2.1.3 with one low (50 µM) and one elevated (200 µM) Cs^+ concentration in the external medium (Tab. 8).

Parameter/variable	Experiment 1	Experiment 2
V_1	100 µL	200 µL
V_2	$25*10^{-9}$ µL	$25*10^{-9}$ µL
V_3	$8.8*10^{-9}$ µL	$8.8*10^{-9}$ µL
N	$2*10^7$ cells	$2*10^7$ cells
c_0	50 µM	200 µM

Table 8. Experimental conditions and known parameters for the uptake experiments.
c_0 is the concentration at t = 0.

For experiment 1, containing the low extracellular Cs^+ concentration, the model parameters given in Tab. 9 were predicted. Statistical analyses were done as described in 4.4.1.

In the wild type, the model predicts a rapid increase of the cytoplasmic Cs^+ with well-defined rate constants k_1 and k_2, as well as a delayed sequestration to the vacuole, which is fast, but less well defined. τ was large and, according to its definition, this describes a fast vacuolar deposition. The fit of the wild type was accurate and it was possible to predict the biphasic structure of the kinetics (Fig. 11a, green curve). The model furthermore allowed the derivation of vacuolar and cytoplasmic concentrations separately (Fig. 11a, red and blue curves, respectively). This revealed that for both compartments, a steady state situation was

assumed. The model estimates Cs^+ concentrations of 0.4 mM in the cytoplasm and of 8.2 mM in the vacuole at the plateau phase of accumulation. In case of the model for the mutant data, a strongly reduced vacuolar deposition, expressed by a significantly reduced τ was predicted (Tab. 9). The saturated concentration in the vacuole was 1.9 mM, while the cytoplasmic concentration was even slightly increased to 0.5 mM compared to the wild type (Fig. 11b).

The robustness of the model was further tested by developing different variants. One variant was created, in which the numerical volume correction, as indicated in Fig. 14, was not done for the test tube and the vacuole, but for the test tube and the cytoplasm[1]. The meaning of τ differs slightly, as it was redefined: $\frac{vacuolar\ concentration\ y}{cytoplasmatic\ concentration\ x}\frac{v3}{v2}=\frac{\tau}{1-\tau}$. This was derived as an expression of the changes in molar masses and not of concentrations like in the first model variant. Still, the model gave the similar fit for the kinetics, only with τ being slightly lower (for wild type, τ was 0.88 instead of 0.95 and for *sec22*Δ it was 0.55 instead of 0.77, respectively), while all other parameters differed only beyond the third decimal point. The outcome was identical: vacuolar sequestration was strongly inhibited in the mutant. For this equivalent model variant, additional tests were performed in order to analyse the meaning of the single model parameters.

Parameter/variable	Wild type	(95 % C I)	*sec22*Δ	(95 % CI)
k_1	30.4 /h	[25.2, 35.5]/h	21.2 /h	[18.8, 23.8]/h
k_2	2.4 /h	[1.78, 3.04]/h	1.76 /h	[1.46, 2.05]/h
k_1/k_2	15.0		12.0	
k_1+k_2	32.8 /h		23.0 /h	
τ	0.95	[0.94, 0.96]	0.77	[0.75, 0.80]
n	4.1	[3.21, 4.99]	7.6	[3.90, 11.40]
thresh	3.7 h	[3.38, 4.02] h	4.5 h	[4.26, 4.83] h

Table 9. Point estimates (model parameters after fitting) and univariate confidence intervals (95 %).
Confidence intervals (C.I.'s) were calculated according to Wald's asymptotic normal approximation (Hall et al., 2011). Model estimations for all time points, as well as the vacuolar and cytoplasmic distribution of Cs^+ inside yeast cells are represented in Fig. 12.

[1] The differential equations in this variant read: $c(t)=c_0-N\frac{v_2+v_3}{v_1}tot(t)$

$$x(t)=\frac{1-\tau_2}{1-(1-s(t))\tau}\frac{v_2+v_3}{v_2}tot(t)$$

$$y(t)=\frac{\varpi(t)}{1-(1-s(t))\tau}\frac{v_2+v_3}{v_3}tot(t).$$

C) Uncertainty analysis.

A graphical display of the uncertainty of the wild type model in comparison to the deviation of the experimental data is shown in Fig. 15. The variation for each model-predicted point builds a narrow framework for the experimental data. Together with the statistical analysis presented in 4.4.1 this emphasizes the uniqueness of the model solution.

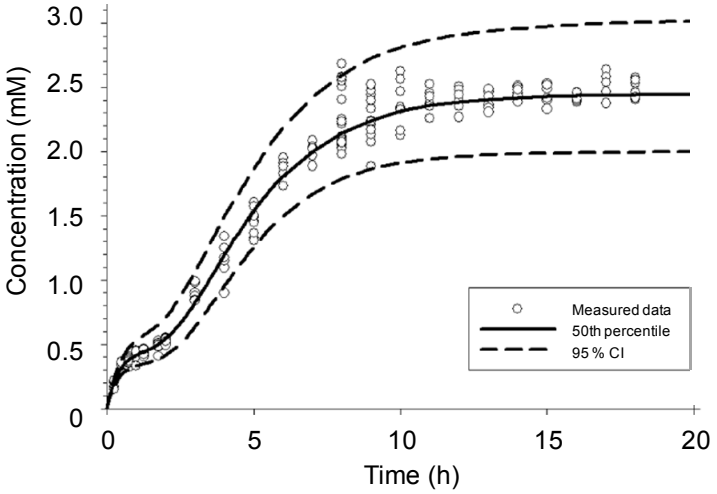

Figure 15. Uncertainty analysis for linear wild-type model prediction versus deviation in the measurement.
The values for 95 % confidence intervals are given in Tab. 9. CI = confidence interval. Only values for the total intracellular concentration *tot* of wild type are plotted.

The remaining questions were whether this unbiased solution for *sec22*Δ accumulation kinetics would be a) the only reasonable solution to the system, b) applicable also to a change in external concentration (e.g. in case of the 200 µM variation) and c) validated by experiments.

D) Uniqueness of the model solution.

To address the question whether the described solution was the only proper fit for the developed model, the wild-type model was used as a basis to a targeted change of single parameters. This artificial bias was exclusively used to get an estimation of single parameter influences on the model predictions and to determine whether these could possibly lead to the *sec22*Δ kinetics.

Single alterations in the parameters k_1, k_2, τ, n and *thresh* were tested. When k_1 is modified, the steady state phase is changed in altitude, as the equilibrium with the non-affected k_2 is reached at different concentrations. A reduction of k_1 to 1/3rd (~ 10 / h) would allow a similar steady state concentration as measured for *sec22*Δ kinetics, but the initial phase could never be adapted (regardless of changes in n or *thresh*). Furthermore, a slower accumulation was expected (plateau reached only at approximately 13 h), which was not true for the experimental dataset. A similar effect could be seen when k_2 was doubled (Fig. 16a). Changes in the plasma membrane fluxes alone could not manage to cause the mutant

kinetics in the model. Still, both fluxes are relevant components for the final intracellular Cs^+ concentration and are not only factors with influence on the time scale. Changing τ alone showed a direct influence on the altitude of the steady state phase, without influencing the initial phase. A reduction to 0.55 (from 0.88 in wild type) fits the mutant kinetics (Fig. 16b). Therefore, τ is able to alter the wild-type kinetics towards the *sec22*Δ situation. Modulation of *thresh* and *n*, expectedly, changed the timing and speed of permeating Cs^+ from the cytoplasm to the vacuole, as they influence the Hill function *s(t)*, but they could not change the altitude of the saturation (Fig. 16c). These tests show the strong influence that the activation of vacuolar deposition had on the shape of the accumulation trajectories, but exclude those factors as relevant for the mutant phenotype. This data proved that a situation as predicted by the model for *sec22*Δ can only be reached with a solution emphasizing the vacuolar deposition, e.g. via changing τ.

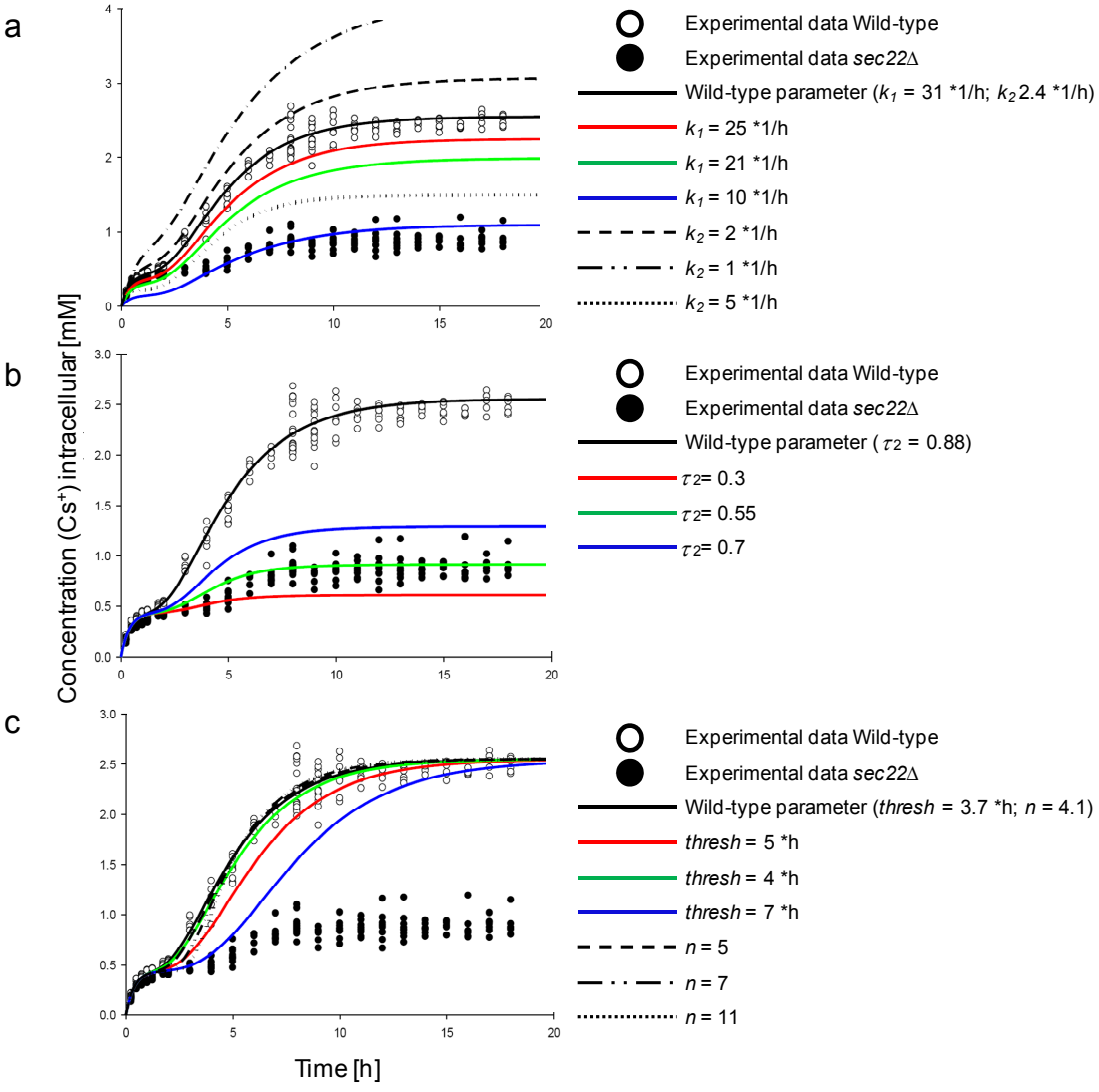

Figure 16. Variation of single parameters in the mathematical model for Cs^+ accumulation in yeast. See figure legend on next page.

Figure 16. Variation of single parameters in the mathematical model for Cs^+ accumulation in yeast.
All modifications were done on the background of the mathematical model described in 2.1.5. Wild-type parameter predictions are indicated in each case. Parameters k_1, k_2 (a), τ (b), *thresh* and *n* (c) were modified and the outcome for total intracellular concentration is displayed.

A different approach to estimate the influence of the single parameters is a sensitivity analysis of the model. **P**artial **r**ank **c**oefficient **c**orrelation (PRCC) was tested, in which the positive correlation (**p**artial **r**ank **c**oefficient (PRC) positive) or inverse correlation (PRC negative) of the parameters to the concentration in the cellular compartments were tested (Fig. 17) (Hamby, 1994; Iman and Conover, 1979; Iman and Davenport, 1982). A correlation coefficient of 1 (-1) stands for direct (indirect) proportional behavior. The outcome of this analysis was in accordance with a biochemical understanding of the compartment model. The cytoplasmic concentration of Cs^+ was direct proportional to those flow rates that increased the cytoplasmic mass of Cs^+ (k_1 and k_4), while k_2 and k_3 had indirect proportional influence on this trait (Fig. 17a). All parameters except k_1 and k_2 (i.e. cellular entry and efflux) tend to lose their influence once the steady state is approached. τ is proportional with the cytoplasmic concentration as long as no Cs^+ is loaded to the vacuole (according to the Hill function), but then becomes indirect proportional, since it increases with the deposition of Cs^+ to the vacuole at the expense of cytoplasmic Cs^+. For the vacuole, the strongest proportionality was found for k_3, followed by k_1, while τ behaved in the opposite manner as for the cytoplasm (Fig. 17b). The flow rates of both, cytoplasm to test tube and vacuole to cytoplasm, acted inversely proportional to the vacuolar concentration. Accordingly, all model parameters behaved in a biochemically reasonable way, which can be seen as a confirmation of the model predictions.

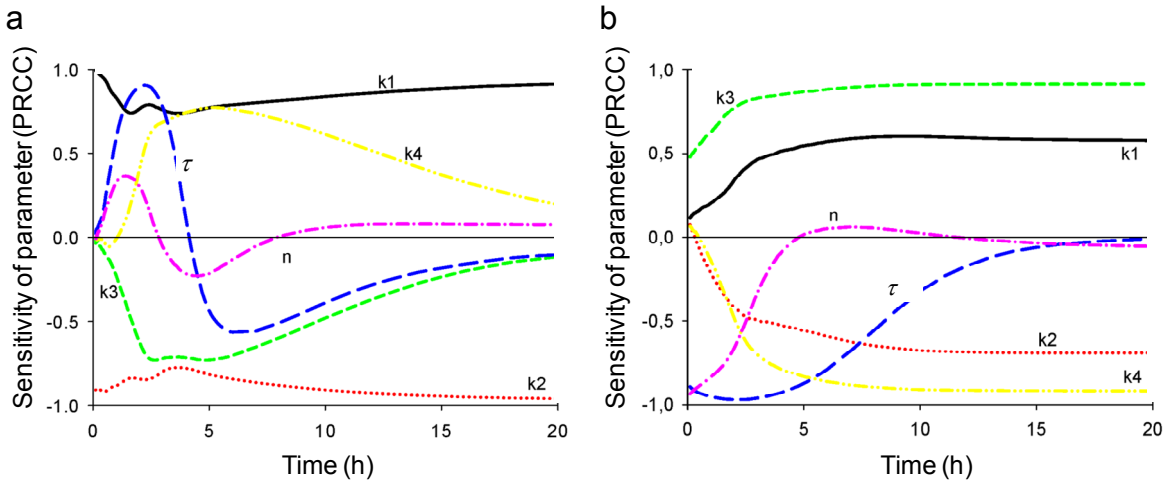

Figure 17. Sensitivity analysis for the model parameter's influence on the traits Cs^+ concentration in the cytoplasm (a) and in the vacuole (b).
PRCC analysis was done for the model described in 2.1.5. The different parameters are indicated. Sensitivity (y-axis) is shown as the RCC (rate correlation coefficient), ranging from 1 (= direct proportional to the trait) over 0 (no effect on the trait) to -1 (indirect proportional effect on the trait).

E) Michaelis Menten variation of k_1c allows predicting high- and low-affinity conditions at once.

In order to address the question regarding the use of the model when experimental setup parameters are changed, we used the data derived at the high-affinity conditions (50 µM) and added the data gained at higher external concentrations (200 µM, low-affinity conditions, *i.e.* experiment 2 in Tab. 8) at the same time. While predictions for the higher concentration alone gave well defined parameters with a similar outcome as the 50 µM condition (not shown) the linear model did not allow an exact prediction of both conditions in parallel. The saturation of fluxes in a system of Michaelis-Menten-kinetics-dependent transporters plays a greater role at higher concentrations. Due to the linear dependence of the fluxes, the model would predict an increase in external concentration to induce a proportional increase in intracellular concentration, which was not confirmed by the experiment. The total internal concentration only was risen 1.4 - and 2.2 - fold. This was probably due to the fact that at 200 µM external CsCl, the Michalis-Menten uptake kinetics should no longer be considered as linear, but dependent on the concentration (Rodriguez-Navarro, 2000; Rodriguez-Navarro and Ramos, 1984). The introduction of Michaelis-Menten terms was possible as a flux $k * c$ will be formulated as $\frac{\hat{k}c}{K_M + c}$. The rate constants and all parameters were labeled with a hat, e.g. $\hat{k}_1$, in order to distinguish the linear from the Michaelis-Menten principle. In case of the Michaelis-Menten conversion, $\hat{k}$ are not canonical rate constants but are equivalent with v_{max} (maximum speed of enzyme activity) of the according reaction. The most crucial change between the two modeling approaches was the change in external Cs^+ concentration, and so the flux to the cytoplasm (k_1c) was first modified to a Michaelis-Menten dependence. This mixed model development is described in Methods chapter 4.4.1. This measure already improved the fits of a joint model for both external conditions for wild type and *sec22*Δ (*Appendix F*). Yet, the modeling was further improved by successively substituting linear fluxes with Michaelis-Menten terms. Besides replacing k_1c, the variants k_1c plus k_3x, k_1c plus k_2x plus k_3x and all Michaelis-Menten were modeled and tested. The fit of both experimental conditions was successful. According to Akaike information criteria (AIC) and Bayesian information criteria (BIC), which indicate the reliability of a model compared to another model (Burnham et al., 2011), the additional substitution of k_3x lead to a considerable improvement of the model, while the infliction of k_2x and k_4y did not further improve the system (Tab. 10). According to literature, a small AIC/BIC value indicates a more reliable model (Burnham and Anderson, 2002; Burnham et al., 2011). The variation of the single parameters became bigger, as the number of estimated parameters was increased. Still, the conclusion of these mixed models was that by making the influx to the cytoplasm and towards the vacuole

concentration-dependent, changes in the external buffer concentration could be included in the model. The basic equations for the variant k_1c and k_3x replaced by Michaelis Menten terms read as follows:

$$c' = N\frac{v_2}{v_1}\left(-\frac{\hat{k}_1 c}{K_{M,1}+c}+\hat{k}_2 x\right)$$

$$x' = \frac{\hat{k}_1 c}{K_{M,1}+c}-\hat{k}_2 x-\frac{\hat{k}_3 s(t) x}{K_{M,3}+x}+\hat{k}_4 y$$

$$y' = \frac{v_2}{v_3}\left(\frac{\hat{k}_3 s(t) x}{K_{M,3}+x}-\hat{k}_4 y\right)$$

$$s(t) = t^n/(thresh^n + t^n).$$

Re-parametrisation was included as:

$$\hat{k}_3 = \hat{\Gamma}\,\hat{\tau}\,mM,$$
$$\hat{k}_4 = \hat{\Gamma}(1-\hat{\tau}),$$
$$\hat{\Gamma} = \hat{k}_3\,mM + \hat{k}_4.$$

The statistical analysis was done as described in 4.4.1. The result for the substitution of k_1c and k_3x regarding the difference between the wild type and the mutant situation was identical to the result of the linear model in that the flux to the vacuole was drastically reduced (Fig. 18; results are included in Fig. 12 as black / grey curves). This was expressed by a reduction in $\hat{k}_{M,3}$, which is equivalent with a decrease in deposition velocity. The delay at the early phase of uptake was still present. It is important to emphasize that such partial integration of Michaelis-Menten terms is problematic as the units of some parameters may differ. The model tried to correct for this incompleteness by partial re-definition of the according parameters. Refinement of the model equations and additional data input is necessary to make the system reliable for a Michaelis-Menten situation.

Reactions changed to Michaelis-Menten	k_1c	k_1c, k_3x	k_1c, k_2x, k_3x	k_1c, k_2x, k_3x, k_4y
AIC_{WT}	- 65.7	-504.9	-502.2	-489.3
BIC_{WT}	- 40.1	-475.7	-469.3	-452.8
AIC_{mut}	-500.3	-607.5	-605.0	-595.5
BIC_{mut}	-474.6	-578.2	-572.0	-555.1

Table 10. Model performance after transformation of individual fluxes into Michaelis-Menten terms. The AIC and BIC diagnostics did not take $\hat{\Gamma}$ into account, which has been interpreted as fixed and known. The Michaelis-Menten formulation of k_1c plus k_3x led to the lowest AIC/ BIC values indicating the most appropriate model (Burnham and Anderson, 2002).

Parameter		Wild type	95 % Confidence intervals	*sec22*Δ	95 % Confidence intervals
$\hat{k}_1$ (=v_{max})	[mM/h]	13.28	[10.38, 16.18]	15.57	[12.15, 19.00]
k_2	[1/h]	4.29	[3.50, 5.07]	4.18	[3.44, 4.92]
$\hat{\Gamma}$	[1/h]	1396	[-530000, 534000]	334	[-20600, 20700]
$K_{M,1}$	[mM]	0.23	[0.19, 0.28]	0.33	[0.26, 0.40]
$K_{M,3}$	[mM]	0.058	[0.04, 0.08]	0.59	[0.40, 0.79]
$\hat{\tau}$		0.91	[0.91, 0.93]	0.84	[0.82, 0.86]
n		3.01	[2.19, 3.82]	3.74	[0.59, 6.88]
thresh	[h]	4.51	[3.46, 5.56]	4.77	[0.69, 8.84]

Table 11. Estimated Parameters with optimal fit for the experimental data. Parameters calculated for the fit of the model with Michaelis-Menten kinetics replacing the linear terms k_1c and k_3x. Point estimates and univariate confidence intervals based on Wald's (linear) asymptotic method.

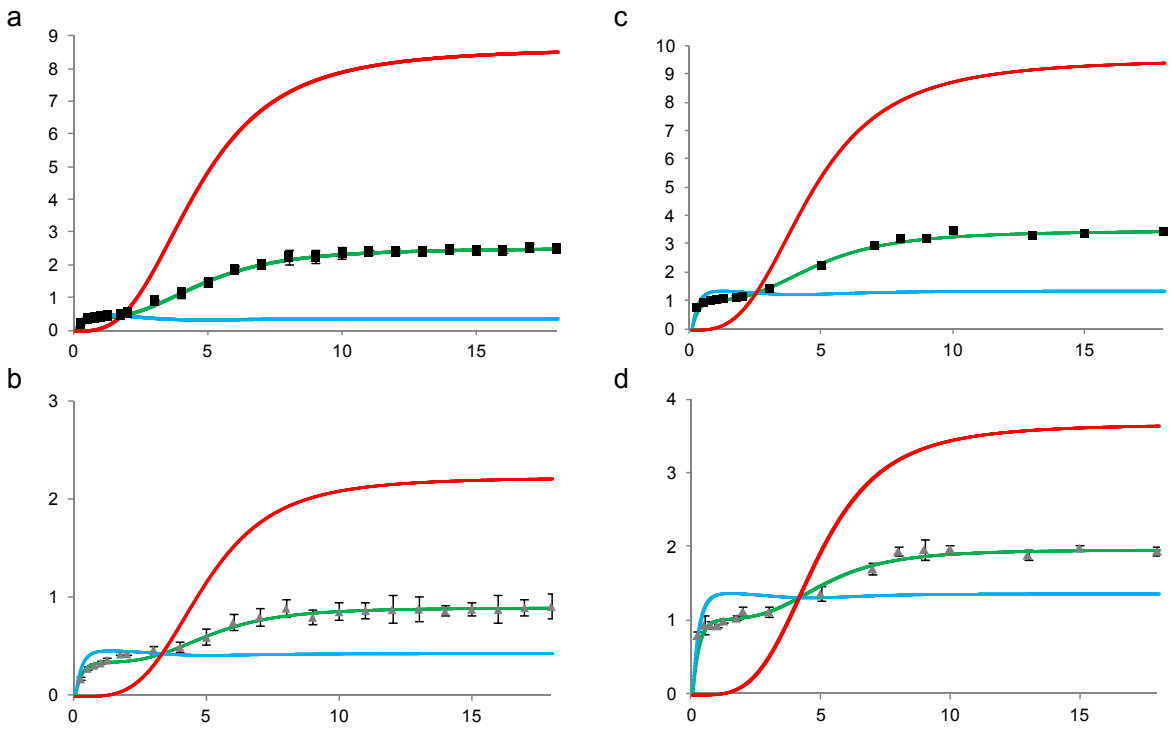

Figure 18. Cytoplasmic and vacuolar concentrations estimated from mathematical modeling after replacing the linear terms k_1 *c* and k_3 *x* by Michaelis-Menten terms.
Data from wild type (a, c) and from *sec22*Δ (b, d) at 50 µM (a, b) and 200 µM (c, d) external Cs^+. Total intracellular concentration (*tot'*) as measured (data points) and as fitted (green trajectory) are shown together with the cytoplasmic (blue) and vacuolar (red) concentration, respectively.

2.1.6 Validation of the mathematical model predictions: Vacuolar Cs^+ deposition is reduced in *sec22*Δ

The most significant alteration for *sec22*Δ against wild type in the mathematical model of the Cs^+ assay was a reduction in vacuolar compartmentalisation of Cs^+ (Tab. 9). To test the assumption Cs^+ laden cells (high-affinity assay conditions) were used to isolate vacuoles and determine the amount of ^{134}Cs tracer retained in this organelle. Density gradient centrifugation in combination with enzymatic tests of the isolated fractions was applied to obtain a pure isolate of intact yeast vacuoles. The standard conditions (buffer concentration 50 µM CsCl and a 4 kBq ^{134}Cs tracer amount) of the uptake experiments could be conserved. The purity and integrity of the expected vacuolar fraction (fraction 3 of the double density gradient centrifugation) were tested by a simultaneous activity analysis of α-mannosidase, a secretory system independent vacuolar membrane marker enzyme (Hutchins and Klionsky, 2001), and carboxypeptidase Y, a secretory system-dependent vacuolar lumen marker enzyme (Stevens et al., 1982). Negative control samples were run with each test (*Appendix G*). The results were balanced by tests for other compartment marker enzymes. No significant difference of α-mannosidase and carboxypeptidase Y activity was found for the wild-type and mutant fractions, pointing towards a generally functional vacuole, but also to a basic conservation of the secretory system, as suggested by literature (Liu and Barlowe, 2002) (Fig. 19). Carboxypeptidase Y activity was strongly reduced in fraction 3 compared to the spheroplast control, which may be due to a low stability of the enzyme. Since none of the enzymes for other cellular components showed specific activity in the vacuolar fraction (fraction 3), we expected no or a negligible contamination by other organelles.

Since α-mannosidase was found to be active exclusively in the vacuole, it was possible to equilibrate a similar amount of intact cells and isolated vacuoles via its activity (Yoshihisa and Anraku, 1990). Accordingly, α-mannosidase was used to adjust the quantity of isolated vacuoles in three biological replicates to a similar amount of intact cells by determining an equally α-mannosidase - active amount of cells. The ^{134}Cs activity could be measured γ-spectrometrically and the portion of Cs^+ deposited to the vacuole could be estimated (Tab. 12).

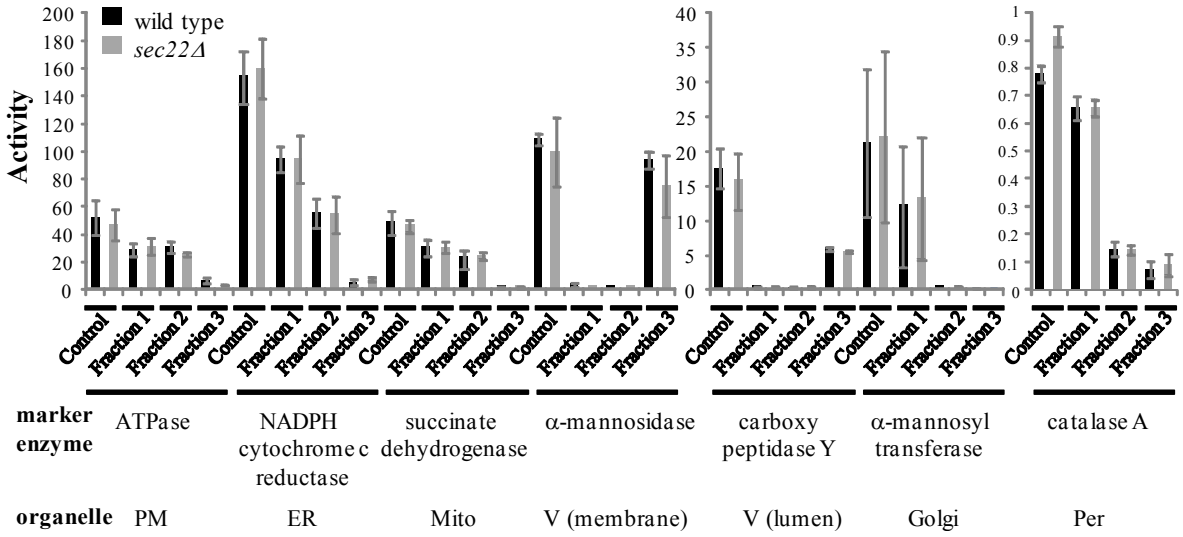

Figure 19. Enzyme activity of different isolated fractions of yeast.
Vacuoles from yeast cells were isolated by Ficoll density gradient centrifugation (see Methods) and the purity of the obtained *fraction 3* was analyzed using marker enzymes. In addition to *fraction 3* (floating material after the second gradient), the following steps were analyzed: *control* - unfractionated spheroblast, *fraction 1* - pellet of first gradient centrifugation and *fraction 2* - pellet of second gradient centrifugation. Marker enzymes and their respective compartment are indicated: PM - plasma membrane; ER - endoplasmic reticulum; Mito - mitochondria; V - vacuole; Golgi - Golgi apparatus; Per - peroxisomes). The activities are indicated in mu / ml in case of the PM, ER, Golgi, mitochondrial and vacuolar markers and by the ratio of reduced H_2O_2/ml for the peroxisomal marker. Mean activities of three independent isolations are shown.
Fraction 3 is enriched in both vacuolar markers, but depleted from all other marker enzymes. Importantly, the activities of vacuolar marker α-mannosidase and carboxypeptidase Y did not differ for wild type and *sec22Δ*. Activity of carboxypeptidase Y was reduced in *fraction 3* compared to the spheroplast control, which might be due to a lower stability of the enzyme under the experimental conditions. See also Appendix G for raw values and negative controls.

Tab. 12 compiles the activities of the isolated vacuolar fraction and the according activities in the cell lysate after normalizing the amount of cells according to the activities of the vacuolar fractions. Six ml of the total isolated fraction were used in each case and the intact cells (derived from the same colony) were diluted to meet the equal activity. The relations of the Cs^+ tracer found in the isolated fraction (vacuole) and in the amount of cells with equal mannosidase activity were calculated. In three repetitions, the vacuolar deposition in wild-type was approximately 80 %, which is in accordance with literature (Avery, 1995; Perkins and Gadd, 1993a). *sec*22Δ, on the other hand, compartmentalized only approximately 36 % of its total Cs^+ content to the vacuole. In direct comparison, a clear picture evolves showing that the low total concentration is mainly due to a reduced vacuolar deposition, while on the other hand the amount in the cytoplasmic part is at least as large as in wild type, or even slightly increased (Fig. 20). The intracellular mass distribution of the ion between wild type and *sec*22Δ is as follows: At 13 h the amount of Cs^+ for the wt was 81 amol, of which 63 amol was in the vacuole, leaving 18 amol in the non-vacuole (= cytoplasm) compartment. The total amount of Cs^+ in the mutant was 30 amol, with 11 amol in the vacuole and 19 amol in the cytoplasm.

Both, the wild type vacuolar compartmentalisation and the compromised deposition in *sec22*Δ are in good agreement with the predictions of the mathematical model.

Isolation	Tissue	α-mannosidase activity (mu / 6 ml)	^{134}Cs activity (CCPM / 6 ml)	^{134}Cs in fraction 3 (vacuoles) relative to whole cells (%)
		Wild-type		
1	Cell lysate	748	333	78.7
	Fraction 3	750	262	
2	Cell lysate	680	183	81.9
	Fraction 3	682	150	
3	Cell lysate	670	254	80.2
	Fraction 3	668	205	
		***sec22*Δ**		
1	Cell lysate	740	373	45.6
	Fraction 3	742	170	
2	Cell lysate	500	186	36
	Fraction 3	510	67	
3	Cell lysate	420	127	29.1
	Fraction 3	420	37	

Table 12. **Intracellular Cs^+ distribution, based on α-mannosidase activity in cell lysate and density gradient centrifugation – isolated vacuoles.**
α – Mannosidase activity was calculated for a fixed volume (6 ml) of the total isolated fractions, based on an activity determination in 500 µl of the isolated fraction and extrapolation to 6 ml. Cell lysates of non-fractionated cells having ~ similar enzyme activity were prepared. ^{134}Cs activity of the according samples was recorded and set in relation. Enzyme activity was measured in triplicate, only mean values are shown.

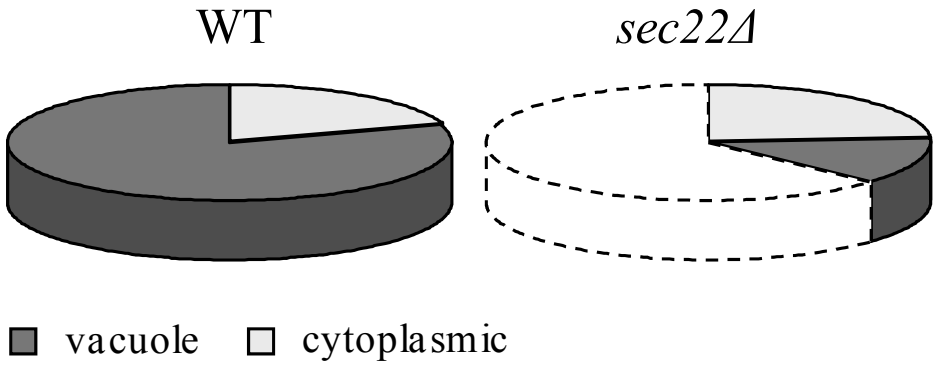

Figure 20. Vacuolar Cs^+ deposition in wild type and *sec22Δ* is changed.
Total Cs^+ uptake and vacuolar Cs^+ compartmentalisation were determined from whole cells after 13 h incubation in 50 µM radiolabelled Cs^+ assay buffer. Caesium amounts were related to equal activity of the vacuolar marker α-mannosidase. Wild type (81.3 +/- 2,3 amol / cell) shows a vacuolar deposition of approximately 63 amol/ cell (80 %, dark grey) leaving 18 amol/ cell (20 %, light grey) in the remaining cellular structures termed *cytoplasmic*. The mutant *sec22Δ* accumulated less than one half of Cs^+, which was distributed to 11 amol/ cell in the vacuole (13 % relative to total wild-type uptake) and to approximately 19 amol/ cell in the cytoplasm (24 %). The experiment was repeated three times.

2.1.7 Cs^+ in the external medium promotes vacuolar fragmentation in *sec22*Δ

The volumes of cells and the vacuoles they include are not different in the mutant (Figs. 4 and 14). Yet, *sec22*Δ exhibits a higher amount of cells containing multiple smaller vacuolar lobes in vital staining as compared to wild-type cells (denoting 3-5 smaller lobes as "fragmented", referring to Li and Kane (2009)). Under assay conditions roughly 25 % more vacuoles showed a fragmented phenotype (50 µM CsCl in the extracellular medium) (Fig. 21). The phenotype was not present when Cs^+ was excluded from the setup, while a slight, but not significant increase of fragmentation was found at further elevated extracellular Cs^+ concentration.

Vacuolar morphology is affected in the mutant, but only in the presence of CsCl at assay conditions, which also means lack of K^+. Thus, a destabilisation of the vacuole by the loss of Sec22p has to be considered, but only in combination with the Cs^+ accumulation behavior.

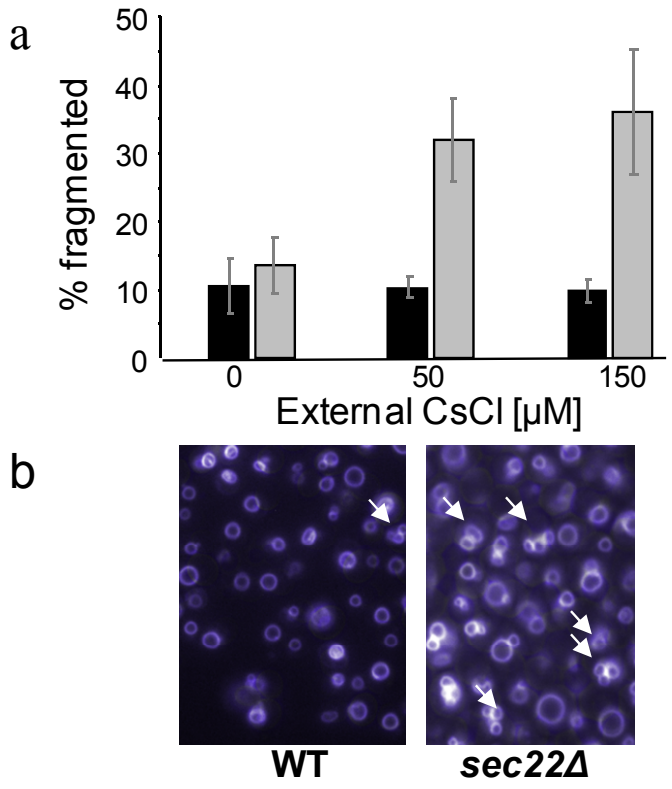

Figure 21. *sec22*Δ cells harbor more fragmented vacuoles in dependence of external Cs^+. Wild-type and mutant cells were analysed for fragmented vacuoles. (a) Relative quantification of fragmented vacuoles. In 3 independent microscopy sessions, 100 cells were inspected each time. The tests were done at three different concentrations of external CsCl (0, 50 and 150 µM). *sec22Δ* has a significantly higher percentage of fragmented vacuoles (32.0 ± 6.0 %) than WT (10.3 ± 1.5 %) under assay conditions (50 µM) (t-test against 0; $p \leq 0.001$). Absence of CsCl abolished this effect (*sec22Δ* 13.7 ± 4.0 %; WT 10.7 ± 4.2 %) while further elevated concentration of CsCl caused no additional increase in fragmentation (*sec22Δ* 36.0 ± 9.2 %; WT 10.0 ± 1.7 %). Representative pictures of wild-type and mutant cells with normal and fragmented vacuoles are shown (b). White arrows indicate typical fragmented vacuoles. Staining is presented as false-colour of 50 ms excited fluorescence recorded with a FM4-64 specific filter.

2.1.8 Cs^+ efflux at the plasma membrane is slightly affected in *sec22*Δ

Eukaryotic cells can reduce their content of potentially toxic ions by an efficient efflux, driven by a set of transporters or channels (Rodriguez-Navarro et al., 1981; Ariño et al., 2010). Changes in plasma membrane turnover of Cs^+ were not predicted to significantly influence the Cs^+ phenotype in the mathematical model (Tab. 9). Still, a possible contribution of such fluxes to the phenotype was tested experimentally. Cells were incubated for 13 h under standard Cs^+ tracer assay conditions, washed and then incubated further in medium containing the 50 µM external CsCl, but excluding the tracer. Thus, the steady state condition of the cells should be conserved, but no tracer could be re-loaded to the cells. Loss of intracellular tracer was recorded (*i.e.* the dilution of tracer by exchange with stable Cs^+ ions) as a means of describing efflux velocities. For 3 h after washing, vital staining revealed a stable viability of the cells, but later, cell death rate increased rapidly (Fig. 22). Therefore, the time up to 3 h after the washing procedure were used for calculating the overall change in intracellular Cs^+ concentration (defined as velocity of efflux = v_{effl}) as the derivation of the e-function that describes the regression at time point t = 0.

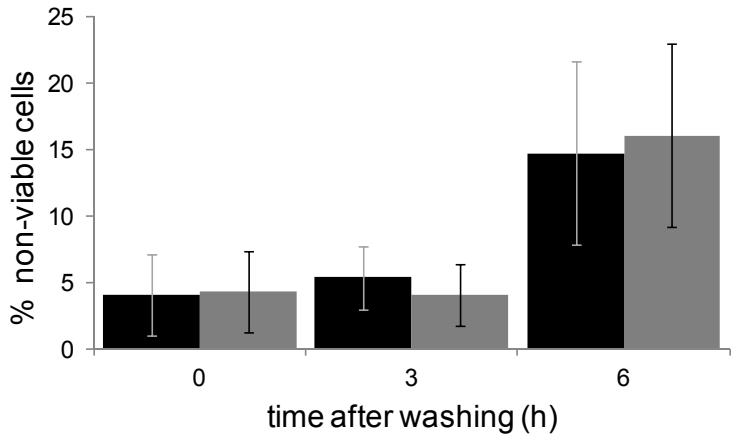

Figure 22. Viability test in yeast cells after the washing procedure for the efflux analyses. Three time points were tested, with 50 cells of both strains analysed. Black = wild type and grey = *sec22*Δ. Vital staining was used as viability marker. Mechanically disrupted cells were excluded from the counting.

An overall slow v_{effl} was found in this experiment (Fig. 23a, b) and the differences between wild type and the mutant regression were significant (p = 0.004; ANCOVA), but the difference in v_{effl} was low. The model has predicted a k_2 of 2.4 / h and 1.8 / h, respectively. The speed of efflux would then be *k2* * $concentration_{cytoplasm}$, in this case 0.96 mM / h and 0.90 mM / h, respectively. The model predictions are about 10 times higher than the comparable value of v_{effl} in the measurement (0.10 mM / h and 0.14 mM / h, respectively). The cells in the washout experiment hesitate to release Cs^+ tracer at steady state. Yet, since the experimentally determined v_{effl} was dependent exclusively on the designated 3 h time scale,

the values might differ in their meaning from the efflux at t = 13 of the Cs^+ accumulation model. Differences between the model and the experiment in this context also have to be considered in the experimental setup. The washing was done in cold buffer, which might have influenced the ion fluxes of a cell, since it was shown that Trk1p is less active below a temperature of 26 °C and might thus impact on the equilibrium of influx and efflux at the plasma membrane (Rodriguez-Navarro and Ramos, 1984). Additionally, starved cells might be stressed by minor changes in external conditions, which could not be implied in the model. Nevertheless, we may state that the overall plasma membrane fluxes are similar for the *sec22Δ* phenotype, which again is in consistence with the model prediction. Raw data of the efflux experiment is given in *Appendix H*.

a

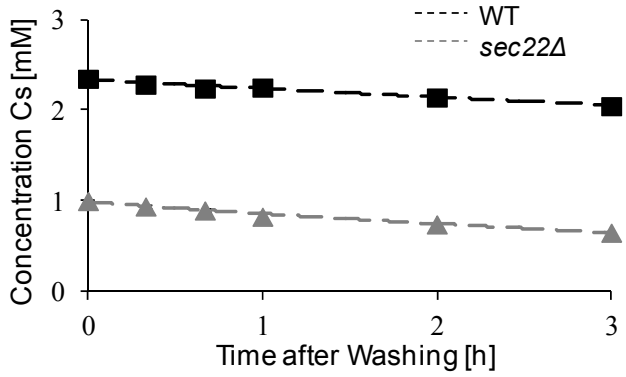

b

WT	
Exponential regression (0 – 3 h after washing)	$c(t) = 2.33*e^{(-0.043*t)}$
Differentiation	$c'(t) = v_{effl} = -0{,}043*2.33*e^{(-0{,}043*t)}$
c[Cs] (t=0) [mM]	2.33
c_{cyt}[Cs] (t=0) [mM] (calc.)	0.45
v_{effl}(t=0) [mM/h]	**0.10**

sec22Δ	
Exponential regression (0 – 3 h after washing)	$c(t) = 0.98*e^{(-0.14*t)}$
Differentiation	$c'(t) = v_{effl} = -0{,}14*0.98*e^{(-0{,}14*t)}$
c[Cs] (t=0) [mM]	0.98
c_{cyt}[Cs] (t=0) [mM] (calc.)	0.61
v_{effl}(t=0) [mM/h]	**0.14**

Figure 23. Tracer efflux kinetics of Cs^+ laden yeast reveal only minor changes in efflux.
Tracer-incubated wild-type (WT) and *sec22Δ* cells were depleted of external tracer, while conserving the concentration of 50 µM external CsCl. Activity was analysed up to 6 hours after washing (a). Data up to 3 h after washing, during which vitality of the cells was not impaired, was considered for calculation. To determine the change of concentration with time (v_{effl}), exponential regression was used (b). The total and cytoplasmic Cs^+ concentrations (the latter one calculated according to the investigated intracellular distribution in the strains), as well as v_{effl} are shown. v_{effl} of wild type versus *sec22Δ* were calculated from the derivation of exponential regression functions fitting the kinetics ($R^2 \geq 0.9$). The slopes of the regression curves are significantly different (ANCOVA: $p \leq 0.004$).

A similar experiment was done, in which the cells were washed and further incubated in assay buffer without any CsCl present. The low speed of efflux was nearly equal to those recorded in the described efflux experiment (v_{effl}(wild type) = 0.9 mM / h; v_{effl}(*sec22Δ*) = 0.9 mM / h).

No significant difference was found between wild type and the mutant. Vital staining was not tested under these conditions. To get a more precise estimation of efflux velocities, the experimental system needs to be refined, e.g. by using pre-warmed buffer during the washing process.

2.2 pH sensitivity of *sec22*Δ is lower than that of V-ATPase loss-of-function mutants

As shown in Fig. 3, a diversity of V-ATPase loss-of-function mutants (compiled as "vacuolar organization") had a tendency to cause reduced Cs^+ accumulation. The connection between Sec22p and Vma22p, a component of the V-ATPase assembly, which also appeared in the screen, was of special interest, since co-response data has proposed a possible functional bond between those gene products (The *S. cerevisiae* co-response database, CSB.DB, MPI, Golm) (Steinhauser et al., 2004). This was supported by the ER localization of Vma22p, similar to Sec22p, which may point toward an interaction between the proteins (Tomashek et al., 1997). However, loss of the V-ATPase function (via mutation of subunits or assembly associated proteins) causes a strict pH sensitive phenotype due to the disturbance of the vacuolar proton gradient (Hill and Stevens, 1995; Nelson and Nelson, 1990). Thus, *sec22*Δ was tested for pH sensitivity (Fig. 24). It shows that *sec22*Δ is compromised by an increase in pH ≥ 8 when compared to wild type or the complemented strain. Still, the sensitivity of V-ATPase mutants (*vma22*Δ and the V-ATPase subunit b mutant *vma2*Δ) was higher.

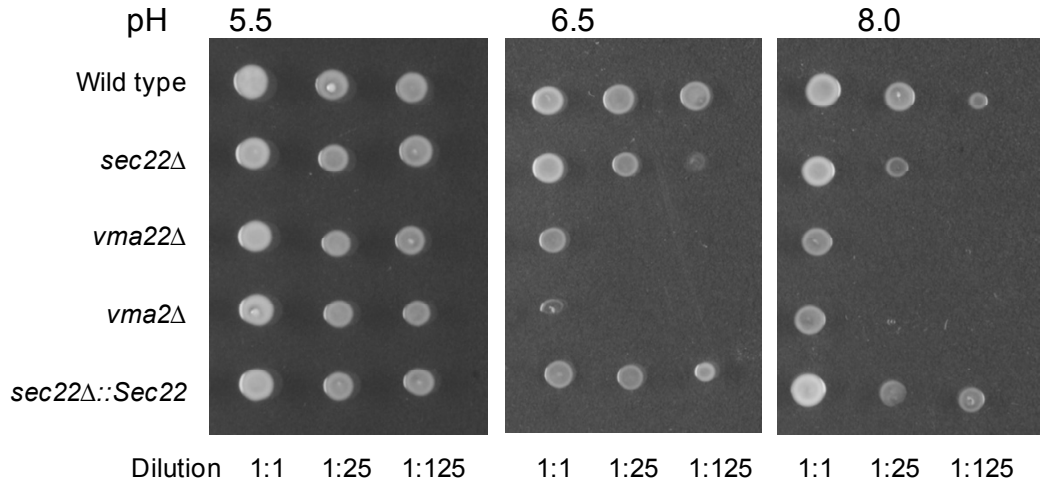

Figure 24. pH sensitivity analysis of yeast strains on YPAD plates
In order to compare *sec22*Δ with the pH sensitive V-ATPase mutants, which also had shown Cs^+ accumulation reduction (Heuck et al., 2010), a pH sensitivity test was applied. Yeast strains (wild type, *sec22*Δ, *vma22*Δ, *vma2*Δ (Liu et al., 1996) and *sec22*Δ*::Sec22* (complemented *sec22*Δ)) were grown overnight +/- Kan containing liquid YPAD media (120 rpm, 30 °C) to OD_{600} = 0.8 – 1.0. A dilution series was prepared and 3 µl drops were pipetted on YPAD plates (pH 5.5). Afterwards, the yeast was replica-plated on plates buffered to different pH (pH 5.5, buffered with 20 mM MES; pH 6.5, buffered with 20 mM MES; pH 8, buffered with 150 mM HEPES). NaOH was used for titrating the correct pH.

2.3 The *Arabidopsis thaliana* orthologue of Sec22p specifically affects the Cs^+ accumulation

2.3.1 The homozygous insertion mutant line *A. thaliana sec22-3* shows tissue specific expression

The model plant *A. thaliana* encodes a protein with 36 % identity to yeast Sec22p, termed SEC22 (Fig. 6). To investigate whether the yeast phenotype accounts for multi-cellular organisms a T-DNA insertion mutant in *A. thaliana* was analysed. In contrast to its *S. cerevisiae* ortholog, A. thaliana SEC22 is essential due to its implication in gametophyte development of the reproductive tissue (El-Kasmi et al., 2011). Still, a homozygous insertion containing line was rescued (*sec22-3* = SALK_042619) (Fig. 25) and tested by RT-PCR (Fig. 26a, b). The insertion of SALK_042619 is positioned in the 5' UTR of *A. thaliana SEC22* (Fig. 26a), disrupting the genomic integrity in an intronic region of an untranslated exon. *SEC22* expression showed a characteristic pattern in this line (Fig. 26b). The *SEC22* transcript was present in flowers, seedlings and young tissue, but was lost in leaf, stem and root. A complementation line was produced (*sec22-3::SEC22*), expressing the gene under control of its native promoter (Fig. 27).

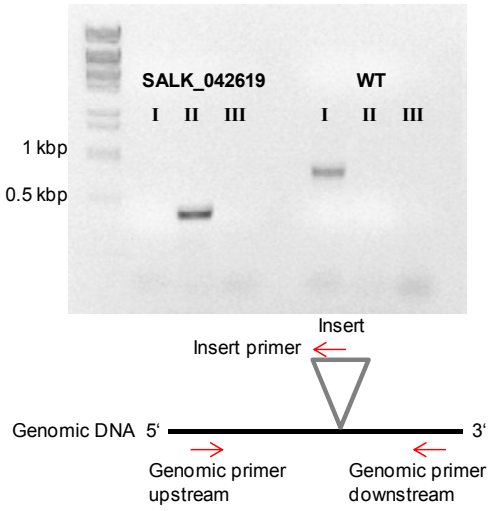

Figure 25. SALK insertion line test.
Confirmation of the homozygous T-DNA insertion in *A. thaliana sec22-3*. Primer combination I: primers on genomic sequence flanking the putative insert in wild type (802 bp fragment); II: Insert-specific primer plus genomic primer downstream of insert (462 bp fragment); III: Insert-specific primer plus genomic primer upstream of insert (150 bp fragment). The expected insertion yields an amplicon in combination II, while wild type should give an amplicon only in combination I. Hemizygous lines would give an amplicon for combinations I + II. 1kb DNA length marker (NEB) was used.

2.3.2 *A. thaliana sec22-3* has a specifically reduced Cs^+ content in leaf and in root

The phenotype of the mutant line was a mirror of the yeast mutant in that approximately 50 % less Cs^+ accumulated in rosette leaves and a reduction by one third in roots (Fig. 28, Raw data: *Appendices I - K*). These results were obtained after 10 days incubation with ^{134}Cs tracer of 10 day old plants grown in rich hydroponic growth medium. Complementation with *A. thaliana SEC22* under its native promoter suppressed the phenotype. Similar to the yeast experiments, the content of essential ions as well as Rb^+ were analysed. None of the other ions showed significant alterations.

a

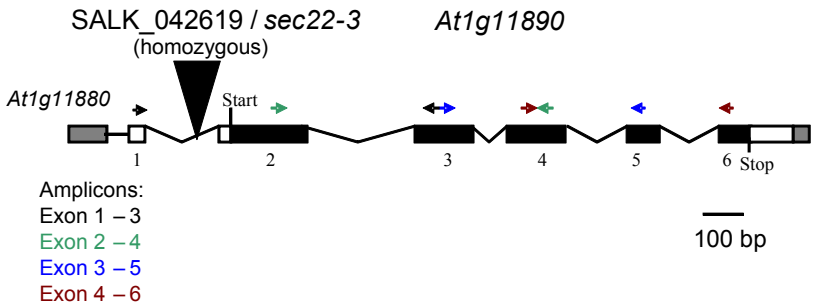

b

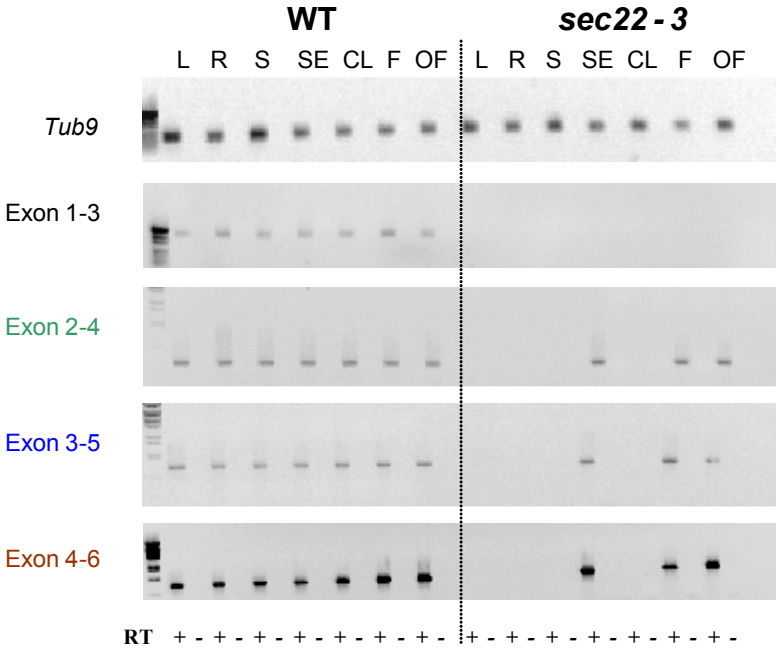

c

	L	R	S	SE	F	OF
Genevestigator (WT)	+	+	+	+	+	+
WT (this work)	+	+	+	+	+	+
sec22-3	-	-	-	+	+	+

Figure 26. Expression analysis of SALK_042619 reveals cryptic expression in young and reproductive tissues in *sec22-3*.
The expression pattern of a homozygous T-DNA insertion line SALK_042619 (*sec22-3*) was analysed. The genomic structure of *At1g11890* is schematically drawn, including the position of the T-DNA insertion (a). Primer combinations for the expression analysis shown in (b) are highlighted as arrows. Exons are labelled with numbers. Primer combinations use these numbers and follow the indicated colour code. Following tissues were analysed by RT-PCR: mature leaf (L), mature root (R), mature stem (S), seedling (1 week after sawing) (SE), cauline leaf (CL), flower stage 7-9 (F, Smyth et al., 1990) and open flower (OF, stage 14, with silique in early stage). All primer combinations were tested +/- Reverse Transcriptase. SE, F and OF growth stages showed expression in the homozygous mutant background. (c) Summary of the expression pattern of *SEC22*, as given by Genevestigator database for WT (NEBION / ETH Zürich) and WT in the course of this work - which is consistent with the database, compared to that found for homozygous SALK_042619 in this study, is shown. + = expression detected.

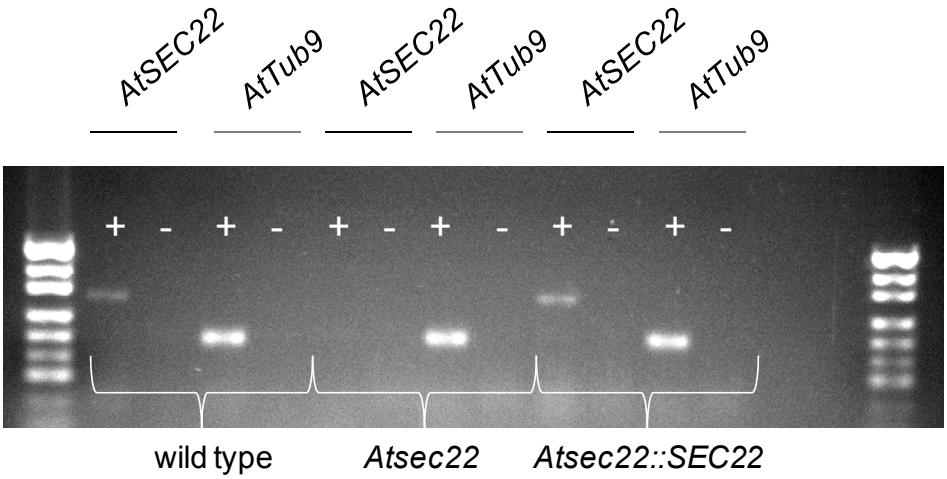

Figure 27. RT-PCR result for leaf material of *sec22-3* and the complemented plant line *sec22-3: SEC22*. Even lanes are – RT. Lanes 1, 2, 5, 6 and 9, 10 are *A. thaliana SEC22* amplicons. Lanes 3, 4, 7, 8, 11 and 12 are *Tub9* amplicons (positive control). Lanes 1-4 are material of wild-type *A. thaliana* Col-0, 5-8 are from *sec22-3* and 9-12 represent material from the complemented line. Fragment sizes were as expected. Size marker: pUC19 (Fermentas).

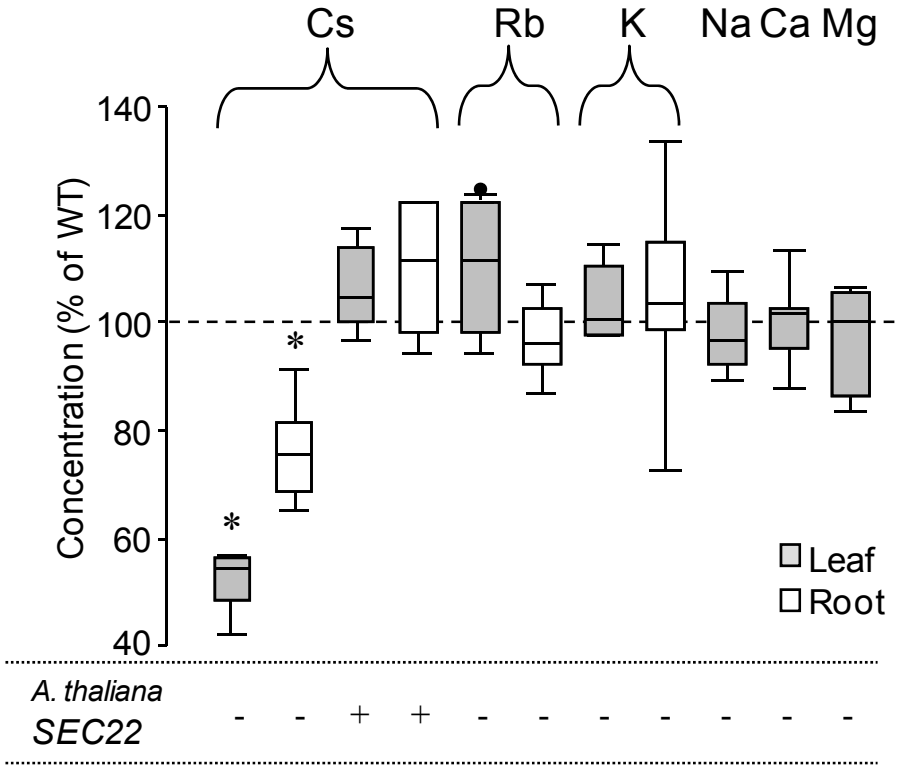

Figure 28. Cation phenotype of *A. thaliana* insertion mutant *sec22-3*.
Boxplot presentation of cation concentrations as relative values compared to the wild-type Col-0 plants. Cs^+ and Rb^+ were analysed in tracer uptake experiments and therefore account to fresh weight, while mass spectrometrical analysis of K^+, Na^+, Ca^{2+} and Mg^{2+} refers to dry weight. One hundred % correspond to: 107.0 ± 8.2 nmol Cs^+/g shoot; 42.5 ± 6.6 nmol Cs^+/g root; 157.8 ± 7.7 nmol Rb^+/g shoot; 52.8 ± 7.4 nmol Rb^+/g root; 1.3 ± 0.4 mmol K^+/g shoot; 0.62 mmol ± 0.08 mmol K^+/g root; K^+/g root; 0.2 ± 0.003 mmol Na^+/g shoot; 0.15 ± 0.01 mmol Ca^{2+}/g shoot; 0.3 ± 0.01 mmol Mg^{2+}/g shoot; The ratio of dry weight / fresh weight (wild type) = 12.1 ± 1.8 and dry weight / fresh weight (*sec22-3*) = 11.6 ± 2.2 (n = 6) was not significantly different in the plant lines.* = significantly different from WT; n ≥ 5; T-test against 0; p ≤ 0,001. The expression of *A. thaliana SEC22* is indicated as + (complemented line) or – (mutant). Outliers are shown as black dots.

2.3.3 *A. thaliana sec22-3* is fully viable

It was essential to test, whether plant growth and propagation was affected in the mutant, since it was shown that a loss-of-function of *A. thaliana SEC22* in reproductive tissue of *A. thaliana* caused strong defects in gametophyte development (El-Kasmi et al., 2011). Visual inspection of the growth (Fig. 29) and recorded germination rates and fresh weight showed no significant differences in the mutant. Fertility was not quantified explicitely, but the plants yield an approximately normal amount of fertile seed.

a

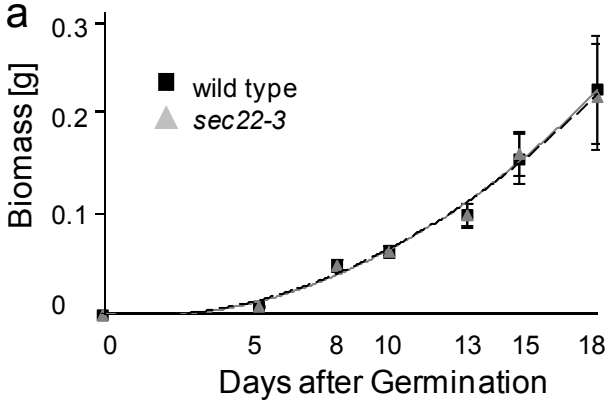

Germination rate	Soil	Hydroponics
wild type	86% 2%	100%
sec22-3	88% 2%	95% 1.5%

b

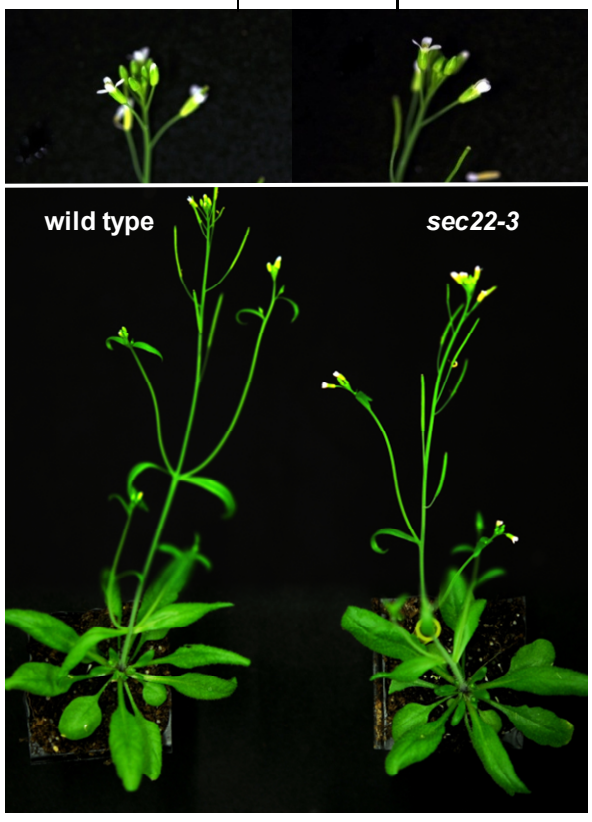

Figure 29. Growth comparison of *A. thaliana* wild type and *sec22-3* does not reveal developmental defects in the mutant.
Wild type (WT) and *sec22-3* were grown on soil or in a hydroponic system. (a) Development of wild type and *sec22-3* was quantified in two different ways: 1. Biomass was determined as fresh weight n ≥ 15. Samples were derived from hydroponic systems with WT and *sec22-3* growing inside the same boxes to ensure equal conditions. grey = *sec22-3*, black = wild type. Regression fits are nearly overlaying. No difference in the biomass and development was found. Germination rates were determined on soil as well as in hydroponic systems, n ≥ 20 (b) Visual inspection of the mutant did not reveal obvious developmental defects in soil grown plants.

2.3.4 *A. thaliana Sec22* is able to functionally substitute for yeast *sec22*Δ

To assess the equivalence in the mutant phenotypes of yeast and plant, the open reading frame of *A. thaliana Sec22* was cloned inside a doxycycline – repressible vector construct. The plant gene was expressed in the yeast mutant background and doxycycline suppressed the expression (Fig. 7). In the Cs^+ uptake experiment, the transformed strain was reaching approximately 85 % of the wild-type level, whereas doxycycline treated cells again showed the reduced Cs^+ phenotype (Fig. 9c). A function of the gene products of both organisms was conserved. Raw data is included in *Appendix A*.

3 DISCUSSION

3.1 Loss of yeast Sec22p causes a defect in vacuolar Cs^+-, but not K^+-deposition

The non-essential alkali ion Cs^+ can be assimilated by organisms like plants due to its similarity to K^+, which also causes the accumulation of radiocaesium in the food chain (White et al., 2010). Attempts to manipulate radiocaesium accumulation in plants are difficult, as long as no process with Cs^+ selectivity is identified (Hampton et al., 2004; Payne et al., 2004; White et al., 2010; Zhu and Smolders, 2000). Still, the fact that Cs^+ differs from K^+ (and Rb^+) in the toxicity for diverse eukaryotes indicated that some distinction must be present intracellularly, based on the incapeability of cells to adapt to Cs^+ as a K^+ substitute (Avery, 1995; Camacho and Rodriguez-Navarro, 1981; Ghosh et al., 1991; Hampton et al., 2004; Perkins and Gadd, 1993a). In this study the yeast *sec22*Δ mutant is shown to specifically discriminate against Cs^+, while retaining other ions including K^+ at wild-type levels (Fig. 9). This discrimination was correlated with a reduced vacuolar deposition of Cs^+ (Fig. 20). Thereby a new function of Sec22p was described in maintaining non-selective ion deposition to the vacuole of yeast cells.

The intracellular concentration of K^+, however, was not altered in *sec22*Δ under the tracer assay conditions (Fig. 8). This data was supported by measurements done in cells grown in full nutrient media (Tab. 6). K^+ homeostasis in yeast species depends on a strict regulation of an intracellular concentration ranging between 200 – 300 mM (Ariño et al., 2010), an optimum that can only be maintained when a cytoplasm-to-vacuole ratio of up to 1:4 can be conserved, since the vacuole is the main storage compartment for K^+ (Avery, 1995; Okorokov et al., 1980). Intracellular concentrations of approximately 240 mM K^+ were found in the experiment (Tab. 6). Considering the microscopically determined cytoplasmic and vacuolar volumes (25 fl and 8.8 fl, respectively) and assuming a vacuolar compartmentalisation of K^+ of approximately 80 % (this would be the case if K^+ is deposited to the vacuole in a similar amount as Cs^+, considering the results shown in Fig. 20), a vacuolar K^+ concentration of approximately 690 mM and a cytoplasmic concentration of 60 – 100 mM is expected for wild type. If K^+ deposition or storage to the vacuole was reduced in *sec22*Δ to the same extent as Cs^+, e.g. to 40 % of wild type, this would decrease the total intracellular concentration to 130 mM K^+, but the concentration in *sec22*Δ was found to be ≥ 200 mM (Tab. 6). Additionally, *sec22*Δ cells grow in an inconspicuous manner, which was highly unlikely if the K^+ concentration was disturbed to such a degree. Therefore, it can be excluded that K^+ storage in the vacuole was affected. Consequentially, the discrimination between Cs^+ and K^+ in *sec22*Δ must be achieved already at the vacuolar membrane. This discrimination is correlated with a lower total Cs^+ concentration at the steady state (Fig. 11),

showing that an effective reduction of the amount of Cs^+ in fully viable cells could be achieved.

A diversity of experiments indicated a generally intact vacuole in *sec22*Δ. The vacuolar volume was not different from wild type (Fig. 4) and the vacuolar membrane and lumen marker enzymes α-mannosidase and carboxypeptidase Y were active in isolated vacuolar fractions similar to the control (Fig. 19). As the function of the vacuole is dependent on the maintenance of the vacuolar pH, which is essential for cell viability at changing growth conditions (Nelson and Nelson, 1990), a pH sensitivity test was analysed. It showed only a slight increase in sensitivity, which was distinct from the phenotype of mutants known to truly affect the vacuolar pH (Fig. 24). *sec22*Δ vacuoles had a tendency of appearing more fragmented than wild-type vacuoles (Fig. 21), but this was dependent on the presence of Cs^+ and may therefore be an attempt of the cell to enhance the defective Cs^+ deposition by increasing the vacuolar membrane-to-volume ratio. It was reported before that *sec22*Δ has an increased sensitivity towards some toxic, cationic treatments like hygromycin B, which depend on a functional vacuolar detoxification and an intact membrane potential (Baretto et al., 2011; Zhou et al., 2009) A slightly increased sensitivity of *sec22*Δ against Cs^+ and Li^+, another toxic alkali ion which depends on vacuolar deposition (Dichtl et al., 1997), was found in the experiments (Fig. 9). This may be interpreted as a disturbance in the detoxification of toxic cationic elements in the cytoplasm of *sec22*Δ and does not necessarily affect the essential K^+ (and the non-toxic Rb^+).

A T-DNA insertion mutant of the model plant *A. thaliana* showed a phenocopy of the yeast *sec22*Δ Cs^+ specific behavior (Fig. 28). The conservation of Sec22p's function in the context of Cs^+ accumulation was supported by the finding that the plant gene was able to substitute for the yeast *sec22*Δ in re-establishing wild-type uptake (Fig. 8c). The measurements in the plant were done in a developmentally controlled mutant that still showed expression in vegetative tissues (Fig. 26) and that could grow and develop without constraints (Fig. 29). Thus, whatever mechanism is responsible for inducing the Cs^+ / K^+ discrimination in the yeast mutant must be translatable into the plant system.

3.2 The cellular functions of Sec22p are diverse

Sec22p/SEC22 is essential for the compartmentalisation and for the accumulation of Cs^+ in the wild type, since its loss-of-function led to a specifically reduced Cs^+ uptake in yeast and *Arabidopsis*. However, it was not shown to use ions as a substrate or to interact with ion permeating proteins. It is surprising that the loss of this protein causes the induction of ion discrimination at the vacuolar membrane. Considering that there is no known single protein, e.g. an ion transporter, that exclusively utilizes Cs^+ as a substrate, a change in the

expression or translation of proteins could not cause a Cs^+ selectivity in *sec22*Δ. Instead, the lack of Sec22p may influence the specificity of already present systems of the ion homeostasis, either by altering their protein structure, their subunit composition (both may affect the selectivity of the ion pore) (Doyle et al., 1998; Noskov et al., 2004) or by changing the working conditions for ion transporters (e.g. by changing their localization or the pH / ion gradient) (Haro and Rodriguez-Navarro, 2002; Rodriguez-Navarro and Ramos, 1984).

Yeast Sec22p has been implicated in diverse aspects of protein targeting and modification, which is summed up in Fig.30. Sec22p's N-terminal Longin domain (Fig. 5), which is considered as regulatory element (Filippini et al., 2001; Mancias and Goldberg, 2007) may be the site of posttranslational modification by palmitoylation (Dietrich et al., 2004; Dietrich et al., 2005). In the ER - Golgi interface Sec22p mediates both, anterograde and retrograde vesicle transport to maintain early protein sorting and protein secretion (Fig. 30, A) (Burri et al., 2003; Liu and Barlowe, 2002). Sec22p's function in this regard is redundant, as the SNARE Ykt6p was found to substitute for the lack of Sec22p. In agreement with this, carboxypeptidase Y activity, which is dependent on a functional early protein sorting (Stevens et al., 1982), was similar in wild type and *sec22*Δ (Fig. 19). Loss of protein sorting *per se* cannot be responsible for the Cs^+ phenotype due to this redundancy. In plants, a similar function in transport of ER derived vesicles towards the Golgi apparatus was described (Chatre et al., 2005). Nevertheless, in *A. thaliana* this function was not substituted by Ykt6p homologous proteins in reproductive and young plant tissue and therefore remained essential (El-Kasmi et al., 2011).

Yeast Sec22p was found to have partial cargo and targeting specificity for the cation transporter Trk1p, which is known for its importance for K^+ and Cs^+ uptake (Avery, 1995; Fell et al., 2011) (Fig. 30, B). This represents a specialization of the protein sorting function and may be non-redundant in opposite to the general vesicle transport. Correct targeting of proteins or regulatory subunits from the ion homeostasis might therefore be a possible function affected when Sec22p is lost.

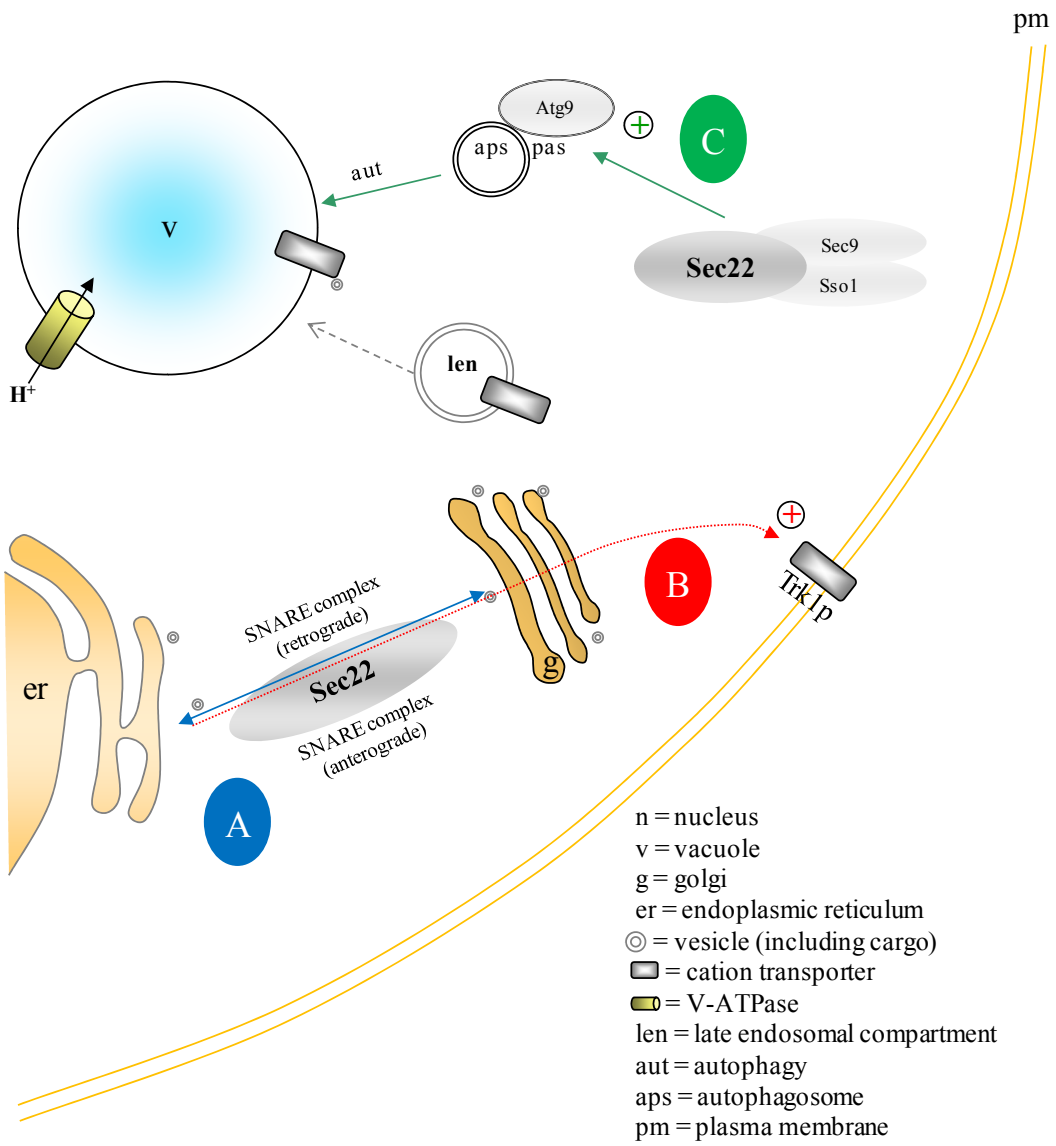

Figure 30. Described functions of Sec22p in *S. cerevisiae*.
Three schematically depicted functions are described that include Sec22p, A) the non-cargo selective, but redundant early proteins sorting between the ER and the Golgi apparatus (blue arrow) (Liu and Barlowe, 2002); B) cargo-selective and only partially redundant protein sorting of Trk1p to the plasma membrane (red arrow) (Fell et al., 2011); C) a co-localization-indicated interaction of Sec22p with two components of the autophagy machinery (Sec9 and Sso1), which are essential to conserve a regular autophagy of the Atg9 pathway (green arrows) (Nair et al., 2011). The late endosomal compartment (len) is indicated, since it is targeting to the vacuole, but can also take up ions itself, but that was not yet shown to involve Sec22p. The membrane potential and pH gradient of the vacuole is maintained via the V-ATPase.

A different, non-redundant function was recently described, as Sec22p turned out to be essential for a specific autophagy pathway, during which it co-localizes with two autophagy-related proteins, Sso1 and Sec9 to enable a normal *Atg9*-driven autophagy (Fig. 30, C) (Nair et al., 2011). These findings proved that the functional identity of Sec22p was diverse and that it might be active at the cell periphery. However, for the explanation of the Cs^+ phenotype of *sec22*Δ autophagy may be of little importance, since on the one hand there was no further indication that any component of the autophagy had an effect on Cs^+

accumulation (Heuck et al., 2010) and on the other hand there are no hints that Sec22p homologous proteins were involved in autophagy pathways of the plant (Bassham, 2007). The importance of autophagy related pathways for the Cs^+ specificity could be analysed using drugs that specifically abolish either the complete autophagy or special autophagy pathways (e.g. 3-methyladenine) (Seglen and Gordon, 1982). Additionally, rapamycin treatment of yeast cells, which is known to induce autophagy, may be tested for an effect on Cs^+ accumulation (Noda and Ohsumi, 1998).

The described functions of Sec22p do not offer an explanation for the observed phenotype, but there are indications for additional functions of this proteins, which may affect the non-selective ion transport to the vacuole.

3.3 Sec22p maintains non-selective vacuolar Cs^+ deposition – hypothetical explanations

High- and low throughput interaction studies, in combination with the already introduced yeast Cs^+ accumulation mutant screen by Heuck and co-workers (2010), have pointed to a link between Sec22p and the vacuole. Vma22p (*i.e.* Yhr060w) was found to be transcriptionally co-responsive with Sec22p and its mutant has shown a reduced Cs^+ accumulation in the screen (Heuck et al., 2010; Steinhauser et al., 2004) (Tab. 5). This putative functional correlation was further substantiated by the fact that the V-ATPase assembly protein Vma22p was localized to the ER, just like Sec22p (Hill and Stevens, 1995). The pH of the vacuole and the membrane potential are created and maintained by the action of the V-ATPase in pre-vacuolar compartments and the vacuolar membrane (Nelson and Nelson, 1990). Loss of Vma22p abolishes the V-ATPase assembly and thereby its function, causing a disturbance in the acidification of the vacuole (Graham et al., 1998) (Fig. 31a). The acidification state of the surrounding of ion transport proteins can affect their selectivity (Rodriguez-Navarro and Ramos, 1984), and thus, a disturbance of V-ATPase activity in *sec22*Δ may indirectly alter the selectivity of ion transporters in the vacuolar membrane. However, reduced acidification of the vacuole makes cells sensitive against neutral and alkaline external pH and causes pleiotropic effects, e.g. by a defective K^+ storage (Nelson and Nelson, 1990). Pleiotropic effects were not found for *sec22*Δ and a pH sensitivity test of *sec22*Δ showed that the SNARE mutant was more tolerant against changes in pH compared to two V-ATPase mutants (*vma22*Δ and *vma2*Δ, which is a mutant of the essential subunit b of the V-ATPase) (Fig. 24). Thus, a considerable reduction of V-ATPase function is not expected for *sec22*Δ and the Cs^+ phenotype of *sec22*Δ is not correlated to a disturbance in vacuolar pH.

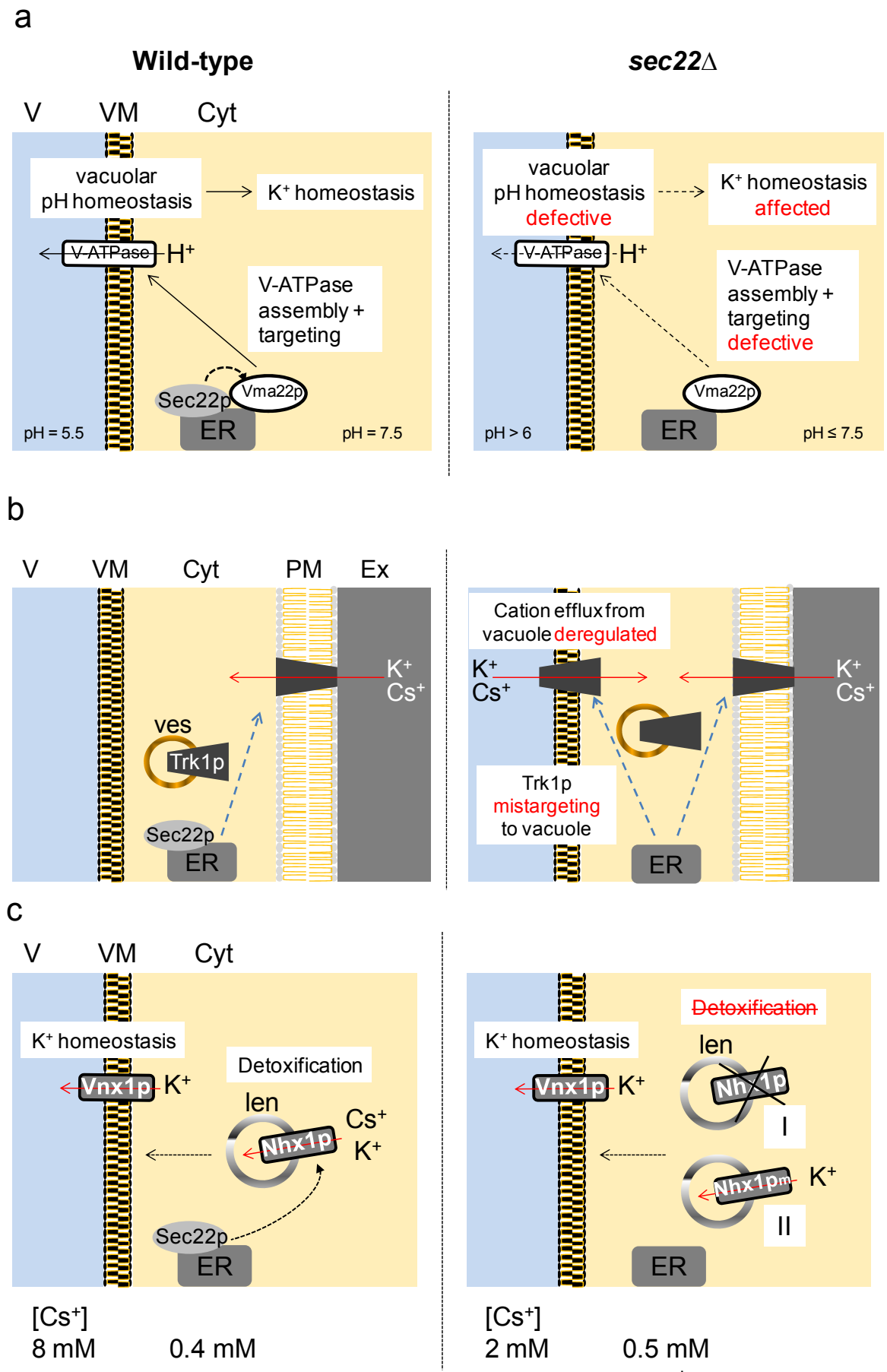

Figure 31. Three hypothetical functions of Sec22p that may affect Cs^+ accumulation and/or discrimination in a yeast cell. See figure legend on next page.

Figure 31. Three hypothetical functions of Sec22p that may affect Cs^+ accumulation and/or discrimination in a yeast cell.
(a) The putative role of Sec22p in the maintenance of vacuolar pH via V-ATPase assembly. In wild type (left), Sec22p and Vma22p interact at the ER to control the assembly and targeting of V-ATPase subunits. The further protein modification and localization is independent of these proteins. V-ATPase activity conserves the high proton concentration in the vacuole and thereby its membrane potential and acidic pH, which is essential for ion storage of the vacuole and the K^+ homeostasis. Loss of Sec22p (right) reduces the efficiency of V-ATPase assembly and therewith causes a disturbed vacuolar pH, membrane potential and, successively, ion transport. (b) Hypothesis for Sec22p's involvement in the correct targeting of a plasma membrane inward rectifying ion transporter, as it was indicated for Trk1p (Fell et al., 2011). Sec22p is necessary for the cargo-specific targeting of the ion transporter Trk1p from the ER to the plasma membrane. In the mutant situation (right) the transporter may be mislocalized to the vacuolar membrane. The selectivity of the transporter can be influenced by the different pH surrounding of the vacuole, but its activity may be conserved after integration to the vacuole membrane. Thereby, this protein would become a vacuolar cation efflux mediator without regulatory control. (c) Hypothesis for Sec22p's role in the activity of Nhx1p. Sec22p is hypothesized to be necessary for the action of Nhx1p in ion detoxification (wild-type situation, left). Nhx1p, located in the membrane of the vacuolar targeted late endosomal compartment can transport both, K^+ and Cs^+ and is essential for cation detoxification. K^+ homeostasis depends mainly on the activity of Vnx1p in the vacuolar membrane, which is not affected by loss of Sec22p (right). In this hypothesis, the ion deposition of essential ions from the cytoplasm to the vacuole is separate from the compartmentalisation of toxic ions. Ion fluxes are indicated as red arrows. Loss of Sec22p may cause a loss of Nhx1p targeting (I) or a modification of its function (II), but both would only influence the regulation of toxic ions and not the K^+ homeostasis. PM = plasma membrane; VM = vacuolar membrane; Cyt = cytoplasm; V = vacuole; ves = vesicle; len = late endosomal compartment.

However, Sec22p may adopt another, non-redundant function affecting the specificity of vacuolar ion transport. This may be correlated to a recently observed cargo specificity in Sec22p-dependent protein sorting (Fell et al., 2011). In this publication, a yeast diploid loss-of-function *Sec22* mutant allele (*sec22*Δ in this thesis is a haploid mutant strain) was described having a reduced Rb^+ content due to a partial mis-targeting of Trk1p. As these experiments were done under different experimental conditions (cells were incubated in a higher concentration of K^+ before the tracer studies were started) and only focused on the initial phase of uptake, these observations are not in contrast to the results presented here. A Rb^+ phenotype at 13 h of incubation, a time when cells were assumed to enter a Rb^+ saturation (Cs^+ is already in saturation at this incubation time) was not detected (Fig. 8). The absolute accumulation was most important for the scope of this work, as we wanted to find measures to reduce the total amount of Cs^+ taken up, while the early phases of uptake were of interest only for the mechanistic interpretation of the *sec22*Δ phenotype. Nevertheless, Fell and colleagues were the first to connect *Sec22* with alkali metal cation homeostasis and proposed that alkali metal cation transporters are specialized cargo of Sec22p-mediated protein sorting. The high-affinity K^+ transporter Trk1p was proven to be less efficiently targeted to the plasma membrane, whereas it was found in intracellular membranous structures, which was not the case in wild type. The experimental setup allows speculating that these intracellular membranes may be vacuolar membranes. Sec22p must have a role in the correct targeting of this protein, even though a non negligible amount of Trk1p was still

found at the plasma membrane (Fell et al., 2011). As it was found for Trk1p that its selectivity of K^+ over Na^+ is dependent on the acidification of its surrounding (Haro and Rodriguez-Navarro, 2002), one may further speculate that a *sec22*Δ-affected mis-targeting of this transporter to the vacuolar membrane – where it would be inserted in the inverse direction (Fig. 31b) – could switch this protein from a low-selectivity plasma membrane uptake transporter to a selective vacuole efflux transporter without regulation. In this process a *sec22*Δ-dependent selective Cs^+ efflux from the vacuole could be generated. Yet, it was not shown so far that Trk1p gets inserted to the vacuolar membrane and it remains speculative whether the selectivity of this transporter could be altered towards a Cs^+ specificity by a drop in pH from 7.5 (cytoplasm) to 5.5 (vacuole). Additional proof would be needed to support that the high-affinity Trk1p could actually function in a vacuolar surrounding. In addition, if the hypothesis of a role of Trk1p holds true and Cs^+ is expelled more from the vacuole, the question remains, which processes serve to save the cytoplasm from the accumulation of toxic cation without altering the K^+ homeostasis at the same time. A minor increase in cytoplasmic Cs^+ concentration may be feasible and might be supported by the slightly increased Cs^+ sensitivity of sec22, however. In the plant system there are several far related non-selective cation transporters with homology to Trk1p, e.g. HKT1, but a cargo-specificity of SEC22 was not indicated so far. Detailed localization / mis-localization studies of selected plasma membrane ion transporters may support this hypothesis.

Besides Trk1p, mis-targeting of other proteins or regulatory subunits may be affected in *sec22*Δ. This could concern ion permeating systems related to the vacuole more directly, namely Vnx1p and Nhx1p (Fig. 2). While there was no indication that the described vacuolar low-affinity cation exchanger Vnx1p was involved in ion specificity, or that it had an effect of Cs^+ accumulation when deleted (Cagnac et al., 2010; Heuck et al., 2010), a possible role of the late endosomal, *i.e.* pre-vacuolar Nhx1p was proposed (Gaxiola et al., 1999; Heuck et al., 2010). Nhx1p, a cation exchanger active in cytosolic, *i.e.* low-affinity conditions, is not ion selective, and – in accordance with this - the yeast mutant screen indicated a reduced Cs^+ as well as Rb^+ accumulation in its loss-of-function mutant. Targeting of Nhx1p is independent of the general secretory system (Wells and Rao, 2001) and might therefore rely on a specialized protein sorting route, which might be mediated via Sec22p.

In the plant system, Nhx1p homologous proteins were described to regulate not only K^+ homeostasis, but also cation detoxification (Bassil et al., 2011; Leidi et al., 2010). In this special case, a situation for yeast and plant may be hypothesized in which Nhx1p is responsible for Cs^+ detoxification via the vacuole (even though it can also transport other cations like Rb^+ and K^+ due to the lacking selectivity) and its function may be altered or even lost in *sec22*Δ (Fig. 31c, variants I or II). Pleiotropic effects for the cell may still be

circumvented via Vnx1p. This vacuolar cation exchanger has no role in Cs^+ detoxification, as *vnx1*Δ did not show any Cs^+ phenotype, and it probably discriminates to a large degree against this Cs^+ (Heuck et al., 2010). The hypothesis suggests that Vnx1p was not affected in *sec22*Δ and may substitute for the loss of Nhx1p in K^+ homeostasis. Reduced ability for ion detoxification would be in accordance with an increased sensitivity against toxic cationic elements, as described above. A possible approach to prove the importance of Nhx1p function in Cs^+ detoxification and the effect of *sec22*Δ on this protein would be to test the Nhx1p protein abundance and localization in *sec22*Δ. Additionally, it could be analysed whether a co-localization of Sec22p and Nhx1p, e.g. at the ER was evident. The *A. thaliana* Nhx1p-homologue NHX1 was shown to substitute for a yeast mutant lacking Nhx1p and other proteins for cation detoxification, proving the exchangeability of the systems (Gaxiola et al., 1999). A double mutant of the *Nhx1* homologous genes *NHX1* and *NHX2* of *A. thaliana* to cause depletion in vacuolar K^+ content (Bassil et al., 2011). In the plant system it would be necessary to analyse the ion selectivity / non-selectivity of the single NHX family members and whether SEC22 co-localizes or interacts with any one of them.

In conclusion, loss of Sec22p in yeast is correlated with a loss of non-selective ion transport at the vacuole, as *sec22*Δ discriminates against Cs^+, which is not true for wild type. Sec22p itself cannot bind or transport ions, but it is involved in a diversity of cellular functions which might affect the selectivity of ion transport. Since essential ion transporting systems are mostly not discriminating between Cs^+ and K^+, it can be speculated that a change in the protein's substrate specificity or a change in the ratio of non-selective against selective systems must be achieved. A number of hypotheses were introduced, of which indications for a cargo specificity were most promising. The putative involvement of Sec22p in the regulation of Nhx1p poses a reasonable explanation for both, the non-selective vacuolar ion transport in wild type, which leads to the high deposition of Cs^+ to the vacuole, and the gain of selectivity in the mutant situation by diminishing the activity of the non-selective vacuolar detoxifier Nhx1p. Pleiotropic effects could be avoided in this case, as the the essential ion homeostasis can be maintained.

3.4 Translation of the yeast *sec22*Δ phenotype to the plant system allows growing a Cs^+ - "safer" *A. thaliana* without growth defects

In the plant *sec22-3* mutant, the Cs^+ phenotype of the yeast *sec22*Δ was copied. Accordingly, a defect in vacuolar deposition of each single cell was also expected in the multicellular system. This might be tested via vacuolar isolation after Cs^+ incubation. Additionally, to prove a uni-cellular effect, single cells (e.g. cell wall free protoplasts) may be analysed for Cs^+ accumulation. The phenotype was found in a developmentally controlled mutant that showed

expression of *A. thaliana SEC22* in young tissue, flowers and reproductive tissue (Fig. 26) and a complemented line was able to suppress the Cs^+ phenotype, confirming that *A. thaliana SEC22* was the responsible gene (Fig. 28). No significant hits in an interaction databases (MIND0.5; www.associomics.org) (BioGRID$^{3.1}$) (Stark et al., 2006), a co-expression database (ATTED-II) (Obayashi et al., 2007), or expression database (Genevestigator) (Zimmermann et al., 2008) supported the connection of *A. thaliana* SEC22 with Cs^+ regulation or a correlation with vacuolar maintenance, so that the observations presented here have to be considered as indications for a novel function of *A. thaliana SEC22* in vegetative tissues. The mutant described here is viable and reproductive and with a reduction of Cs^+ accumulation by approximately one half, it can be the basis to develop safer crop strategies. The necessity of dealing with a developmentally controlled mutant could be overcome, once the mechanistic background of the phenotype is fully revealed and additional targets may be identified.

A “safer crop” strategy involving SEC22 may be suggested: The organ specific suppression of SEC22 could be combined with other findings, e.g. by manipulating ion transporters, which affect Cs^+ uptake (e.g. altering the KIRC / VICC expression level), but that are not detrimental if they are lost (White et al., 2010). This could further be supplied with targeted fertilization programs (NH_4^+ and K^+ rich fertilization) or a slight acidification of the soil. Such a mixture of classical soil-based counteracting and organism-encoded limitation of Cs^+ uptake may synergistically restrict radiocaesium uptake by plants.

4 MATERIAL AND METHODS

4.1 MATERIAL

4.1.1 Radioactive isotopes and radioactively labelled chemicals

Chemical (abbreviation in this work)	Activity (at Date of Arrival)	Company
^{134}CsCl (^{134}Cs)	3.2 MBq (500 µl)	AEA Technology, Germany
^{86}RbCl (^{86}Rb)	22 MBq (500 µl)	GE Healthcare, UK
Guanosindiphosphate – mannose (1-^{14}C) (GDP – [^{14}C] – mannose)	30 kBq (1 ml)	Hartmann Analytic, Germany

Table 13. Radioactive isotopes and labelled chemicals

4.1.2 Consumables and standard chemicals

Consumable material (reaction tubes, falcon tubes and pipette tipps) was obtained from Eppendorf (Germany), Greiner Bio One (Germany) or VWR (Germany). Standard buffer substances, agars and chemicals, if not mentioned otherwise, were obtained from Merck (Germany), Roth (Germany), Sigma (Germany), Duchefa (Netherlands) or Biozyme (Germany).

4.1.3 Yeast strains

Yeast strains used and//or modified in this work are listed in Tab. 14. The mutant strains from a genome- wide haploid mutant collection are all based on the strain BY4741 with a Kanamycine (Kan) resistance cassette inserted in the according genomic region (Brachmann et al., 1998; Kumar and Snyder, 2001; Winzeler et al., 1999).

Strain (Trivial name)	Attributes	Selection	Source
BY4741 (WT or BY4741 WT)	MATa; *his2Δ1; leu2Δ0; met15Δ0; ura3Δ0*	Synthetic complete (SC) medium lacking histidine (His) and uracil (Ura)	a
ylr268wΔ (*sec22Δ*)	MATa; *his2Δ1; leu2Δ0; met15Δ0; ura3Δ0; ylr268wΔ::KanMX4*	Kan	a
*ybr127c*Δ (*vma2*Δ)	MATa; *his2Δ1; leu2Δ0; met15Δ0; ura3Δ0; ybr127cΔ::KanMX4*	Kan	a
*yhr060w*Δ (*vma22*Δ)	MATa; *his2Δ1; leu2Δ0; met15Δ0; ura3Δ0; yhr060wΔ::KanMX4*	Kan	a

Table 14. Yeast strains used or created in this study.
[a] Euroscarf (Frankfurt am Main), [b] Stephan Dräxl (this work)
Table is continued on next page.

Strain (Trivial name)	Attributes	Selection	Source
ypr029cΔ (*apl4Δ*)	MATa; *his2Δ1; leu2Δ0; met15Δ0; ura3Δ0; yhr060wΔ::KanMX4*	Kan	a
yjl024cΔ (*aps3Δ*)	MATa; *his2Δ1; leu2Δ0; met15Δ0; ura3Δ0; yhr060wΔ::KanMX4*	Kan	a
yjl154cΔ (*vps35Δ*)	MATa; *his2Δ1; leu2Δ0; met15Δ0; ura3Δ0; yhr060wΔ::KanMX4*	Kan	a
ylr268wΔ::5'UTR$_{YLR268W}$::ORF(YLR268W)::3'UTR$_{YLR268W}$ (*sec22Δ::Sec22*)	MATa; *his2Δ1; leu2Δ0; met15Δ0; ura3Δ0; ylr268wΔ::KanMX4* transiently transformed with YEp352_YLR268Wcomp	Ampicillin (Amp)	b
ylr268wΔ::OE_YLR268W (*sec22Δ*_OE)	MATa; *his2Δ1; leu2Δ0; met15Δ0; ura3Δ0; ylr268wΔ::KanMX4* transiently transformed with pCM189_YLR268W	Amp; Doxicycline (Dox)-repressible	b
ylr268wΔ::AT1G11890 (*sec22Δ_AtSEC22*)	MATa; *his2Δ1; leu2Δ0; met15Δ0; ura3Δ0; ylr268wΔ::KanMX4* transiently transformed with pCM189_*AT1G11890*	Amp; Dox-repressible	b

Table 14. Yeast strains used or created in this study (continued).
[a] Euroscarf (Frankfurt am Main), [b] Stephan Dräxl (this work)

4.1.4 Plant material

Tab. 15 contains all *A. thaliana* lines purchased or created for analyses in the course of this project. All lines stated are based on the ecotype Columbia-0 (Col-0).

Line (Trivial name)	AGI code	Attributes	Selection	Source
A. thaliana Col – 0 (WT)	-	-	-	*a*
SALK_042619 (*sec22-3*)	*At1g11890*	T-DNA insertion line	Kan; genotyping by PCR	b
SALK_042619::pBGW(5'UTR$_{At1g11890}$:*At1g11890:3'UTR$_{At1g11890}$*) (*sec22-3::SEC22*)	*At1g11890*	Complementation of SALK_042619 homozygous line with *At1g11890* under control of its native promoter	BASTA; RT-PCR expression analysis	c

Table 15. Plant lines used in this strudy.
[a] *Arabidopsis* Biological Research Center (ABRC, Ohio, USA), [b] Nottingham *Arabidopsis* Stock Center (NASC, Nottingham, UK), [c] Stephan Dräxl (this work)

4.1.5 Bacterial strains

All bacterial strains were produced as shuttle system to clone DNA fragments in vectors used for yeast or plant transformation, except *Agrobacterium tumefaciens* (*A. tumefaciens*) strains, which were directly used to create transgenic *A. thaliana* lines (Tab. 16).

Escherichia coli (*E. coli*) heat competent strain DH5α and *A. tumefaciens* strain GV3101 (pMP90) were used.

Bacterium	Vector	Purpose	Selection
E.coli	pBGW(5'UTR$_{At1g11890}$:*At1g11890:3'UTR$_{At1g11890}$*)	Complementing *A. thaliana sec22-3* with *A. thaliana Sec22*	-
E.coli	YEp352(*5'UTR$_{YLR268W}$::ORF (YLR268W)::3'UTR$_{YLR268W}$*)	Complementing *S. cerevisiae sec22Δ* with *Sec22*.	Amp
E.coli	pCM189_YLR268W	Constitutive expression of *Sec22* in *S. cerevisiae sec22Δ.*	Amp
E.coli	pCM189_*AT1G11890*	Constitutive expression of *A. thaliana Sec22* in *S. cerevisiae sec22Δ.*	Amp
A. tumefaciens	pBGW(5'UTR$_{At1g11890}$:*At1g11890:3'UTR$_{At1g11890}$*)	Complementation of *A. thaliana sec22-3* with *A. thaliana SEC22* under its native promoter.	Amp, Rifampicine, Spectinomycine

Table 16. Bacterial stems transformed with vectors produced in this work.

4.1.6 Vectors

The vectors listed in Tab. 17 were used as empty vector controls or were modified by restriction digest and ligation, as described in methods (chapter 4.2.4.7).

Vector	Purpose	Source	Reference
pCM189	Constitutive expression of a gene of interest (GOI) in yeast; doxycycline repressible.	a	(Gari et al., 1997)
pYEp352	Complementation of yeast mutant with a genomic construct under its native promoter.	a	(Hill et al., 1986)
pBGW,0	Gateway® Cloning – ready vector for expression of GOI under control of its native promoter in plants.	b	(Karimi et al., 2002)

Table 17. Vectors used as basis for different contructs created in this work.
[a]Euroscarf, Frankfurt am Main; [b]Invitrogen, KarsruheTable

4.1.7 PCR Primers

Tab.18 contains all oligonucleotides, purchased from Sigma (Germany), that were used for PCR based strategies to amplify a genomic region of interest or to proof expression of a GOI on cDNA level. All primers were designed in this work. Selection of suitable primers was done with primer3 (Untergasser et al., 2007). An exception is SALK*_LBb1.3* which was designed according to http://signal.salk.edu/cgi-bin/tdnaexpress (Alonso and Stepanova, 2003).

Name	Sequence (5' – 3')	Purpose
SEC22coXmaIfw	GAGAGGGCCCGGGAGTGAAAAGGATGGTTGC	Ligation of *ScSec22* in YEp352
SEC22coHindIIIrv	GAGAAAGCTTTTATTGTCTTGATATCGGTCC	Ligation of *ScSec22* in YEp352
ScSec22ClaIfw	GAGAATCGATATGATAAAGTCAACACT	Ligation of ScSec22 in pCM189
ScSec22NotIrev	GAGAGCGGCCGCCTATTTGAGGAAGATCC	Ligation of ScSec22 in pCM189
PromSecfwXmaI	GAGACCCGGGATGATCACGAGCTCGTATTCGA	Cloning of genomic *At1g11890* (Promoter)
PromSecrevClaI	GAGAATCGATCTTTGCCTTATTACTTCT	Cloning of genomic *At1g11890* (Promoter)
TermSecfwXhoI	GAGACTCGAGAAAAAAAAGGAGGAATCT	Cloning of genomic *At1g11890* (3'UTR)
TermSecrevPstI	GAGACTGCAGTGAAATCAAACCCAA	Cloning of genomic *At1g11890* (3'UTR)
SEC22fwClaI	GAGAATGCATCGATATGGTGAAAATGACATTGA	Cloning of *At1g11890*
SEC22revXhoI	GAGACTCGAGTTACCATAGCTTGTTCTTGACC	Cloning of *At1g11890*
SEC22revNotI	GAGAGCGGCCGCTTACCATAGCTTGTTCTTGA	Cloning of *At1g11890* (yeast transformation)
RTiScSEC22fw	TGAACAAAAGCAAAAGGTGAAAATC	Expression analysis of *Sec22 S. cerevisiae*
RTiScSEC22rev	GCCTCCGTGGCAGACTGT	Expression analysis of *Sec22 S. cerevisiae*
SEC22_RTPCRfw	AACGTGTCAATGGGCCTAAC	Expression analysis of *SEC22 A. thaliana*
SEC22_RTPCRrv	ATGTTAACCGGCTCGACATC	Expression analysis of *SEC22 A. thaliana*
SEC22LP	TTTGGGATCGGAACTTTGAG	Genotyping of SALK_042619 *A. thaliana*
SEC22RP	GGAAAACATAGGGGCCAGTT	Genotyping of SALK_042619 *A. thaliana*
SALK_LBb1.3	ATTTTGCCGATTTCGGAAC	Genotyping of SALK_042619 *A. thaliana*
Exon1-3fw	TCCAGTTTTAAAAACGCTAAGATGAAT	Expression analysis of *SEC22 A. thaliana*
Exon1-3rev	TCCAGGTATTGGAAAGCGAGTTTCT	Expression analysis of *SEC22 A. thaliana*
Exon2-4fw	ACAACAGGTCAAAGCTTTGTTTAAG	Expression analysis of *SEC22 A. thaliana*
Exon2-4rev	CTAAGACTTCTTGCACATTCCGGGT	Expression analysis of *SEC22 A. thaliana*
Exon3-5fw	ATGGGCCTAACATTGAAACAGCTGC	Expression analysis of *SEC22 A. thaliana*
Exon3-5rev	TATACGAGATTCAGATGTTAACCGG	Expression analysis of *SEC22 A. thaliana*
Exon4-6fw	TCTATGAGGTTCATCAAATAATGAC	Expression analysis of *SEC22 A. thaliana*
Exon4-6rev	TGACCCAGAAAAGGAGGAAGACTAC	Expression analysis of *SEC22 A. thaliana*

Table 18. Oligonucleotides used in this study.
Table is continued on next page.

Name	Sequence (5' – 3')	Purpose
Exon1-3fw	TCCAGTTTTAAAAACGCTAAGATGAAT	Expression analysis of *SEC22* *A. thaliana*
Exon1-3rev	TCCAGGTATTGGAAAGCGAGTTTCT	Expression analysis of *SEC22* *A. thaliana*
AtS16fw	TTTACGCCATCCGTCAGAGTAT	RT – PCR positive control *A. thaliana*
AtS16rev	TCTGGTAACGAGAACGAGCAC	RT – PCR positive control *A. thaliana*
AtTUB9fw	GTACCTTGAAGCTTGCTAATCCTA	RT – PCR positive control *A. thaliana*
AtTUB9rev	GTTCTGGACGTTCATCATCTGTTC	RT – PCR positive control *A. thaliana*
ScAct1RTfw	TCGTTCCAATTTACGCTGGTT	RT-PCR positive control *S. cerevisiae*
ScAct1RTrev	CGGCCAAATCGATTCTCAA	RT-PCR positive control *S. cerevisiae*
ScTub1RTfw	TGTCGGTCAAGCTGGTTGTCA	RT-PCR positive control *S. cerevisiae*
ScTub1RTrev	TTGTAATTTCTGACACAGAGT	RT-PCR positive control *S. cerevisiae*

Table 18. Oligonucleotides used in this study.
Continued.

4.1.8 Antibiotics

Antibiotic	Source	Final concentration in media
Ampicilline	Roche	100 µg/ml
Doxycycline	Sigma	10 µg/ml
Kanamycine	Sigma	50 µg/ml
Rifampicine	Sigma	100 µg/ml

Table 19. Antibiotics supplied to media for selection or repression of doxycycline-regulated expression in pCM189 constructs.

4.1.9 Media

Standard media for growth of yeast and plants are given in Tab. 20, while specialized media for accumulation assays, kinetic studies, yeast vacuole extraction, gel electrophoresis etc. are described in the according methods. Sources of media components are included in chapter 4.1.2.

Medium	Component	Concentration
Luria Broth	LB Broth high salt NaOH +/- Bactoagar +/- Antibiotics	2.5 g/l 600µl/l of 5N stem solution 10 g/l see 4.1.3 / 4.1.4.
½ Murashige & Skoog (MS)	MS medium including vitamins Sucrose +/- Bactoagar	2.2 g/l 1 % (w/v) pH 5.8 (KOH) 1 % (w/v)

Table 20. Basic media recipes.
Continued on next page.

Medium	Component	Concentration
Yeast Peptone Dextrose plus Adenine hemisulfate (YPAD)	Yeast extract	10 g/l
	Peptone	20 g/l
	Glucose	20 g/l
	Adenine hemisulfate	0.1 g/l
	+/- Bactoagar	1 % (w/v)
Synthetic Complete (SC)	Yeast Nitrogen Base w/o amino acids	6.8 g/l
	Glucose	20 g/l
	SC Dropout Mix	0.85 g/l
		pH 5.7 (10 N NaOH)
	+/- Bactoagar	1 % (w/v)
SC Dropout Mix (Amino acids marked red are omitted for selective SC – His/SC – Ura media)	Adenine hemisulfate; Arginine HCl; Histidine HCl; Isoleucine; Leucine; Lysine HCl; Methionine; Tyrosine	2 g each
	Phenylalanine; Tryptophane	3 g
	Homoserine	6 g
	Uracil	1.2 g
	Caline	9 g

Table 20. Basic media recipes.
Continued.

4.2 METHODS

4.2.1 Microscopy

Microscopic analyses were performed with an Olympus BX61 (Olympus, Germany). The software Cell*P (Olympus Soft Imaging Solutions, USA) was used for acquisition and image analysis.

4.2.2 Staining of yeast cells

FM6-64 staining of yeast vacuoles in proliferating cells was modified from an established protocol (Vida and Emr, 1995); 15 µM SnyptoRed C2 (Biotium, Germany) instead of FM4-64 was added to the yeast culture (OD_{600} < 1.0). Cells were analysed at 50 ms exposure time with 525 nm excitation and 647 nm emission.

4.2.3 Quantification of yeast cells and isolated vacuoles

Yeast cells were quantified by correlating microscopically achieved standard growth curves to optical density. Vacuoles were counted and quantified by enzymatic activity tests (see chapter 4.2.7.3.7).

Vacuoles were counted in a Neubauer Haemacytometer.

Cell number estimations via Optical Density (OD_{600}) measurement were done in a Biophotometer (Eppendorf, Germany) or in a Safire2 plate reader (Tecan, Germany).

4.2.4 Radioactive measurements

4.2.4.1 Liquid Scintillation Counting

The method originates from the protocol of (Broser and Kallmann, 1947). ^{14}C standard and samples were dissolved in 1 ml Triskem Ultima Gold/Hi Safe 2 LSC cocktail, placed in a 20ml PET vial and measured in a Beckman LS 6500 Scintillation Counter (Beckman Coulter, Germany). Measurement time was set to 3600 s per sample. Empty vials and vials containing LSC cocktail excluding sample were used for background normalisation.

4.2.4.2 γ - spectrometrical Analysis of ^{134}Cs / ^{86}Rb.

Yeast cells on filters and yeast vacuole fractions were resuspended in 3 ml 3 M HNO_3 to achieve a homogenous dilution suitable for γ-spectrometrical analysis. Plant material was directly placed in 3 ml of 3 M HNO_3. Measurements were done in a Wallac WIZARD 1480 (Perkin Elmer, USA), analysing the two expected spectral peaks for ^{134}Cs (605 and 796 keV).

Counting time was set to 3600 s. Background and buffer measurements were supplied for each experiment. For ^{86}Rb, a similar procedure was applied, analysing the main peak at 1077 keV. In case of isolated vacuoles, α-mannosidase activity of the isolated fraction was determined (Yoshihisa and Anraku, 1990) and an amount of cells with equal enzyme activity was isolated. A detailed description is given in 4.2.7.3.7ff.

a) Calculating accumulated Cs^+/Rb^+ in yeast samples using tracer estimation:

Gammaspectrometrical measurement gives a value of (CCPM, which are already internally normalized. In addition, we always include tracer- free buffer solution for additional background correction. For estimating the amount of tracer included in the sample, we further need to record the decays in a given volume of pure tracer solution and the counts of the tracer- loaded buffer without cells. In addition, it is necessary to know the concentration of stable CsCl/RbCl added to the experimental setup. With this information, we can use, for both, plant and yeast material and for Cs^+ and Rb^+ determination the following equations:

Amount compound (Cs^+/Rb^+) per CCPM (buffer) = conc (mol/L buffer)/CCPM (buffer);

Normalization: CCPM in 2.0 * 10^7 cells (or according sample) – CCPM (background) = CCPM (sample);

Amount compound in sample (mol) = CCPM (sample) * Amount compound per CCPM.

b) Calculating accumulated Cs^+/Rb^+ in plant samples using tracer estimation:

For estimating the amount of tracer included in the sample, we further need to record the decays in a given volume of pure tracer solution and the counts of the tracer- loaded buffer without cells. By knowing the concentration of stable CsCl/RbCl added to the experimental setup. With this information we can use for both, plant and yeast material and for Cs^+ and Rb^+ determination following equations:

Amount compound (Cs^+/Rb^+) per CCPM (buffer) = conc (mol/L buffer)/CCPM (buffer);

Amount compound in sample (mol) = CCPM (sample) * Amount compound per CCPM.

The next calculation step was done according to the recorded fresh weight (f.wt.) in order to get a comparable unit ($mol/g_{f.wt.}$).

4.2.5 Determination of metal concentrations in yeast and plants

S. cerevisiae and *A. thaliana* samples were prepared as described in the according chapters (4.2.7.3.10 and 4.2.8.2.2, respectively). Analysis was done at the Central Anorganic Analytical Unit of the Helmholtz Zentrum München (Research Unit Analytical

BioGeoChemistry). For concentration measurements of K^+, Na^+, Ca^{2+} and Mg^{2+}, freeze dried samples were digested. The digests were introduced to an inductively coupled plasma atomic emission spectrometer (ICP-AES) using a peristaltic pump and a seaspray nebulizer fitting to a cyclon spray chamber. The following element lines were measured: Ca^{2+}: 317.933 nm; K^+: 766.490 nm; Mg^{2+}: 279.077 nm; Na^+: 589.592 nm. Concentrations were determined by external calibration.

4.2.6 General molecular biological methods

4.2.6.1 Polymerase Chain Reaction (PCR)

This method was applied to amplify short (approximately 300 bp – 5 kb) DNA sequences from a double stranded DNA template molecule. The temperatures and the length of elongation steps were according to the melting temperature of the used oligonucleotides and the size of the desired DNA fragment. The elongation *in vitro* was catalysed by the Polymerase Phusion® (M0530L) from Thermo Fisher Scientific (Germany) or Taq DNA Polymerase from Agrobiogen GmbH (Germany). The protocols for both polymerases are given below. Phusion polymerase is supposed to amplify longer fragments with less base exchanges.

Protocol for Phusion PCR (20 µl reaction volume):

Mix the following components in the indicated order.

Component	**Amount (µl)**	**Concentration**
Nuclease – free water	to 20	-
5x Phusion Polymerase HF buffer	4	1x
10 mM dNTPs	0.4	200 µM
10 µM Forward Primer	1	0.5 µM
10 µM Reverse Primer	1	0.5 µM
Template DNA	2	100 – 200 ng
Phusion HF Polymerase	0.2	0.4 units

Protocol for Agrobiogen Taq polymerase (20 µl reaction volume):

Mix following components in the order indicated.

Component	Amount (µl)	Concentration
Nuclease – free water	to 20	-
10x Reaction buffer	2	1x
2 mM $MgCl_2$	1.2	0.12 mM
10 µM Forward Primer	1	0.5 µM
10 µM Reverse Primer	1	0.5 µM
10 mM dNTPs	0.4	200 µM
Agrobiogen Taq	0.1	0.5 units

PCR reaction cycles were automated using a Multicycler PTC-500 (Biozym, Germany) with following standard program (including modifications for optimizing single reactions according to the product properties):

Temperature (°C)	Number of cycles	Length (min)
95	1	5
95		0.5
52 – 62	30-35	0.5
72		1 per kb product
72	1	10

4.2.6.2 Reverse transcription

In both, yeast and plant, the presence of chosen transcripts can be used to confirm knockout (KO) mutant lines (loss of transcript) in comparison to WT (presence of transcript) or stable and transiently transformed mutants (presence of native or modified transcript). To this end, total RNA was isolated from the organisms as described in the according sections. For the reverse transcription (RT), 500 ng of RNA was used. First strand synthesis was done using the Invitrogen Reverse Transcription SuperScript II kit. The reaction set-up was modified from instructors manual as follows:

Component	Final concentration
Total RNA	500 ng
5x first – strand – synthesis buffer	1 x
dNTP mix (MBI Fermentas, Germany)	1 mM
DTT (5M)	0.01 M
Rnase Inhibitor (MBI Fermentas, Germany)	40 units
Oligo $(dT)_{15}$ (Promega, Germany)	0.17 µg (0.34 µl of a 0.5 µg/µl stock)
Nuclease – free water	to 20 µl
Incubate 10 min at room temperature	
Reverse transcriptase Superscript II	67 u (1µl of a 1:1 dilution in 1x first – strand – synthesis buffer)

Negative reactions (-RT) were run without addition of reverse transcriptase in order to estimate the contamination of samples with genomic DNA.

To produce cDNA, the mixture was incubated in a Multicycler PTC-200 (Biozym, Germany) for 30min at 42°C, 40 min at 50°C and 5 min at 95°C (to inactivate the enzyme).

4.2.6.3 Agarose gel electrophoresis to visualize DNA fragments

Separation of DNA fragments by size was done by agarose gel electrophoresis as described (Sambrook and Russell, 2001). A concentration of 0.5 µg/ml ethidium bromide was added directly to the gel. Appropriate size markers were run in each gel to estimate the size of fragments. Visualization and recording of DNA gels was done using a Bio-Rad Gel Doc 2000 (Bio – Rad, Germany) and evaluated with Quantity One Software.

Agarose gels were prepared by adding 1- 2 g Agarose (Biozyme, Germany)/ 100 ml TAE buffer (40 mM Tris, 20 mM Acetate, 1 mM Na_2 – EDTA, pH 8.5). Samples were diluted in 5x loading buffer (1µl loading buffer per 10µl sample).

Recipe loading buffer (5x): 36 % Glycerine; 1x TAE; 2.5 mg/ml Orange G in ddH_2O

4.2.6.4 Gel extraction of DNA fragments

Purification of DNA from gel was done using the Quiaquick® PCR Purification kit (Quiagen, Germany). No changes were made to the manufacturer's manual.

4.2.6.5 DNA sequencing

Gel-extraction purified PCR fragments or purified plasmids were subjected to sequencing, performed by Eurofins MWG Operon (Germany) with following preparation:

Component	Final concentration
DNA template	100 ng/µl
Forward or Reverse Primer	15 pmol
Nuclease – free water	to 15 µl

4.2.6.6 Determination of DNA and RNA concentration

Absorption at 260 and 280 nm can be used to measure the concentration of DNA and RNA. Furthermore, the ratio of these values gives a clue about the purity of the material. The spectrometrical analysis was done in a Nanodrop ND-1000 spectrophotometer (Kisker-Biotech, Germany). Since all DNA and RNA samples were dissolved in ddH_2O, water was used as blank reference. Only spectra with acceptable quality (ratio absorbance 260/280 ≥ 1.8) were further used.

4.2.6.7 Restriction and ligation of DNA fragments

For site-directed insertion of PCR – or plasmid – derived fragments into target vectors restriction/ligation procedures were performed according to the standard protocols of the manufacturer. The enzymes were either purchased from Fermentas or NEB and were used in combination with the reaction buffers recommended for maximum activity.

Standard procedure:

Component	Amount (µl)
10x reaction buffer	1.0
ddH_2O	6.5
DNA (insert: 100-200 ng/µl; plasmid: 300 ng/µl)	1.0
Restriction enzyme	1.0

Incubation was done for 1.5 h at 37°C. The reaction was stopped by placing it for 10 min at 65°C. If indicated by the company, BSA was added. Restrictions digests were confirmed on agarose gels.

Restriction digest-produced fragments were ligated into accordingly digested Multiple Cloning Sites (MCSs) of target vectors using the T4 DNA Ligase from NEB (M0202), following the protocol given in the instruction manual except of following modifications: the ratio of fragment:vector was 3:1 with a minimum vector amount of 200 ng; The reaction was incubated at 24°C for 2 h and then transformed to the relevant bacteria Correct ligation was tested by either another restriction digest with agarose gel electrophoresis and/or sequencing.

4.2.7. Microbiological methods

4.2.7.1 Molecular biological methods in *E. coli*

Escherichia. coli laboratory strains are a useful system for cloning and propagation of vectors.

4.2.7.1.1 Preparing competent *E. coli*

Treatment of *E. coli* with chemicals can make them more susceptible for cell wall permeation and accordingly, transformation with plasmids (Hanahan, 1983).

2.5 ml Rich broth (RB) medium was inoculated with a single colony of *E. coli* DH5α and incubated overnight (37°C, 250 rpm). *E. coli* were than further subcultured in 250 ml RB medium with 20 mM $MgCl_2$, until an OD_{600} of maximum 0.6 was reached. Cells were collected by centrifugation (1000 x g for 5 min, 4°C). One hundred ml of ice cold transformation buffer 1 (30 mM K-acetate, 100 mM RbCl, 10 mM $CaCl_2$, 50 mM $MnCl_2$ in 15 % glycerol at pH 5.8, adjusted with acetic acid) were used to gently resuspend the cells, which were then kept on ice for 5 min. Centrifugation was repeated and resuspension was done in 10 ml of cold transformation buffer 2 (10 mM MOPS, 75 mM $CaCl_2$, 10 mM RbCl in 15 % glycerol, pH= 6.5, adjusted with KOH). Following an incubation of maximum 1 h on ice, 50 µl aliquots were prepared and frozen in liquid nitrogen. The efficiency was inspected with a selective vector construct transformation.

4.2.7.1.2 Transformation of heat shock competent *E. coli*

One aliquot of competent *E.coli* was thawed on ice and heat shock transformation was performed as described (Sambrook and Russell, 2001). Roughly 100 ng DNA was pipetted to the aliquot as soon as the cells were defrosted and the mixture was kept on ice for 15 min. Heat shock was done for 30-35 sec at 42°C in a water bath. Cells were then kept on ice for 5 min, before 200µl of fresh LB medium was added and the suspension was transferred to glass reaction tubes, where another 800 µl of LB medium was added. After incubation for 1.5 h at 37°C with gentle shaking, the cells were spun down and 30 µl were plated on selective

LB agar plates. Transformed *E. coli* was grown over-night at 37°C on LB medium plates containing the antibiotic vector-encoded antibiotic.

4.2.7.1.3 Plasmid isolation from *E. coli*

Plasmids derived from bacterial clones were isolated using the NucleoSpin® Plasmid purification kit by Macherey Nagel (Germany). Two to three ml of an overnight culture of bacteria (OD_{600} ≈ 0.8) were centrifuged (6000 x g, 1 min) to collect cells. Cell lysis, clarification of the lysate, silica-column binding and washing were done according to the instruction manual. Elution was in 50 µl ddH_2O.

4.2.7.2 Molecular biological methods in *Agrobacterium tumefaciens*

All *Agrobacterium* experiments were done with the electro- competent strain GV3101 (pMP90).

4.2.7.2.1 Preparing competent *A. tumefaciens*

A single colony was used to inoculate an overnight culture of *A. tumefaciens*. The cells were incubated at 28°C, shaking with 100 rpm to an OD_{600} < 1.0. A fresh 300 ml of LB medium including antibiotics (Rifampicin) was inoculated with 2 ml of this suspension and incubated until an OD_{600} of 0.6 was reached. The bacteria were cooled on ice for 30 min, centrifuged for 20 min (150 x g at 4°C in a Rotanta 460R centrifuge (Hettich, Germany)). After resuspending the pellet in 125 ml cold water and another incubation on ice (30 min), cells were washed again, followed by an incubation step on ice of 60 min. Cells were resuspended again in water and washed for a third time. The pellet was dissolved in 3 ml ice – cold glycerol (15 %) and aliquots of 50 µl were prepared, frozen and stored at -80°C.

4.2.7.2.2 Transformation of competent *A. tumefaciens* by electroporation

Plasmids for creating complementation lines in *A. thaliana* need to be introduced into *A. tumefaciens* via electroporation. To this end the competent bacteria were quickly thawed and 1µl plasmid DNA (20 – 40 ng/µl, diluted in TE buffer) was mixed to the aliquot. The suspension was directly transferred to a 0.1 cm electroporation cuvette. The following setup was used in a BioRad Gene Pulser with BioRad Puls Controller and BioRad Capacitance Extender (BioRad, Germany):

Feature	Setting
Capacitance	250 µFD
Voltage	1.25 kV
Resistance	400 Ω

When the time constant was close to 9.6, 1 ml of room temperature LB medium was added to the cuvette and the mixture was gently transferred to a Falcon reaction tube (15 ml) and incubated for 1.5 h with gentle shaking at 24°C. Cells became dense by centrifugation 1000 x g, 1 min to remove approximately 700 µl of supernatant. Twenty µl of the remaining suspension were spread on LB agar plates including the antibiotic selection of the *Agrobacteria* and the plasmid. Colonies were inspected 2.5 days after incubation at 28°C.

4.2.7.3 Molecular biological methods in *S. cerevisiae*

Saccharomyces cerevisiae was the most important model organism of this study, as it was established already as effective tool to study Cs^+ uptake (Heuck et al., 2010).

4.2.7.3.1 Yeast growth conditions and sterile stock cultures

Basic yeast growth conditions were followed (Sherman, 1991). Yeast was grown on YPAD medium (solid or liquid) at 30°C, if not noted otherwise. In case of toxicity or pH growth tests, liquid YPAD cultures were dropped on the appropriate media and/or the colonies were transferred by replica plating (Replicator and sterile velvet tissue by Roth, Germany). Growth on plates was stopped by transferplates to 4°C after 1 d or 2 d (in case of selective media) of growth. Liquid cultures (inoculated by a single colony or from a glycerol stock) were shaken at 100 -120 rpm and incubated until aspired OD_{600} was reached. In case of toxicity tests, additional concentrations of the according salts were added to non-selective SC plates. All media were autoclaved before use.

Sterile stock cultures were created by gently mixing a fresh overnight culture to 100 % glycerol (sterile) in 1:4 ratio. Stocks were directly frozen in liquid N_2 and kept at -80°C until use.

4.2.7.3.2 Transient transformation of yeast (Li-acetate method)

Yeast transformation was performed according to an established protocol (Gietz et al., 1995). An amount of 2 x 10^8 cells were harvested and washed in 100 mM Li-acetate. A volume of 240 µl PEG3500 50 % (w/v), 36 µl 1 M Li-acetate 36 µl, 50 µl carrier ssDNA (2 mg / ml) and plasmid (500 ng) in 34 µl H_2O were added successively. The mixture was incubated 15 min at 30°C, heat-shocked at 42°C for 45 min and regenerated 2 h at 30°C, before plating on selective YPAD plates.

4.2.7.3.3 Isolation of genomic DNA from yeast

Up to 10 ml of an over-night culture were harvested and resuspended in 100 µl 25 mM Tris-HCl pH=8, 1 mM EDTA pH=8 and 50 mM Glucose. Two hundred µl of 200 mM NaOH and 1 % sodium dodecyl sulphate (SDS) were mixed to the homogenate by inverting. A volume of

125 µl glass beads (diameter 0.25 mm, Roth, Germany) was placed in the reaction tube and vortexed for 8 minutes. The cell debris was sedimented, while the supernatant was incubated with 150 µl 3 M Na-acetate, pH 4.8 for 10 minutes on ice. After centrifugation the DNA of the supernatant was precipitated with 400 µl 100 % isopropanol. The DNA was washed in 80 % ethanol, dried and solved in ddH_2O.

4.2.7.3.4 Isolation of plasmid DNA from yeast ("Lazy bones protocol")

This plasmid isolation is modified from the lazy bones protocol (Burke et al., 2000). To rescue plasmids from transformed yeast, 2 ml of overnight culture were pelleted (1000 rpm, 5 min). An amount of 0.2 ml of a mixture of 2 % Triton-X- 102, 1 % SDS, 100 mM NaCl, 10 mM Tris- HCl (pH 8.0) and 1 mM Na-EDTA (not autoclaved) was used for resuspension. On top 0.2 ml phenol: chloroform: isoamylalcohol (25:24:1) solution and 0.3 ml acid-washed glass beads (diameter: 0.3 – 0.5 mm) were added. Samples were vortexed for 5 min and centrifuged at maximum speed for another 5 min. A volume of 120 µl of the aqueous phase was transferred to a new tube and the DNA was precipitated in 1 x volume isopropanol (100 %). For precipitation, the mix was kept at -20 °C for > 30 min. Afterwards, the DNA was pelleted by centrifugation (6000 x g, 2 min) and washed in 120 µl 70 % ethanol. The pellet was dried in the air for > 30 min, before the plasmids were resolved in ddH_2O.

4.2.7.3.5 Isolation of RNA from yeast

An overnight culture of yeast (5 ml) was harvested, washed in 1 ml H_2O, resuspended in 400 µl AE buffer (50 mM Na-acetate and 10 mM EDTA, pH 5.3), to which 40 µl 10 % SDS were added. The suspension was incubated together with 440 µl Phenol (pH 5.3) after vortexing at 65°C for 5 minutes. Dry ice was used to rapidly cool the mixture. After centrifugation, the supernatant was overlayed with Chloroform (400 µl), flipped three times and incubated at room temperature for 5 minutes. The upper phase was used to precipitate RNA with 1/10 V 3 M Na-acetate pH 5.3 and 2.5 V of 100 % ethanol by keeping the solution at -20°C for 2 hours.

4.2.7.3.6 Cloning strategies in yeast

All plasmids were propagated in *E. coli* (see chapter 4.2.7.1.2). Yeast transformation was done according to chapter 4.2.7.3.2. Isolated plasmids were tested by restriction digest and sequencing. Expression was tested by RT-PCR.

4.2.7.3.6.1 Creating a complemented *S. cerevisiae sec22*Δ*::Sec22* strain

For amplification of the genomic sequence of *YLR268W* (*Sec22*) the primers Sec22coXmaIfw and SEC22coHINDIIIrv were used. Restriction digest and ligation into

YEp352 with the following cloning in *E. coli* were done as described, resulting in Yep352_(5'UTR$_{YLR268W}$::ORF(*YLR268W*)::3'UTR$_{YLR268W}$). The according yeast strain was named *sec22*Δ*::Sec22*.

4.2.7.3.6.2 Creating a *S. cerevisiae Sec22* overexpression strain

The ORF of *YLR268W* (*Sec22*) was amplified using the primers ScSec22ClaIfw and ScSec22NotIrev. The amplicon was ligated to pCM189 after restriction digest with ClaI and NotI (Gari et al., 1997). The expression vector construct was transformed into *sec22*Δ as described in 4.2.7.3.2. Ten µg/ml doxycycline were used to silence the expression mediated by pCM189.

4.2.7.3.6.3 Creating a *A. thaliana SEC22* overexpression strain in a *S. cerevisiae sec22*Δ background

In order to construct the doxycycline repressible expression vectors for yeast containing *A. thaliana SEC22*, *At1g11890* was amplified using following oligonucleotides: AtSEC22ClaIfw: and AtSEC22NotIrevstop. The PCR products were cut by restriction enzymes (ClaI and NotI) together with the expression vector pCM189, and ligated with T4 DNA ligase as described. Ten µg/ml doxycycline were used to silence the expression induced by this construct.

4.2.7.3.7 Isolation of intact vacuoles from yeast

The protocol was modified from (Bankaitis et al., 1986). Yeast cells were grown until an OD_{600} of 0.8 was reached. Cells were harvested at 3000 rpm for 5 minutes (Sorvall RC-5B, using a GS-3 rotor, ThermoFisher Scientific, Germany) at room temperature. Sediments were resuspended in 2 x 25 ml wash buffer (stock solution: 10 ml 1 M Tris-HCl pH 9.4, 1.0ml 1M DTT, 89ml ddH_2O) by manual shaking in 50 ml reaction tubes (Greiner Bio-One GmbH, Germany). Samples were additionally shaken at 50 rpm for 10 minutes before washing in ddH_2O. For spheroplasting, the cells were resuspended in 15 ml of spheroplast buffer (50 mM PIPES-KOH, pH 6.8 and 600 mM Sorbitol in 0.2 % YPAD) and 100 µl/ml freshly prepared enzyme mixture (1000 u/ml each of Glusulase (Perkin Elmer, USA), Zymolase (US Biological, USA) and Glucanex (SIGMA, Germany) were added. The reaction was incubated for 1.5 hours at 30°C with shaking 60 rpm plus manual swirling every 15 minutes. All following steps were done at 4°C. Spheroplasts were pelleted 2 min at 900 x g (Hettich Rotanta 460R, Hettich, Germany) and resolved in 7.5 % Ficoll (SIGMA, Germany, diluted in 1.1 M Sorbitol). After centrifugation for 20 min at 900 x g, the pellet was solved in 6 volumes of lysisbuffer (10 mM Tris-MES, PH 6.9, 12 % Ficoll, 0.1 mM $MgCl_2$ and 10 µl protease inhibitor cocktail (SIGMA, Germany)). Homogenization was done with a 40 ml Dounce homogenizer (VWR, UK) using pistille size "A" on ice with 15 strokes, the solution was filled

in an appropriate ultracentrifugation tube and overlaid with 10 ml of lysis buffer. All following ultracentrifugation steps were performed in a Beckman Optima LE70 Ultracentrifuge with a SW28 swing out rotor (Beckmann Coulter, Germany). Samples were centrifuged at 140000 x g, 30 min. The upper fraction and the pellet were collected, and aliquots were saved for enzymatic tests. The upper fraction should contain crude vacuoles and was diluted in 10ml lysis buffer per 2ml collected fraction. Five additional strokes in the homogenizer were made and the solution was overlaid in an ultracentrifuge tube with 10ml of a solution similar to lysis buffer, but with 8 % Ficoll instead of 12% and a second overlay was done with the mixture containing 4 % Ficoll. Centrifugation for 45 min, 140000 x g, separated floating vacuoles from other organelles.

4.2.7.3.7 Enzymatic tests to proof purity and integrity of the isolated vacuole fractions

In total, 3 fractions and one positive control were tested after density centrifugation: spheroplasts (positive control), the pellet of the first centrifugation (Fraction 1), as well as pellet (Fraction 2) and floating fraction (Fraction 3) of the second density gradient. The following tests were carried out to show the content of the fractions and the possible contaminations by unexpected organelles. Fig. 32 shows an overview of the expected enzyme activities in the different fractions.

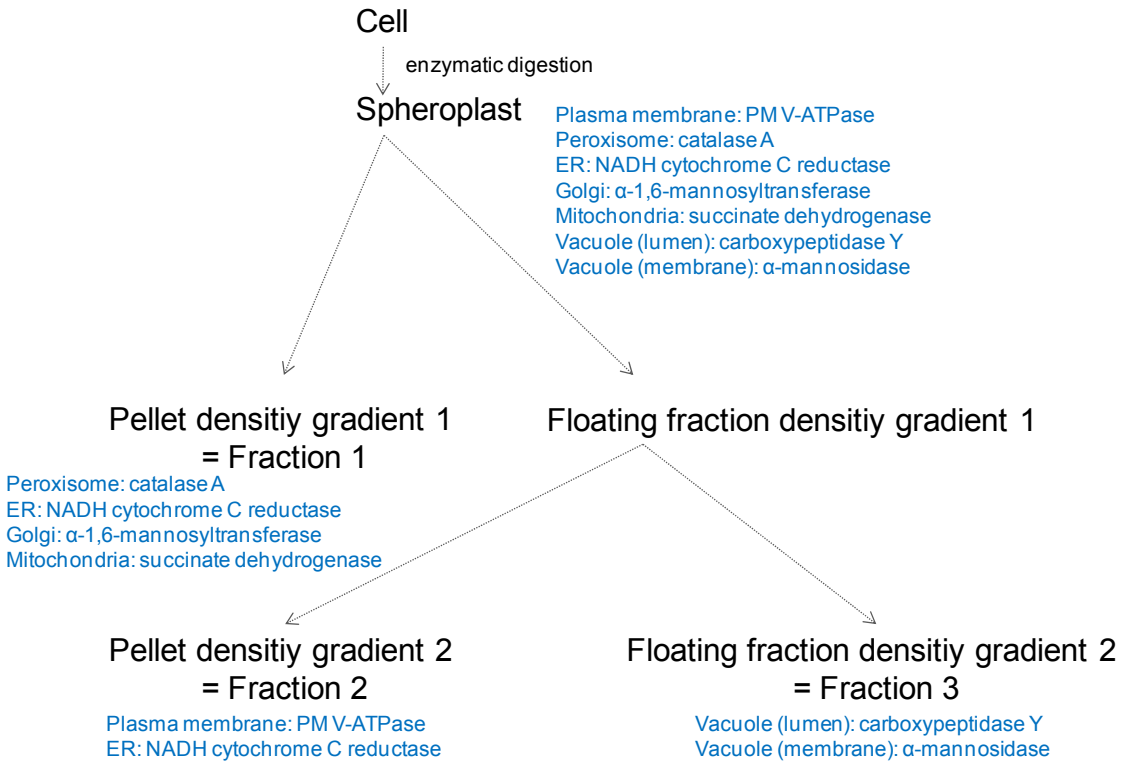

Figure 32. Scheme for vacuole isolation from yeast cells and enzymatic tests.
Spheroplast (yeast cells with enzymatically digested cell walls) were used as positive control, since they should harbour all functional enzymes. The enzyme activity expected in the different fractions is indicated in blue.

Plasma membrane ATPase (vanadate sensitive) measurement was described before (Bowman and Slayman, 1979; Serrano, 1978). Sixty µl fractions were used. All reagent volumes were reduced to 1/4th of the protocol. No further changes were made. The absorbance was taken at 750 nm and the activity was calculated using a standard curve produced by the similar assay with $(NH_4)_2HPO_4$ as substrate. We also added plus/minus vanadate controls (20 µM). Only vanadate sensitive activity was considered to originate from PM ATPase.

Catalase A activity (peroxisomal marker) was assayed by the titanium oxysulfate method according to a classical protocol (Lück, 1963), with recent modifications (Rieder and Emr, 2001). Freshly prepared substrate mixture: 8.5 ml peroxide stock solution (0.67 g 30 % (w/w) H_2O_2 with Tris/BSA to 200 ml) diluted in 100 ml Tris/BSA (0.2 g BSA in 100 ml H_2O + 4 ml 1 M Tris-HCl, pH 7) was mixed with 200 ml H_2O. One ml Titanium oxysulfate reagent control (SIGMA, Germany) and 0.5 ml substrate mixture were combined and absorbance at 405 nm was recorded. Thirty µl of sample buffer (2 g Triton X 100 in 100 ml H_2O, diluted 1:2 in Tris/BSA solution) plus 10µl fraction was prepared. As negative control, 40 µl of sample buffer were used. All steps were done on ice. To each reaction tube, 0.5 ml of substrate mixture were added (with 10 sec intervals from one reaction well to the next). After exactly 1 min, 1 ml of titanium oxysulfate reagent was pipetted on top, in similar time intervals. Precipitate was removed by centrifugation (2 min at maximum speed, 4 °C). Reactions were transferred to room temperature and the absorbance at 405 nm was measured against 0.5 ml Tris/BSA + 1 ml titanium oxysulfate reagent as blank. The activity was calculated by deducting the test absorbance of the sample from the reagent control.

NADPH cytochrome c reductase (ER marker) was assayed using the protocol published by Graham for mammalian cell cultures (Graham, 1993), with described modifications (Rieder and Emr, 2001). Sample volume was 50µl (40 µl reaction buffer + 10 µl of fraction). We used rotenone (SIGMA, Germany) to exclude a reaction caused by mitochondrial protein. Activity was measured via the absorbance at 550 nm using a molar extinction coefficient of 27000/ cm*M.

α-1,6-Mannosyltransferase (Golgi marker) was tested according to established methods (Jelinek-Kelly et al., 1985; Nakajima and Ballou, 1975), using GDP-[^{14}C]-mannose, 700 Bq per assay, with α-1,6-mannobiose (Merck, Germany) as acceptor and 1-Deoxy-mannojirimycin (Merck, Germany) as mannosidase inhibitor. Fourty µl of the fraction sample in a total volume of 50 µl per assay were used. Liquid Scintillation Counting (LSC) measurements were done after purifying the samples over a Dowex 1-X8 column (1 ml,

SIGMA, Germany) and diluting the sample in 1 ml Ultima Gold / Hi Safe 2 LSC cocktail (Triskem, Germany). Efficiency of the measurement was determined by a standard curve (a dilution series of GDP-[^{14}C]-mannose).

Succinate dehydrogenase (mitochondrial marker) was assayed as described (Ackrell et al., 1978; Rieder and Emr, 2001), with following modifications: 0.1 ml of 10 mM succinate solution (in phosphate buffer, pH 7.4) were mixed with 10 µl of isolated fraction. Samples were incubated for 20 min at 37 °C and 0.1 ml INT solution (25 mg p-Iodonitrotetrazolium violet in 10 ml phosphate buffer, pH 7.4) was added. The reaction was terminated by 500 µl stop solution (10 g $C_2HCl_3O_2$, 50 ml $C_4H_8O_2$, 50 ml C_2H_6O). Negative controls were done by including stop solution before adding INT solution. The assay was performed in 96 well Nunclon 96ft plates. Absorbance at 490 nm was measured. Activity was calculated using a molar extinction coefficient of 19300 / cm*M.

Carboxypeptidase Y determination was done following the protocol of Stevens (1986) in a sample volume of 200µl containing 50µl of the fraction (Stevens et al., 1986). The substrate n-CBZ-L-Phe-L-Leu was obtained from SIGMA, Germany. No further changes were made to the protocol. To calculate activity the absorbance at 540 nm was recorded and compared to standard curve using 0.05 M L-leucine (VWR, Germany) as substrate. Activity = OD_{540} / (slope of standard curve * 0.05 M * 30 min).

α-Mannosidase assays were done according to a published method (Sarry et al., 2007), on the basis of the protocol established by (Opheim, 1978). Ten µl 0.4 mM p-nitrophenyl-α-D-mannopyranoside (SIGMA) and 70 µl 40 mM Na-acetate, pH 6.4 were added to 60 µl of fraction. The assay was incubated at 28°C for 30 min. The reaction was stopped by addition of 200 µl 1 M Na_2CO_3, while for a negative control Na_2CO_3 was added at the beginning of the reaction. Absorbance at 405 nm was recorded. For activity calculation, a molar extinction coefficient for p-nitrophenyl-α-D-mannopyranoside of 19000/cm*M was used.

Activity calculation (in cases where a molar extinction coefficient is used):
Activity = Absorbance * (Assay-Volume ml * 1000)/((molar extinction coefficient/1000) * (Sample-volume ml * min)
Photometrical quantification in 96-well format was done in a Safire2 plate reader (Tecan, Germany).

The activity was calculated by subtracting the test absorbance of the sample from the reagent control.

4.2.7.3.8 Preparation of yeast for ^{86}Rb and ^{134}Cs assays

Cs^+ accumulation assays in 96-well format MultiScreen HTS plates (Millipore, USA) were performed using 2 x 10^7 cells per well suspended in 100 µl (Heuck et al., 2010). In short, the cells were washed in H_2O and resuspended in 50 µl assay-buffer (50 mM HEPES-Tris pH 7.0, 2 % glucose). After 1 h regeneration, an equal amount of assay buffer supplied with 100 µM CsCl containing 4 kBq/ml ^{134}Cs as a radioactive tracer was added, and the plates were incubated at 30°C on a shaker at 100 rpm. At defined time points up to 18 h after Cs^+ addition, assays were stopped by washing the cells twice with HEPES-Tris pH 7.0 using a Multicreen HTS Vacuum Manifold (Millipore, USA). The retained radioactivity was measured using a Wallac WIZARD 1480 counter (Perkin Elmer, USA). For determination of the Rb^+ content after 13 h, a similar approach was performed using 50 µM RbCl, which contained 50 kBq/ml ^{86}Rb radioactive tracer. Alternatively, an equal setup was prepared using a final volume of 2 x 100 µl and a final concentration of 0.2 mM CsCl (similar tracer concentration). In case of the efflux experiments, a 50 µM uptake experiment including ^{134}Cs tracer was stopped after 13 h by removal of the medium and two washes with 100 µl cold, tracer-free assay buffer. Incubation was continued with the assay buffer including 50 µM tracer-free CsCl.

4.2.7.3.9 Cs^+ partitioning to yeast vacuoles and cell lysates

To analyse Cs^+ partitioning to vacuoles, Cs^+ from tracer-laden cells and from isolated vacuoles from such cells was determined. Cells had been grown in YPAD medium and the medium was exchanged with assay buffer. These cells, at an OD_{600} of 0.5 - 1.2, were incubated in the presence of 4 kBq/mL $^{134}Cs^+$ for 13 h. The number of cells used for radioactivity measurements were related to the isolated vacuoles based on equal amounts of α-mannosidase activity. The total vacuolar fraction from 1 L cells at O.D. 0.8 (except for the parts used for enzyme activity measurements) was dispersed in 6 ml and used for scintillation counting. The activity of α-mannosidase assay from cell lysates was determined according to the method described in 4.2.7.3.7 with following modifications: 2 mL samples of cells in assay buffer with tracer were vortexed with glass beads. Ten units of a protease inhibitor mixture (Roche Applied Science) was added and 500 µL of reagent mixture were applied. The reaction was stopped by addition of 400 µL of Na_2CO_3; the samples were centrifuged after 30 min incubation at 28 °C. The supernatant was transferred to 500 µL Tris-glycine, pH 10.4 and the absorbance was measured.

For szintillation counting, samples were dissolved in 3 ml HNO_3 for γ-spectrometrical analysis as described (chapter 4.2.2.2).

4.2.7.3.10 Preparation of yeast for determination of metal concentrations

Cultures were shaken (100 rpm) for 13 h at 30°C either in 50 ml YPAD or in 50 ml assay buffer. Cells (OD_{600} ≈ 0.7) were collected on 45 µm filters using a vacuum manifold and washed two times with ddH_2O. The filters with the harvested cells were dissolved in 2 ml of 30 % HNO_3 at 60°C over-night. After a threefold dilution with H_2O 5 ml were analysed.

4.2.7.3.11 pH sensitivity analysis of yeast strains on YPAD plates

Yeast strains WT, *sec22*Δ, *vma22*Δ, *vma2*Δ and *sec22*Δ*::Sec22* (complemented *sec22*Δ) were grown over-night in antibiotica containing liquid YPAD media (120 rpm, 30 °C) to OD_{600} = 0.8 – 1.0. A dilution series was created, and 3 µl drops were pipetted on selective YPAD plates (pH 5.5). Afterwards, the yeast was replica-plated on plates of buffered to different pH. The pH was adjusted before adding bactoagar by using the following buffers. NaOH was used for titration of the correct pH.

pH	buffer
5.5	20 mM MES
6.5	20 mM MES
8	150 mM HEPES

4.2.8 Plant methods

4.2.8.1 Plant growth conditions

4.2.8.1.1 Plant seed sterilisation and stratification

Seeds were sterilized in 80 % ethanol for 5 minutes, washed 5 times in ddH_2O and stratified for 2 days in the dark at 4°C in a volume of 500 µl ddH_2O. Alternatively, seeds were spread on sterile filter paper, soaked with 80 % ethanol and left there for 5 minutes before being transferred to soil or hydroponic cultures. In the latter case, a 2- 3 day incubation of the growth media with seeds at 4°C in the dark, covered with plastic foil, was included. Afterwards, the seeds were transferred to growth chambers for germination and the foil was removed 4 days later.

4.2.8.1.2 Cultivation of *A. thaliana* on soil

“Floragard Floradur B fein” (Floragard, Germany) was used as soil. A roughly 4:1 mixture of sieved soil to fine sand (silica) was filled in standard plant growth pods, according to the amount of plants needed. The soil was watered two times, before the swollen seeds were distributed on top. Growth conditions were either 16/8 hour light/dark cycle at 21 °C and a

relative humidity of approximately 60 %, or 14/10 hour cycle with similar conditions (Light intensity: 75 µmol*m^{-2}*s^{-1}). Longer light periods were used to achieve faster seed propagation and enhanced growth for genotyping.

4.2.8.1.3 Cultivation of *A. thaliana* in hydroponic systems

Hydroponic cultures were prepared as described by Tocquin and colleagues (2003) and modified by Kanter et al. (2010). Sterile and stratified seeds were placed on 1.5 ml Eppendorf reaction tubes, which were filled with 0.65 % Bactoagar (Difco, USA) and cut at the tip (Dremel® with PROXXON metal cutting blades, 22 mm). The preparation was done under semisterile conditions. Hydroponic growth medium was a modified Hoagland's liquid medium, containing 1.5 mM $Ca(NO_3)_2$ x 4 H_2O, 1.25 mM KNO_3, 0.75 mM $MgSO_4$ x 7 H_2O, 0.5 mM KH_2PO_4, 0.1 mM Na_2O_3Si x 9 H_2O, 0.072 mM Fe-EDTA, 0.05 mM KCl, 0.05 mM H_3BO_3, 0.01 mM $MnSO_4$ x H_20, 0.002 mM $ZnSO_4$ x 7 H_2O, 0.0015 mM $CuSO_4$ x 5 H_2O, 0.075 µM $(NH_4)_6MO_{24}$ with 0,5 g/l MES to adjust a pH of 5 to 6 (Gibeaut et al., 1997). The containers were kept air tight for 7 days, and another 3 days with limited aeration. Growth conditions were according to the long day conditions described for soil growth with humidity of 70 %. After 10 days, the media was refreshed and supplied with a mixture of tracer and stable ion as described in chapter 4.2.8.2.

4.2.8.2 Plant ion determinations

4.2.8.2.1 Cs^+/Rb^+ accumulation assays in hydroponic cultures

To determine the total cellular concentration of Cs^+ in *A. thaliana*, plants were grown for 10 days in hydroponic medium. Normal plant growth and root development was monitored and the medium was exchanged to fresh hydroponic solution (see 4.2.8.1.3). Twelfe kBq/l of ^{134}Cs (AEA Technology, Germany) together with 0,005 mM CsCl, or 24kBq/l Rb-86 (GE Healthcare, UK) and 0,005 mM RbCl. Plants were incubated for additional 10 days. After the incubation, root and shoot material was carefully rescued from the boxes, washed 2 times in water to get rid of radioactive tracer on the outside of the samples, and pooled (a minimum of 8 plants per sample). The harvested fresh samples were weighed and directly measured in a well type gamma spectrometer WIZARD 1480 (Perkin Elmer, USA) (see 4.2.2.2).

4.2.8.2.2 Preparation of plants for determination of stable metal ion concentrations

Plants were grown for 20 days in hydroponic medium, control plants mixed randomly with test plants within one box. Healthy plants were carefully detached from the agar filled Eppendorf tubes and leaf material was separated from root. Ten plants were pooled per sample, freeze dried over-night and grinded with mortar and pistille. Two mg of powder were collected and sent to analysis, as described in chapter 4.2.3.

4.2.8.3 Molecular biological methods in *A. thaliana*

4.2.8.3.1 DNA extraction from *A. thaliana* (CTAB method)

2 – 6 rosette leaves were used for extraction of 1 sample. Custom made pistilles (made of heated blue pipetting tips) were used to grind the material inside reaction tubes under liquid nitrogen. A volume of 250 µl 2 % CTAB buffer (1.4 M NaCl, 2 % CTAB, 20 mM EDTA and 100 mM Tris- HCl; pH 8 with freshly added 0.2 % Mercaptoethanol) was added on top. The solution was incubated at 65°C for 20 min in a water bath. After the samples cooled down, 200 µl of a mixture of chloroform/isoamylalcohol (24:1) was pipetted on top, and the mixture was vortexed 1 min. After centrifugation 2 min at 2000 x g, the upper phase was transferred to a new tube, avoiding the interphase. These new tubes already contained 1 µl of a 1 % LPA (linear polyacrylamide) solution. Six hundred µl of 100 % ethanol was used to precipitate the nucleic acids, by carefully mixing the solution and incubating it at -20°C for 1 hour. DNA was pelleted (4000 x g at 4°C for 10 min) and washed in 70 % ethanol, before being air-dried. Fifty µl of ddH_2O was used to resolve the DNA.

4.2.8.3.2 RNA extraction from *A. thaliana*

4.2.8.3.2.1 RNA extraction using a commercial kit

An amount of 2- 6 cauline leaves, 10 flowers, 10 stems, a single rosette, 3 seedlings or approximately 5 mg of root material were used for extraction respectively. Total RNA extraction was done using the RNeasy Plant Mini Kit (Quiagen, Germany) according to the manual, with the following changes: Material was grinded with a custom made pistille inside a reaction tube. Grinding was performed in liquid nitrogen.

4.2.8.3.2.2 RNA extraction using the Trizol® method

Plant material (approximately 5 – 50 mg) was ground in liquid nitrogen inside a reaction tube. Three hundred µl Trizol® reagent (SIGMA, Germany) was added on top by flooding the custom made pistilles. Samples were vortexed for 60 sec, and the solution was incubated at 60 °C in a water bath for 5 min with additional vortexing in between. Sixty µl of chloroform were added on top. The tubes were vortexed for 15 sec and incubated at room temperature for 5 min, before a centrifugation step of 15 min at 2000 x g was done. The aqueous phase was transferred to a new tube, which already contained 2 µl of a high salt solution (50 mM Na- citrate and 100 mM NaCl). Five hundred µl of isopropanol (100 %) were added. Incubation at -20°C for 1 hour was included. After a centrifugation at maximum speed for 10 min at 4°C, the pellet was washed with 500 µl of 80 % ethanol (centrifuge 2 min at maximum speed in the cold), before the pellet was air dried. The RNA was resolved in 40 µl RNAse free water.

4.2.8.4 Genotyping of SALK_042619

PCR-based genotyping of genomic DNA isolated from the mutant line was done with the following three fragments: I) SEC22_RP + SEC22_LP; II) SEC22_RP + SALK_LBb1.3; III) SEC22_LP + SALK_LBb1.3. Homozygous progeny was selected and loss of segregation was monitored in the next generation.

4.2.8.5 Cloning strategy for stable transformation of *A. thaliana* SALK_042619 with a promoter:*At1g11890*:terminator construct

Genomic *A. thaliana SEC22* including promoter, genomic sequence and 3' UTR of *At1g11890*, was constructed by amplification of three separate fragments, using I) *PromSecfwXmaI*, + *PromSecrevClaI*; II) *SEC22fwClaI* + *SEC22revXhoI*; III) *TermSecfwXhoI* + *TermSecrevPstI*, cut by restriction digest (XmaI, XhoI or PstI), together with the vector pBGW,0 (Invitrogen) (XmaI and PstI). Ligation of the desired fragments was done using T4 DNA ligase. Constructs were cloned in *E. coli* DH5α and tested by restriction digest of extracted plasmids and sequencing.

4.2.8.6 Transformation of *A. thaliana* with *A. tumefaciens* (floral dip)

This method was described as an easy and efficient way of stably transforming *A. thaliana* (Clough and Bent, 1998). Optimal efficiency was found for plants grown at 16 h light cycle in 22°C for roughly 4 weeks. Flower opening was used as the time for transformation. Already opened flowers were cut off before dipping. The bacterial suspension was prepared from a single positively selected colony. From a 2 ml overnight culture, 300 ml of fresh LB medium (including antibiotics) was inoculated (1 ml) and grown overnight at 170 rpm shaking , 28°C to an OD_{600} of 1.5. Bacteria were centrifuged for 10 min at 4°C with 1000 x g, and the cells were resuspended in 50 ml of infiltration medium (5 % sucrose and 0.05 % Silwet L-77 from Lehleseeds, USA) and diluted to OD_{600} = 0.8. A sterile glass container was flooded with the suspension, and the plants (in soil pods) were dipped with their inflorescence for 10 s. After 20 min at room temperature plants were transferred back to the growth conditions, covered in plastic. The developing seed generation was named T_0 and subjected to a selection process following the Mendelian rules. For selection of pBGW,0- construct transformed plants, a Basta™ resistance was used (spraying Basta™ on 5 day old seedlings, 2 times a week). For confirmation, DNA was extracted, and a PCR-based genotyping was done.

4.3 Bioinformatics and Webtools

Alignments were done with GeneDoc (www.psc.edu/biomed/genedoc) (Nicholas et al., 1997). . Plasmid construction was planned using APE (a plasmid editor) by equi4 software. Alignment based phylogeny was prepared at

http://www.phylogeny.fr/version2_cgi/advanced.cgi. BLAST searches for Sec22p homologues were done online at http://web.expasy.org/blast/ (Altschul et al., 1997). Additional services and tools are indicated in the figure legends. Yeast interaction database search was carried out with BioGrid (http://thebiogrid.org). Co-response analysis was done at CSB.DB (http://csbdb.mpimp-golm.mpg.de/cgi-bin/csbdb_cor.cgi) by the Comprehensive System Biology Project of the Max Planck Institute, Golm.

4.4 Mathematical modelling approach: Caesium flux model

Programs used were R (R Development Core Team), SAAMII (Barrett et al., 1998) and SimbTUM v.0.23 by Prof. Dr. Christina Kuttler and Prof. Dr. Johannes Müller (TUM, July 2012). The source code for the calculation can be requested from Prof. Dr. Johannes Müller, Center for Mathematical Sciences, Technische Universtität München.

We develop a linear model for Cs^+ flux in yeast cells. Time scale analysis is used to reduce dimension and number of parameters of the model. Data for wild type and mutant are analysed, and significance tests for the difference of parameters are performed. The model is extended to Michaelis-Menten kinetics in order to obtain estimates of K_m-values.

4.4.1 Model

Model development. With all-linear reaction kinetics the changes in the cytoplasmic Cs^+ concentration due to the corresponding fluxes at the surfaces to the external medium and to the vacuole can be formulated (parameters defined according to Fig. 13): k_1c denotes the flow from outside into the cytoplasm with rate constant k_1 and k_2x describes the efflux from the cytoplasm into the outer space with rate constant k_2; similarly, k_3x denotes the flux from cytoplasm into the vacuole with rate constant k_3 and k_4y the flux from the vacuole into the cytoplasm with rate constant k_4 [2].

To describe the changes in concentration in the external medium and in the vacuole, the transferred molar amounts, i.e. the product of rate constant, concentration and volume of a compartment, are divided by the volume of the respective compartments, i.e. V_1 and V_3. Then the equations describing the changes in time of the concentrations in the different compartments read

[2] We only refer to specific characteristics of a single cell as reference point in order to obtain an invariance of the rate constants with respect to change of the test volume V_1 or change of the cell number N.

$$c' = N\frac{V_2}{V_1}\left(-k_1 c + k_2 x\right)$$
$$x' = k_1 c - k_2 x - k_3 x + k_4 y$$
$$y' = \frac{V_2}{V_3}\left(k_3 x - k_4 y\right).$$

The biphasic behavior of the uptake curves indicated that the flow from cytoplasm into the vacuole is not fully present from the beginning, but is activated in reaction to the Cs^+ influx into the cytoplasm (and thus, increasing *x*). In a further step of the modeling, we use this interpretation of the data as a hypothesis to refine the set-up slightly. We introduce the function *s(t)* by

$$s(t) = t^n / (thresh^n + t^n).$$

This Hill function modulates the rate k_3, allowing to model a situation where after a certain time this transport process is switched on (compare Fig. 15). Thus, we obtain the model

$$c' = N\frac{V_2}{V_1}\left(-k_1 c + k_2 x\right)$$
$$x' = k_1 c - k_2 x - k_3 s(t) x + k_4 y$$
$$y' = \frac{V_2}{V_3}\left(k_3 s(t) x - k_4 y\right)$$
$$s(t) = t^n /(thresh^n + t^n).$$

c, *x* and *y* are not measured directly, but the average concentration within the cells *tot*

$$tot = \frac{V_2 x + V_3 y}{V_2 + V_3}.$$

Dimension reduction. Next we aimed at reducing the three-dimensional model developed above to a one-dimensional model. On the one hand, simulations become faster and the numerical error of the simulations is decreased. At the same time, we are able to scale away one parameter about which the experimental data only give imprecise information: in accordance to earlier experiments (Avery, 1995) preliminary data analysis has found that the time scale for the transport through the vacuole membrane is fast (once it is “switched on”), but the exact time scale is hard to recognize. As a parameter that is only vaguely known is likely to spill statistics, singular perturbation theory is applied in order to remove this parameter from the model (assuming a quasi-steady state for the concentrations in the vacuole). Together with mass conservation the three-dimensional model can be reduced to a one dimensional equation.

Thereto, it is convenient to re-parametrize the rates k_3 and k_4

$$k_3 = \Gamma\tau,\ k_4 = \Gamma(1-\tau),$$
$$\Gamma = k_3 + k_4.$$

τ denotes the equilibrium ratio between x and y in the stationary state (with $s(t) \rightarrow 1$ and $k_3 x = k_4 y$), i.e. τ contains the information about the asymptotic ratio between x and y, while Γ represents the time scale at which this ratio is assumed, given that $s(t) = 1$.

$$\lim_{1\to\infty} \frac{y(t)}{x(t)} = \frac{\tau}{1-\tau}.$$

The reparametrization leads to:

$$c' = N\frac{V_2}{V_1}\left(-k_1 c + k_2 x\right)$$
$$x' = k_1 c - k_2 x - \Gamma\tau\, s(t)x + \Gamma\,(1-\tau)y$$
$$y' = \frac{V_2}{V_3}\left(\Gamma\tau\, s(t)x - \Gamma\,(1-\tau)y\right).$$

As mentioned above, a preliminary analysis of the present dataset indicates that Γ is large, which would be also in accordance with biological experience that vacuolar Cs^+ compartmentalisation is large (Avery, 1995). We express this observation by defining

$$\Gamma = 1/\varepsilon,\ \ 0 < \varepsilon << 1.$$

And thus:

$$c' = N\frac{V_2}{V_1}\left(-k_1 c + k_2 x\right)$$
$$x' = k_1 c - k_2 x - \frac{1}{\varepsilon}\tau\, s(t)x + \frac{1}{\varepsilon}(1-\tau)y$$
$$\varepsilon y' = \frac{V_2}{V_3}\left(\tau\, s(t)x - (1-\tau)y\right).$$

For *tot* we obtain the equation

$$tot' = \frac{V_2}{(V_2+V_3)}(k_1 c - k_2 x).$$

Replacing x by means of $V_2 x = (V_2 + V_3)\, tot - V_3 y$, a system in the standard form of singular perturbation theory is obtained:

$$c' = N\left\{-k_1\frac{V_2}{V_1}c + k_2\frac{1}{V_1}\left[(V_2+V_3)\,tot - V_3 y\right]\right\} \quad \text{(I)}$$

$$tot' = k_1\frac{V_2}{(V_2+V_3)}c - k_2\frac{1}{(V_2+V_3)}\left[(V_2+V_3)\,tot - V_3 y\right] \quad \text{(II)}$$

$$\varepsilon y' = \frac{1}{V_3}\tau\, s(t)\left[(V_2+V_3)\,tot - V_3 y\right] - \frac{V_2}{V_3}(1-\tau)\, y.$$

The singular limit ε → 0 yields the slow manifold, i.e. the quasi-steady state,

$$0 = \frac{1}{V_3}\tau\, s(t)\left[(V_2+V_3)\,tot - V_3 y\right] - \frac{V_2}{V_3}(1-\tau)\, y$$

$$\Rightarrow y = \frac{(V_2+V_3)\,\tau\, s(t)}{V_3\,\tau\, s(t) + V_2(1-\tau)}\,tot.$$

x can be computed from the definition of *tot* and this relation:

$$x = \frac{(V_2+V_3)\,tot - V_3 y}{V_2} = \frac{(V_2+V_3)(1-\tau)}{V_3\tau\, s(t) + V_2(1-\tau)}\,tot.$$

Replacing *y* in the equations (I) and (II) yields the slow system. We obtain

$$c' = N\frac{V_2}{V_1}\left[-k_1 c + k_2\frac{(V_2+V_3)(1-\tau)}{V_3\tau\cdot s(t) + V_2(1-\tau)}\,tot\right]$$

$$tot' = k_1\frac{V_2}{(V_2+V_3)}c - k_2\frac{V_2(1-\tau)}{V_3\tau\, s(t) + V_2(1-\tau)}\,tot.$$

It is possible to reduce the system to one dimension: mass conservation implies

$$\frac{d}{dt}\left[V_1 c + N(V_2+V_3)tot\right] = 0.$$

Defining $c_0 = c(0)$, we find

$$V_1 c = V_1 c_0 - N(V_2+V_3)tot.$$

Using this relation, we find an equation for *tot* alone

$$tot' = k_1\frac{V_2}{(V_2+V_3)}c_0 - \left(N\frac{V_2}{V_1}k_1 + \frac{V_2(1-\tau)}{V_3\tau\cdot s(t) + V_2(1-\tau)}\,k_2\right)tot.$$

The time dependence of all other concentrations can be computed once we know *tot(t)*,

$$c(t) = c_0 - N\frac{V_2 + V_3}{V_1}\,tot(t)$$

$$x(t) = \frac{(V_2 + V_3)\,(1-\tau)}{V_3\,\tau\,s(t) + V_2\,(1-\tau)}\,tot(t)$$

$$y(t) = \frac{(V_2 + V_3)\,\tau\,s(t)}{V_3\,\tau\cdot s(t) + V_2\,(1-\tau)}\,tot(t).$$

Statistical tests for parameter estimations. Log-likelihood ratio tests were performed according to Mood, Graybill and Boes (1963). First, the wild-type and mutant data are fitted with independent sets of parameters. In order to test whether a certain parameter differs significantly between wild type and mutant, the model is fitted again to both parameter sets, but this time under the restriction that this single parameter is identical for wild-type and mutant. All other eight parameters are still allowed to differ. Necessarily, the log-likelihood for this fit is smaller than that for the fit with all ten parameters. Asymptotically, for many data, the doubled difference between the two log-likelihood values is distributed according to a Chi square distribution with one degree of freedom,

T = 2 * (conditioned log-likelihood – unconditioned log-likelihood) ~ χ^2.

As we perform seven tests, we use the Bonferoni-principle to correct for multiple testing, i.e. we multiply each significance level by the number of tests performed (Tab. 21). The most significant parameter was τ.The results of the linear *de-novo* model for the described experiment allowed a fit of the biphasic experimental data (Fig. 12) with well defined parameters (Tab. 9) and a significant reduction of the parameter τ to estimate the mutant data.

parameter	T	p-value	p-value with Bonferoni correction
k_1	13.4	$2.5*10^{-4}$	$1.76*10^{-3}$
k_2	4.6	0.03	0.21
k_1/k_2	0.43	0.511	≈ 1
$k_1 + k_2$	12.36	$4.4*10^{-4}$	0.003
τ	66.6	$3.3*10^{-16}$	$2.3*10^{-15}$
n	5.87	0.015	0.077
thresh	16.1	$6.1*10^{-5}$	$4.2*10^{-4}$

Tab. 21. **Log-likelihood ratio tests for equality of parameters between wild type and mutant.**

Modeling of Cs^+ fluxes including Michaelis-Menten terms.

Since the experiment with 200 µM Cs^+ in the external medium resulted in much lower than fourfold changes in the cellular Cs^+ concentration in comparison to the 50 µM experiment, both experiments could not be jointly interpreted by an all-linear model. Instead, the saturation of fluxes due to Michaelis-Menten kinetics at higher concentrations plays a greater role. The strongest change in Cs^+ concentration (fourfold) occurred in the external medium, whereas the total internal concentration only was risen 1.4- and 2.2-fold.

Therefore, we first considered to include a Michaelis-Menten term for the flux dependent on the external concentration, i.e. to substitute the linear term $k_1 c$ by $\frac{\hat{k}_1 c}{K_{M,1} + c}$, to jointly model the data sets from both experiments with an initial external concentration of 50 µM and 200 µM Cs^+. The rate constants and all parameters are labeled with a hat, e.g. $\hat{k}_i$, to distinguish between the linear model and the Michaelis-Menten including model; in case of Michaelis-Menten terms, $\hat{k}_i$ are not canonical rate constants but indicate $v_{max,i}$ of these fluxes.

This measure (for details of the modeling, see below) already improved the fits in a joint analysis of wild type and *sec22Δ* mutant data at both external Cs^+ concentrations. Thus, the Michaelis-Menten repression of the influx at 200 µM external Cs^+ was an important factor. To further improve the modeling we systematically substituted additional processes by Michaelis-Menten terms, such as $k_1 c$ plus $k_3 x$, $k_1 c$ plus $k_2 x$ plus $k_3 x$, and $k_1 c$ *plus* $k_2 x$ *plus* $k_3 x$ *plus* $k_4 y$. According to both Akaike and Bayesian information criteria (AIC, BIC) these additional changes lead to a considerable further improvement of the modeling. Yet, the replacement of all fluxes by Michaelis-Menten terms was not superior to replacing only of $k_1 c$ plus $k_3 x$, i.e. the additional consideration of $k_2 x$ and $k_4 y$ did not further improve the fit. In particular, the $k_2 x$-related flux tended to stay in the linear phase indicated by a large k_M value ($k_{M,2} \approx 278$ mM for wild type). Thus, substituting k_1 and k_3 by Michaelis-Menten terms could be used as a preliminary expansion of the model, leaving the fluxes $k_2 x$ and $k_4 y$ linear:

$$c' = N \frac{V_2}{V_1} \left(- \frac{\hat{k}_1 c}{K_{M,1} + c} + \hat{k}_2 x \right)$$

$$x' = \frac{\hat{k}_1 c}{K_{M,1} + c} - \hat{k}_2 x - \frac{\hat{k}_3 s(t) x}{K_{M,3} + x} + \hat{k}_4 y$$

$$y' = \frac{V_2}{V_3} \left(\frac{\hat{k}_3 s(t) x}{K_{M,3} + x} - \hat{k}_4 y \right)$$

$$s(t) = t^n / (thresh^n + t^n).$$

We again assume a separation of time scales and re-parameterize the system[3] according to

$$\hat{k}_3 = \hat{\Gamma}\,\hat{\tau}\,mM,$$
$$\hat{k}_4 = \hat{\Gamma}(1-\hat{\tau}),$$
$$\hat{\Gamma} = \hat{k}_3\,mM + \hat{k}_4.$$

In order to fit this model we do not reduce it by means of time scale analysis. However, in this case we rather focus on sensible point estimates, and not on statistical tests for differences; this task requires only less sophisticated methods.

The model procedure is equivalent to the one described above for the linear model.

4.4.2 Uncertainty of model parameters

Uncertainties were calculated using described evaluation methods (Li et al., 2011) and will not be repeated here in detail.

4.4.3 Sensitivity analysis

The influence of the single parameters on certain traits in the compartment model (Global sensitivity analysis) was assessed using a partial rank correlation component (PRCC) analysis, according to Saltelli et al., 2008 and Li et al., 2011. The partial correlation coefficient describes the power of correlation between selected output and the input parameters, while eliminating effects caused by correlation between this chosen output and other input parameters. The single parameters used as “input” parameters in our model were tested against the Cs^+ concentration in cytoplasm and the vacuole. Analysis was done with a program using a code modified from Fortran 77 computer program (Iman et al., 1985), called Fortran 95 program.

[3] Since not all fluxes are changed to Michaelis-Menten terms, the units of the parameters are different.

References

Aberth, W., and Burlingame, A.L. (1984). Comparison of three geometries for a cesium primary beam liquid secondary ion mass spectrometry source. Anal Chem *56*, 2915-2918.

Ackrell, B.A., Kearney, E.B., and Singer, T.P. (1978). Mammalian succinate dehydrogenase. Methods Enzymol *53*, 466-483.

Adelman, W.J., Jr., and French, R.J. (1978). Blocking of the squid axon potassium channel by external caesium ions. J Physiol *276*, 13-25.

Alemán, F., Nieves-Cordones, M., Martinéz, V., and Rubio, F. (2011). Root K^+ acquisition in plants: the *Arabidopsis thaliana* model. Plant Cell Physiol *52*, 1603-1612.

Alexakhin, R.M., Frissel, M.J., Schulte, E.H., Prister, B.S., Vetrov, V.A., and Wilkins, B.T. (1993). Change in land use and crop selection. Sci Total Environ *137*, 169-172.

Alexakhin, R.M., Sanzharova, N.I., Fesenko, S.V., Spiridonov, S.I., and Panov, A.V. (2007). Chernobyl radionuclide distribution, migration, and environmental and agricultural impacts. Health Phys *93*, 418-426.

Alonso, J.M., and Stepanova, A.N. (2003). T-DNA mutagenesis in Arabidopsis. Methods Mol Biol *236*, 177-188.

Altschul SF*, et al.* (1997) Gapped BLAST and PSI-BLAST: a new generation of protein database search programs. *Nucleic Acids Res* 25(17):3389-3402.

Amtmann, A., Fischer, M., Marsh, E.L., Stefanovic, A., Sanders, D., and Schachtman, D.P. (2001). The wheat cDNA LCT1 generates hypersensitivity to sodium in a salt-sensitive yeast strain. Plant Physiol *126*, 1061-1071.

Ariño, J., Ramos, J., and Sychrová, H. (2010). Alkali metal cation transport and homeostasis in yeasts. Microbiol Mol Biol Rev *74*, 95-120.

Armstrong, W.M., and Rothstein, A. (1964). Discrimination between Alkali Metal Cations by Yeast. I. Effect of Ph on Uptake. J Gen Physiol *48*, 61-71.

Armstrong, W.M., and Rothstein, A. (1967). Discrimination between alkali metal cations by yeast. II. Cation interactions in transport. J Gen Physiol *50*, 967-988.

Arpin, M., Reboud, A.M., and Reboud, J.P. (1972). Conformational changes of large ribosomal subunits of rat liver, induced by some monovalent cations. Biochim Biophys Acta *277*, 134-139.

Avery, S.V. (1995). Caesium accumulation by microorganisms: uptake mechanisms, cation competition, compartmentalization and toxicity. J Ind Microbiol *14*, 76-84.

Avery, S.V. (1996). Fate of caesium in the environment: Distribution between the abiotic and biotic components of aquatic and terrestrial ecosystems. J Environ Radioactiv *30*, 139-171.

Avery, S.V., Codd, G.A., and Gadd, G.M. (1993). Transport kinetics, cation inhibition and intracellular location of accumulated caesium in the green microalga *Chlorella salina*. J Gen Microbiol, 827 - 834.

Bakken, L.R., and Olsen, R.A. (1990). Accumulation of radiocaesium in fungi. Can J Microbiol *36*, 704-710.

Balague, C., Lin, B., Alcon, C., Flottes, G., Malmstrom, S., Kohler, C., Neuhaus, G., Pelletier, G., Gaymard, F., and Roby, D. (2003). HLM1, an essential signaling component in the hypersensitive response, is a member of the cyclic nucleotide-gated channel ion channel family. Plant Cell *15*, 365-379.

Bankaitis, V.A., Johnson, L.M., and Emr, S.D. (1986). Isolation of yeast mutants defective in protein targeting to the vacuole. Proc Natl Acad Sci U S A *83*, 9075-9079.

Banuelos, M.A., and Rodriguez-Navarro, A. (1998). P-type ATPases mediate sodium and potassium effluxes in *Schwanniomyces occidentalis*. J Biol Chem *273*, 1640-1646.

Baretto, L., Canadell, D., Petrezsélyová, S., Navarrete, C., Marešová, L., Peréz-Valle, J., Herrera, R., Olier, I., Giraldo, J., Sychrová, H.*, et al.* (2011). A Genomewide Screen for Tolerance to Cationic Drugs Reveals Genes Important for Potassium Homeostasis in *Saccharomyces cerevisiae*. Eukaryot Cell *10*, 1241-1250.

Barrett, P.H., Bell, B.M., Cobelli, C., Golde, H., Schumitzky, A., Vicini, P., and Foster, D.M. (1998). SAAM II: Simulation, Analysis, and Modeling Software for tracer and pharmacokinetic studies. Metabolism *47*, 484-492.

Bassham, D.C. (2007). Plant autophagy--more than a starvation response. Curr Opin Plant Biol *10*, 587-593.

Bassham, D.C., and Blatt, M.R. (2008). SNAREs: cogs and coordinators in signaling and development. Plant Physiol *147*, 1504-1515.

Bassil, E., Tajima, H., Liang, Y.C., Ohto, M.A., Ushijima, K., Nakano, R., Esumi, T., Coku, A., Belmonte, M., and Blumwald, E. (2011). The Arabidopsis Na^+/H^+ antiporters NHX1 and NHX2 control vacuolar pH and K^+ homeostasis to regulate growth, flower development, and reproduction. Plant Cell *23*, 3482-3497.

Beger, R.M., and Buerger, M.J. (1967). The crystal structure of the mineral pollucite. Proc Natl Acad Sci U S A *58*, 853-854.

Benito, B., Quintero, F.J., and Rodriguez-Navarro, A. (1997). Overexpression of the sodium ATPase of *Saccharomyces cerevisiae*: conditions for phosphorylation from ATP and Pi. Biochim Biophys Acta *1328*, 214-226.

Bertl, A., Ramos, J., Ludwig, J., Lichtenberg-Frate, H., Reid, J., Bihler, H., Calero, F., Martinez, P., and Ljungdahl, P.O. (2003). Characterization of potassium transport in wild-type and isogenic yeast strains carrying all combinations of *trk1*, *trk2* and *tok1* null mutations. Mol Microbiol *47*, 767-780.

Bertl, A., Reid, J.D., Sentenac, H., and Slayman, C.L. (1997). Functional comparison of plant inward-rectifier channels expressed in yeast. J Exp Bot *48 Spec No*, 405-413.

Bihler, H., Eing, C., Hebeisen, S., Roller, A., Czempinski, K., and Bertl, A. (2005). TPK1 is a vacuolar ion channel different from the slow-vacuolar cation channel. Plant Physiol *139*, 417-424.

Bihler, H., Slayman, C.L., and Bertl, A. (1998). NSC1: a novel high-current inward rectifier for cations in the plasma membrane of *Saccharomyces cerevisiae*. FEBS Lett *432*, 59-64.

Borst-Pauwels, G.W. (1981). Ion transport in yeast. Biochim Biophys Acta *650*, 88-127.

Bossemeyer, D., Schlosser, A., and Bakker, E.P. (1989). Specific cesium transport via the *Escherichia coli* Kup (TrkD) K^+ uptake system. J Bacteriol *171*, 2219-2221.

Bowman, B.J., and Slayman, C.W. (1979). The effects of vanadate on the plasma membrane ATPase of *Neurospora crassa*. J Biol Chem *254*, 2928-2934.

Brachmann, C.B., Davies, A., Cost, G.J., Caputo, E., Li, J., Hieter, P., and Boeke, J.D. (1998). Designer deletion strains derived from Saccharomyces cerevisiae S288C: a useful set of strains and plasmids for PCR-mediated gene disruption and other applications. Yeast *14*, 115-132.

Bresinsky, A., Körner, C., Kadereit, J.W., Neuhaus, G., and Sonnewald, U. (2008). Strasburger - Lehrbuch der Botanik, 36th edn (Heidelberg, Spektrum Akademischer Verlag).

Broadley, M.R., Escobar-Gutierrez, A.J., Bowen, H.C., Willey, N.J., and White, P.J. (2001). Influx and accumulation of Cs^+ by the *akt1* mutant of *Arabidopsis thaliana* (L.) Heynh. lacking a dominant K^+ transport system. J Exp Bot *52*, 839-844.

Broadley, M.R., Willey, N.J., and Mead, A. (1999). A method to assess taxonomic variation in shoot caesium concentration among flowering plants. Environ Pollut *106*, 341-349.

Broadley, M.R., and White, P.J. (2012). Some elements are more equal than others: soil-to-plant transfer of radiocaesium and radiostrontium, revisited. Plant and Soil *355*, 23-27.

Broser, I., and Kallmann, H. (1947). The Elementary Process of Light Stimulation in Luminous Substances by alpha-Particles, Fast Electrons, and gamma-Quanta, II. Journal Name: Zeitschrift fuer Naturforschung (West Germany) Divided into Z Nautrforsch, A, and Z Naturforsch, B: Anorg Chem, Org Chem, Biochem, Biophys,; Journal Volume: Vol: 2a; Other Information: Orig Receipt Date: 30-JUN-49, Medium: X; Size: Pages: 642-650.

Burke, B., Dawson, D., and Stearns, T. (2000). Methods in Yeast Genetics: A Cold Spring Harbor Laboratory Course Manual (Cold Spring Harbor, New York, Cold Spring Harbor Laboratory Press).

Burnham, K.P., and Anderson, D.R. (2002). Model selection and multimodel inference: a practical information-theoretic approach (Berlin, Springer).

Burnham, K.P., Anderson, D.R., and Huyvaert, K.P. (2011). AIC model selection and multimodel inference in behavioral ecology: some background, observations, and comparisons. Behav Ecol Sociobiol *65*, 23-35.

Burri, L., Varlamov, O., Döge, C.A., Hofmann, K., Beilharz, T., Rothman, J.E., Söllner, T.H., and Lithgow, T. (2003). A SNARE required for retrograde transport to the endoplasmic reticulum. Proc Natl Acad Sci U S A *100*, 9873-9877.

Cabrera, E., Alvarez, M.C., Martin, Y., Siverio, J.M., and Ramos, J. (2012). K^+ uptake systems in the yeast *Hansenula polymorpha*. Transcriptional and post-translational mechanisms involved in high-affinity K^+ transporter regulation. Fungal Genet Biol. 49(9):755-763

Cagnac, O., Aranda-Sicilia, M.N., Leterrier, M., Rodriguez-Rosales, M.P., and Venema, K. (2010). Vacuolar cation/H^+ antiporters of *Saccharomyces cerevisiae*. J Biol Chem *285*, 33914-33922.

Cagnac, O., Leterrier, M., Yeager, M., and Blumwald, E. (2007). Identification and characterization of Vnx1p, a novel type of vacuolar monovalent cation/H^+ antiporter of *Saccharomyces cerevisiae*. J Biol Chem *282*, 24284-24293.

Camacho, M., J., R., and Rodriguez Navarro, A. (1981). Potassium requirements of *Saccharomyces cerevisiae*. Current Microbiology *6*, 295-299.

Carini, F. (2001). Radionuclide transfer from soil to fruit. J Environ Radioact *52*, 237-279.

Carini, F. (2009). Radionuclide transfer to fruit in the IAEA TRS 364 Revision. J Environ Radioact *100*, 752-756.

Chatre, L., Brandizzi, F., Hocquellet, A., Hawes, C., and Moreau, P. (2005). Sec22 and Memb11 are v-SNAREs of the anterograde endoplasmic reticulum-Golgi pathway in tobacco leaf epidermal cells. Plant Physiol *139*, 1244-1254.

Cline, J.F., and Hungate, F.P. (1960). Accumulation of Potassium, Cesium, and Rubidium in Bean Plants Grown in Nutrient Solutions. Plant Physiol *35*, 826-829.

Clough, S.J., and Bent, A.F. (1998). Floral dip: a simplified method for Agrobacterium-mediated transformation of *Arabidopsis thaliana*. Plant J *16*, 735-743.

Collander, R. (1941). Selective Absorption of Cations by Higher Plants. Plant Physiol *16*, 691-720.

Coronado, R., Rosenberg, R.L., and Miller, C. (1980). Ionic selectivity, saturation, and block in a K^+-selective channel from sarcoplasmic reticulum. J Gen Physiol *76*, 425-446.

Davenport, R. (2002). Glutamate receptors in plants. Ann Bot *90*, 549-557.

Davis, J.J. (1963). Cesium and its relationships to potassium in ecology. In Radioecology, V. Schultz, and A.W. Klement, eds. (New York, Reinhold), pp. 339-356.

Demidchik, V., Davenport, R.J., and Tester, M. (2002). Nonselective cation channels in plants. Annu Rev Plant Biol *53*, 67-107.

Dichtl, B., Stevens, A., and Tollervey, D. (1997). Lithium toxicity in yeast is due to the inhibition of RNA processing enzymes. EMBO J *16*, 7184-7195.

Dietrich, L.E., Gurezka, R., Veit, M., and Ungermann, C. (2004). The SNARE Ykt6 mediates protein palmitoylation during an early stage of homotypic vacuole fusion. EMBO J *23*, 45-53.

Dietrich, L.E., LaGrassa, T.J., Rohde, J., Cristodero, M., Meiringer, C.T., and Ungermann, C. (2005). ATP-independent control of Vac8 palmitoylation by a SNARE subcomplex on yeast vacuoles. J Biol Chem *280*, 15348-15355.

Dighton, J., Clint, G.M., and Poskitt, J. (1991). Uptake and accumulation of ^{137}Cs by upland grassland soil fungi: a potential pool of Cs^+ immobilization. Mycol Res *95*, 1052-1056.

Doyle, D.A., Morais Cabral, J., Pfuetzner, R.A., Kuo, A., Gulbis, J.M., Cohen, S.L., Chait, B.T., and MacKinnon, R. (1998). The structure of the potassium channel: molecular basis of K^+ conduction and selectivity. Science *280*, 69-77.

El-Kasmi, F., Pacher, T., Strompen, G., Stierhof, Y.D., Müller, L.M., Koncz, C., Mayer, U., and Jürgens, G. (2011). Arabidopsis SNARE protein SEC22 is essential for gametophyte development and maintenance of Golgi-stack integrity. Plant J *66*, 268-279.

Entry, J.A., Vance, N.C., Hamilton, M.A., Zabowski, D., Watrud, L.S., and Adriano, D.C. (1996). Phytoremediation of soil contaminated with low concentrations of radionuclides. Water Air Soil Pollut, 167-176.

Epstein, E. (1972). Mineral nutrition of plants: principles and perspectives (New York, Wiley).

Fell, G.L., Munson, A.M., Croston, M.A., and Rosenwald, A.G. (2011). Identification of yeast genes involved in K^+ homeostasis: loss of membrane traffic genes affects K^+ uptake. G3 (Bethesda) *1*, 43-56.

Filipović-Vinceković, N., Barišić, D., Mašić, N., and Lulić, S. (2005). Distribution of fallout radionuclides through soil surface layer. J Radioanal Nucl Ch *148*, 53-62.

Filippini, F., Rossi, V., Galli, T., Budillon, A., D'Urso, M., and D'Esposito, M. (2001). Longins: a new evolutionary conserved VAMP family sharing a novel SNARE domain. Trends Biochem Sci *26*, 407-409.

Garciadeblas, B., Rubio, F., Quintero, F.J., Banuelos, M.A., Haro, R., and Rodriguez-Navarro, A. (1993). Differential expression of two genes encoding isoforms of the ATPase involved in sodium efflux in *Saccharomyces cerevisiae*. Mol Gen Genet *236*, 363-368.

Gari, E., Piedrafita, L., Aldea, M., and Herrero, E. (1997). A set of vectors with a tetracycline-regulatable promoter system for modulated gene expression in *Saccharomyces cerevisiae*. Yeast *13*, 837-848.

Gaxiola, R.A., Rao, R., Sherman, A., Grisafi, P., Alper, S.L., and Fink, G.R. (1999). The *Arabidopsis thaliana* proton transporters, AtNhx1 and Avp1, can function in cation detoxification in yeast. Proc Natl Acad Sci U S A *96*, 1480-1485.

Gaymard, F., Pilot, G., Lacombe, B., Bouchez, D., Bruneau, D., Boucherez, J., Michaux-Ferriere, N., Thibaud, J.B., and Sentenac, H. (1998). Identification and disruption of a plant shaker-like outward channel involved in K^+ release into the xylem sap. Cell *94*, 647-655.

Gerstmann, U.C., and Schimmack, W. (2006). Soil-to-grain transfer of fallout ^{90}Sr for 28 winter wheat cultivars. Radiat Environ Biophys *45*, 187-194.

Ghosh, A., Ghosh, A.K., Sharma, A., and Talukder, G. (1991). Modification of cesium toxicity by calcium in mammalian system. Biol Trace Elem Res *31*, 139-145.

Ghosh, A., Sharma, A., and Talukder, G. (1993). Effects of cesium on cellular systems. Biol Trace Elem Res *38*, 165-203.

Gibeaut, D.M., Hulett, J., Cramer, G.R., and Seemann, J.R. (1997). Maximal biomass of *Arabidopsis thaliana* using a simple, low-maintenance hydroponic method and favorable environmental conditions. Plant Physiol *115*, 317-319.

Gietz, R.D., Schiestl, R.H., Willems, A.R., and Woods, R.A. (1995). Studies on the transformation of intact yeast cells by the LiAc/SS-DNA/PEG procedure. Yeast *11*, 355-360.

Graham, J. (1993). The identification of subcellular fractions from mammalian cells. Methods Mol Biol *9*, 1-18.

Graham, L.A., Hill, K.J., and Stevens, T.H. (1998). Assembly of the yeast vacuolar H^+-ATPase occurs in the endoplasmic reticulum and requires a Vma12p/Vma22p assembly complex. J Cell Biol 142, 39-49.

Hall, P., Pham, T., Wand, M.P., and Wang, S.S.J. (2011). Asymptotic Normality and Valid Inference for Gaussian Variational Approximation. Ann Stat *39*, 2502-2532.

Hamby, D.M. (1994). A review of techniques for parameter sensitivity analysis of environmental models. Environmental Monitoring and Assessment *32*, 135-154.

Hampton, C.R., Bowen, H.C., Broadley, M.R., Hammond, J.P., Mead, A., Payne, K.A., Pritchard, J., and White, P.J. (2004). Cesium toxicity in *Arabidopsis*. Plant Physiol *136*, 3824-3837.

Hampton, C.R., Broadley, M.R., and White, P.J. (2005). Short Review: the mechanisms of radiocaesium uptake by *Arabidopsis* roots. Nukleonika *50*, 3-8.

Hanahan, D. (1983). Studies on transformation of *Escherichia coli* with plasmids. J Mol Biol *166*, 557-580.

Haro, R., Garciadeblas, B., and Rodriguez-Navarro, A. (1991). A novel P-type ATPase from yeast involved in sodium transport. FEBS Lett *291*, 189-191.

Haro, R., and Rodriguez-Navarro, A. (2002). Molecular analysis of the mechanism of potassium uptake through the TRK1 transporter of *Saccharomyces cerevisiae*. Biochim Biophys Acta *1564*, 114-122.

Heuck, S., Gerstmann, U.C., Michalke, B., and Kanter, U. (2010). Genome-wide analysis of caesium and strontium accumulation in *Saccharomyces cerevisiae*. Yeast *27*, 817-835.

Hill, J.E., Myers, A.M., Koerner, T.J., and Tzagoloff, A. (1986). Yeast/*E. coli* shuttle vectors with multiple unique restriction sites. Yeast *2*, 163-167.

Hill, K.J., and Stevens, T.H. (1995). Vma22p is a novel endoplasmic reticulum-associated protein required for assembly of the yeast vacuolar H^+-ATPase complex. J Biol Chem *270*, 22329-22336.

Hille, B. (1978). Ionic channels in excitable membranes. Current problems and biophysical approaches. Biophys J *22*, 283-294.

Holden, N.E. (1987 (revised 2004)). Table of the Isotopes (Upton, NY (US), Brookhaven National Lab.).

Howard, B.J., Beresford, N.A., Nisbet, A., Cox, G., Oughton, D.H., Hunt, J., Alvarez, B., Andersson, K.G., Liland, A., and Voigt, G. (2005). The STRATEGY project: decision tools to aid sustainable restoration and long-term management of contaminated agricultural ecosystems. J Environ Radioact *83*, 275-295.

Hutchins, M.U., and Klionsky, D.J. (2001). Vacuolar localization of oligomeric alpha-mannosidase requires the cytoplasm to vacuole targeting and autophagy pathway components in *Saccharomyces cerevisiae*. J Biol Chem *276*, 20491-20498.

Iman, R.L., and Conover, W.J. (1979). The use of the rank transform in regression. Technometrics *21*, 499-509.

Iman, R.L., and Davenport, J.M. (1982). Rank correlation plots for use with correlated input variables. Communications in Statistics - Simulation and Computation *11*, 335-360.

Iman, R.L., Shortencarrier, M.J., and Johnson, J.D. (1985). FORTRAN 77 program and user's guide for the calculation of partial correlation and standardized regression coefficients (Albuquerque, NM (USA), Sandia National Labs).

Isenberg, G. (1976). Cardiac Purkinje fibers: cesium as a tool to block inward rectifying potassium currents. Pflugers Arch *365*, 99-106.

Jacob, P., Fesenko, S., Firsakova, S.K., Likhtarev, I.A., Schotola, C., Alexakhin, R.M., Zhuchenko, Y.M., Kovgan, L., Sanzharova, N.I., and Ageyets, V. (2001). Remediation strategies for rural territories contaminated by the Chernobyl accident. J Environ Radioact *56*, 51-76.

Jelinek-Kelly, S., Akiyama, T., Saunier, B., Tkacz, J.S., and Herscovics, A. (1985). Characterization of a specific alpha-mannosidase involved in oligosaccharide processing in *Saccharomyces cerevisiae*. J Biol Chem *260*, 2253-2257.

Jorgensen, P., Nishikawa, J.L., Breitkreutz, B.J., and Tyers, M. (2002). Systematic identification of pathways that couple cell growth and division in yeast. Science *297*, 395-400.

Kanter, U., Hauser, A., Michalke, B., Dräxl, S., and Schäffner, A.R. (2010). Caesium and strontium accumulation in shoots of *Arabidopsis thaliana*: genetic and physiological aspects. J Exp Bot *61*, 3995-4009.

Kaplan, B., Sherman, T., and Fromm, H. (2007). Cyclic nucleotide-gated channels in plants. FEBS Lett *581*, 2237-2246.

Karimi, M., Inze, D., and Depicker, A. (2002). GATEWAY vectors for *Agrobacterium*-mediated plant transformation. Trends Plant Sci *7*, 193-195.

Ketchum, K.A., Joiner, W.J., Sellers, A.J., Kaczmarek, L.K., and Goldstein, S.A. (1995). A new family of outwardly rectifying potassium channel proteins with two pore domains in tandem. Nature *376*, 690-695.

Kinclová-Zimmermannová, O., Flegelová, H., and Sychrová, H. (2004). Rice Na^+/H^+-antiporter Nhx1 partially complements the alkali-metal-cation sensitivity of yeast strains lacking three sodium transporters. Folia Microbiol (Praha) *49*, 519-525.

Kirchhoff, G., and Bunsen, R. (1861). Chemische Analyse durch Spectralbeobachtungen. Ann Phys *189*, 337.381.

Klionsky, D.J., Herman, P.K., and Emr, S.D. (1990). The fungal vacuole: composition, function, and biogenesis. Microbiol Rev *54*, 266-292.

Krebs, M., Beyhl, D., Gorlich, E., Al-Rasheid, K.A., Marten, I., Stierhof, Y.D., Hedrich, R., and Schumacher, K. (2010). *Arabidopsis* V-ATPase activity at the tonoplast is required for efficient nutrient storage but not for sodium accumulation. Proc Natl Acad Sci U S A *107*, 3251-3256.

Kumar, A., and Snyder, M. (2001). Genome-wide transposon mutagenesis in yeast. Curr Protoc Mol Biol *Chapter 13*, Unit13 13.

Lacombe, B., Becker, D., Hedrich, R., DeSalle, R., Hollmann, M., Kwak, J.M., Schroeder, J.I., Le Novere, N., Nam, H.G., Spalding, E.P.*, et al.* (2001). The identity of plant glutamate receptors. Science *292*, 1486-1487.

Lasat, M.M., Norvell, W., and Kochian, L.V. (1997). Potential for phytoextraction of ^{137}Cs from a contaminated soil. Plant and Soil *195*, 99-106.

Leidi, E.O., Barragan, V., Rubio, L., El-Hamdaoui, A., Ruiz, M.T., Cubero, B., Fernandez, J.A., Bressan, R.A., Hasegawa, P.M., Quintero, F.J.*, et al.* (2010). The AtNHX1 exchanger mediates potassium compartmentation in vacuoles of transgenic tomato. Plant J *61*, 495-506.

Leng, Q., Mercier, R.W., Hua, B.G., Fromm, H., and Berkowitz, G.A. (2002). Electrophysiological analysis of cloned cyclic nucleotide-gated ion channels. Plant Physiol *128*, 400-410.

Li, S.C., and Kane, P.M. (2009). The yeast lysosome-like vacuole: endpoint and crossroads. Biochim Biophys Acta *1793*, 650-663.

Li, W.B., Greiter, M., Oeh, U., and Hoeschen, C. (2011). Reliability of a new biokinetic model of zirconium in interanl dosimetry: Part I, Parameter Uncertainty Analysis. Health Phys *101*, 660-676.

Linkov, I., Carini, F., Collins, C., Eged, K., Mitchell, N.G., Mourlon, C., Ould-Dada, Z., Robles, B., Sweeck, L., and Venter, A. (2006). Radionuclides in fruit systems: model-model intercomparison study. Sci Total Environ *364*, 124-137.

Liu, Q., Kane, P.M., Newman, P.R., and Forgac, M. (1996). Site-directed mutagenesis of the yeast V-ATPase B subunit (Vma2p). J Biol Chem *271*, 2018-2022.

Liu, Y., and Barlowe, C. (2002). Analysis of Sec22p in endoplasmic reticulum/Golgi transport reveals cellular redundancy in SNARE protein function. Mol Biol Cell *13*, 3314-3324.

Loukin, S.H., and Saimi, Y. (2002). Carboxyl tail prevents yeast K^+ channel closure: proposal of an integrated model of TOK1 gating. Biophys J *82*, 781-792.

Lück, H. (1963). Catalase. In Methods of Enzymatic Analysis, H.U. Bergmeyer, ed. (San Diego, Academic Press), pp. 885-894.

Madrid, R., Gomez, M.J., Ramos, J., and Rodriguez-Navarro, A. (1998). Ectopic potassium uptake in *trk1 trk2* mutants of *Saccharomyces cerevisiae* correlates with a highly hyperpolarized membrane potential. J Biol Chem *273*, 14838-14844.

Mancias, J.D., and Goldberg, J. (2007). The transport signal on Sec22 for packaging into COPII-coated vesicles is a conformational epitope. Mol Cell *26*, 403-414.

Marovic, G., Franic, Z., Sencar, J., Bituh, T., and Vugrinec, O. (2008). Mosses and some mushroom species as bioindicators of radiocaesium contamination and risk assessment. Coll Antropol *32 Suppl 2*, 109-114.

Martinez, P., and Persson, B.L. (1998). Identification, cloning and characterization of a derepressible Na^+-coupled phosphate transporter in *Saccharomyces cerevisiae*. Mol Gen Genet *258*, 628-638.

Michel, R., and Voigt, G. (2006). Die Wege der Radionuklide. Physik Journal *5*, 37-42.

Middleton, L.J. (1959). Radioactive strontium and caesium in the edible parts of crop plants after foliar contamination. International Journal of Radiation Biology *1*, 387-402.

Mood, A.M., Graybill F.A. and Boes D.C. (1961). Introduction to the theory of statistics 3rd ed. (New York, MacGraw-Hill).

Nair, U., Jotwani, A., Geng, J., Gammoh, N., Richerson, D., Yen, W.L., Griffith, J., Nag, S., Wang, K., Moss, T.*, et al.* (2011). SNARE proteins are required for macroautophagy. Cell *146*, 290-302.

Nakajima, T., and Ballou, C.E. (1975). Yeast manno-protein biosynthesis: solubilization and selective assay of four mannosyltransferases. Proc Natl Acad Sci U S A *72*, 3912-3916.

Nakamura, R.L., and Gaber, R.F. (2009). Ion selectivity of the Kat1 K^+ channel pore. Mol Membr Biol *26*, 293-308.

Nass, R., and Rao, R. (1998). Novel localization of a Na^+/H^+ exchanger in a late endosomal compartment of yeast. Implications for vacuole biogenesis. J Biol Chem *273*, 21054-21060.

Nelson, H., and Nelson, N. (1990). Disruption of genes encoding subunits of yeast vacuolar H(+)-ATPase causes conditional lethality. Proc Natl Acad Sci U S A *87*, 3503-3507.

Nicholas, K.B., Nicholas, H.B.J., and Deerfield, D.W.I. (1997). GeneDoc: Analysis and Visualization of Genetic Variation. EMBNEWNEWS *4*.

Nieves-Cordones, M., Alemán, F., Martinéz, V., and Rubio, F. (2010). The *Arabidopsis thaliana* HAK5 K^+ transporter is required for plant growth and K^+ acquisition from low K^+ solutions under saline conditions. Mol Plant *3*, 326-333.

Nisbet, A.F. (1993). Effect of soil-based countermeasures on solid-liquid equilibria in agricultural soils contaminated with radiocaesium and radiostrontium. Sci Total Environ *137*, 99-118.

Nisbet, A.F., Konoplev, A.V., Shaw, G., Lembrechts, J.F., Merckx, R., Smolders, E., Vandecasteele, C.M., Lönsjö, H., Carini, F., and Burtoni, O. (1993). Application of fertilisers and ameliorants to reduce soil to plant transfer of radiocaesium and radiostrontium in the medium to long term — a summary. Sci Total Environ *137*, 173–182.

Noda, T., and Ohsumi, Y. (1998). Tor, a phosphatidylinositol kinase homologue, controls autophagy in yeast. J Biol Chem *273*, 3963-3966.

Noskov, S.Y., Berneche, S., and Roux, B. (2004). Control of ion selectivity in potassium channels by electrostatic and dynamic properties of carbonyl ligands. Nature *431*, 830-834.

Nowikovsky, K., Reipert, S., Devenish, R.J., and Schweyen, R.J. (2007). Mdm38 protein depletion causes loss of mitochondrial K^+/H^+ exchange activity, osmotic swelling and mitophagy. Cell Death Differ *14*, 1647-1656.

Obayashi, T., Kinoshita, K., Nakai, K., Shibaoka, M., Hayashi, S., Saeki, M., Shibata, D., Saito, K., and Ohta, H. (2007). ATTED-II: a database of co-expressed genes and cis elements for identifying co-regulated gene groups in *Arabidopsis*. Nucleic Acids Res *35*, D863-869.

Okorokov, L.A., Andreeva, N.A., Lichko, L.P., and Valiakhmetov, A. (1983). Transmembrane gradient of K^+ ions as an energy source in the yeast *Saccharomyces carlsbergensis*. Biochem Int *6*, 463-472.

Okorokov, L.A., Lichko, L.P., and Kulaev, I.S. (1980). Vacuoles: main compartments of potassium, magnesium, and phosphate ions in *Saccharomyces carlsbergenis* cells. J Bacteriol *144*, 661-665.

Opheim, D.J. (1978). alpha-D-Mannosidase of *Saccharomyces cerevisiae*. Characterization and modulation of activity. Biochim Biophys Acta *524*, 121-130.

Ould-Dada, Z., Carini, F., Eged, K., Kis, Z., Linkov, I., Mitchell, N.G., Mourlon, C., Robles, B., Sweeck, L., and Venter, A. (2006). Radionuclides in fruit systems: model prediction-experimental data intercomparison study. Sci Total Environ *366*, 514-524.

Pardo, J.M., Cubero, B., Leidi, E.O., and Quintero, F.J. (2006). Alkali cation exchangers: roles in cellular homeostasis and stress tolerance. J Exp Bot *57*, 1181-1199.

Payne, K.A., Bowen, C., Hammond, J.P., Hampton, C.R., Lynn, J.R., Mead, A., Swarup, R., Bennett, M.J., White, P.J., and Broadley, M.R. (2004). Natural genetic variation in caesium (Cs) accumulation by *Arabidopsis thaliana*. New Phytol, 535-548.

Perkins, J., and Gadd, G. (1993a). Caesium toxicity, accumulation and intracellular localization in yeasts. Mycol Res *97*, 717-724.

Perkins, J., and Gadd, G.M. (1993b). Accumulation and intracellular compartmentation of lithium ions in *Saccharomyces cerevisiae*. FEMS Microbiol Lett *107*, 255-260.

Petruska, J.A., Melaika, E.A., and Tomlinson, R.H. (1955). The Fission Yields of the Cesium Isotopes formed in the Thermal Neutron Fission of U-235 and the Neutron Absorption Cross Section of Xe-135. Canadian Journal of Physics *33*, 640-649.

Prister, B., Loshchilov, N., Perepelyatnikova, L., Perepelyatnikov, G., and Bondar, P. (1992). Efficiency of measures aimed at decreasing the contamination of agricultural products in areas contaminated by the Chernobyl NPP accident. Sci Total Environ *112*, 79-87.

Putyatin, Y., Seraya, T., Petrykevich, O., and Howard, B. (2006). Comparison of the accumulation of ^{137}Cs and ^{90}Sr by six spring wheat varieties Radiat Environ Bioph, 289-298.

Qi, Z., Hampton, C.R., Shin, R., Barkla, B.J., White, P.J., and Schachtman, D.P. (2008). The high affinity K^+ transporter AtHAK5 plays a physiological role in planta at very low K^+ concentrations and provides a caesium uptake pathway in *Arabidopsis*. J Exp Bot *59*, 595-607.

Ramirez, J., Ramirez, O., Saldana, C., Coria, R., and Pena, A. (1998). A *Saccharomyces cerevisiae* mutant lacking a K^+/H^+ exchanger. J Bacteriol *180*, 5860-5865.

Ramos, J., Alijo, R., Haro, R., and Rodriguez-Navarro, A. (1994). TRK2 is not a low-affinity potassium transporter in *Saccharomyces cerevisiae*. J Bacteriol *176*, 249-252.

Ramos, J., and Rodriguez-Navarro, A. (1986). Regulation and interconversion of the potassium transport systems of *Saccharomyces cerevisiae* as revealed by rubidium transport. Eur J Biochem *154*, 307-311.

Rhodes, N., Morris, C.N., Ainsworth, S., and Kinderlerer, J. (1986). The regulatory properties of yeast pyruvate kinase. Effects of NH_4^+ and K^+ concentrations. Biochem J *234*, 705-715.

Rieder, S.E., and Emr, S.D. (2001). Isolation of subcellular fractions from the yeast *Saccharomyces cerevisiae*. Curr Protoc Cell Biol *Chapter 3*, Unit 3 8.

Rodriguez-Navarro, A. (2000). Potassium transport in fungi and plants. Biochim Biophys Acta *1469*, 1-30.

Rodriguez-Navarro, A., Quintero, F.J., and Garciadeblas, B. (1994). Na^+-ATPases and Na^+/H^+ antiporters in fungi. Biochim Biophys Acta *1187*, 203-205.

Rodriguez-Navarro, A., and Ramos, J. (1984). Dual system for potassium transport in *Saccharomyces cerevisiae*. J Bacteriol *159*, 940-945.

Rodriguez-Navarro, A., Sancho, E.D., and Perez-Lloveres, C. (1981). Energy source for lithium efflux in yeast. Biochim Biophys Acta *640*, 352-358.

Rodríguez-Rosales, M.P., Gálvez, F.J., Huertas, R., Aranda, M.N., Baghour, M., Cagnac, O., and Venema, K. (2009). Plant NHX cation/proton antiporters. Plant Signal Behav *4*, 265-276.

Roller, A., Natura, G., Bihler, H., Slayman, C.L., Eing, C., and Bertl, A. (2005). In the yeast potassium channel, Tok1p, the external ring of aspartate residues modulates both gating and conductance. Pflugers Arch *451*, 362-370.

Rubio, F., Gassmann, W., and Schroeder, J.I. (1995). Sodium-driven potassium uptake by the plant potassium transporter HKT1 and mutations conferring salt tolerance. Science *270*, 1660-1663.

Rubio, F., Nieves-Cordones, M., Alemán, F., and Martínez, V. (2008). Relative contribution of AtHAK5 and AtAKT1 to K^+ uptake in the high-affinity range of concentrations. Physiol Plant *134*, 598-608.

Sacher, M., Stone, S., and Ferro-Novick, S. (1997). The synaptobrevin-related domains of Bos1p and Sec22p bind to the syntaxin-like region of Sed5p. J Biol Chem *272*, 17134-17138.

Sahr, T., Voigt, G., Paretzke, H.G., Schramel, P., and Ernst, D. (2005). Caesium-affected gene expression in Arabidopsis thaliana. New Phytol *165*, 747-754.

Salt, D.E., Blaylock, M., Kumar, N.P., Dushenkov, V., Ensley, B.D., Chet, I., and Raskin, I. (1995). Phytoremediation: a novel strategy for the removal of toxic metals from the environment using plants. Biotechnology (N Y) *13*, 468-474.

Saltelli, A., Ratto, M., Andres, T., Campolongo, F., Cariboni, J., Gatelli, D., Saisana, M., and Tarantola, S. (2008). Global Sensitivity Analysis: The Primer (Chichester, West Sussex, England John Wiley and Sons, Ltd.).

Sambrook, J., and Russell, D. (2001). Molecular Cloning: A Laboratory Manual (New York, CSHL Press).

Sarry, J.E., Chen, S., Collum, R.P., Liang, S., Peng, M., Lang, A., Naumann, B., Dzierszinski, F., Yuan, C.X., Hippler, M.*, et al.* (2007). Analysis of the vacuolar luminal proteome of *Saccharomyces cerevisiae*. FEBS J *274*, 4287-4305.

Schachtman, D.P. (2000). Molecular insights into the structure and function of plant K^+ transport mechanisms. Biochim Biophys Acta *1465*, 127-139.

Schachtman, D.P., and Schroeder, J.I. (1994). Structure and transport mechanism of a high-affinity potassium uptake transporter from higher plants. Nature *370*, 655-658.

Schimmack, W., and Bunzl, K. (1992). Migration of radiocesium in two forest soils as obtained from field and column investigations. Sci Total Environ *116*, 93-107.

Schimmack, W., Zimmermann, G., Sommer, M., Dietl, F., Schultz, W., and Paretzke, H.G. (2004). Soil-to-grain transfer of fallout ^{137}Cs for 28 winter wheat cultivars as observed in field experiments. Radiat Environ Biophys *42*, 275-284.

Schneider, K., Kuznetzov, V.K., Sanzharova, N.I., Kanter, U., Telikh, K.M., and Khlopuk, M.S. (2008). Soil-to-plant and soil-to-grain transfer of Cs-137 in field-grown maize hybrids during two contrasting seasons: assessing the phenotypic variability and its genetic component. Radiat Environ Bioph *47*, 241-252.

Scholl, R.L., May, S.T., and Ware, D.H. (2000). Seed and molecular resources for *Arabidopsis*. Plant Physiol *124*, 1477-1480.

Scott, S.V., Hefner-Gravink, A., Morano, K.A., Noda, T., Ohsumi, Y., and Klionsky, D.J. (1996). Cytoplasm-to-vacuole targeting and autophagy employ the same machinery to deliver proteins to the yeast vacuole. Proc Natl Acad Sci U S A *93*, 12304-12308.

Seglen, P.O., and Gordon, P.B. (1982). 3-Methyladenine: specific inhibitor of autophagic/lysosomal protein degradation in isolated rat hepatocytes. Proc Natl Acad Sci U S A *79*, 1889-1892.

Serrano, R. (1978). Characterization of the plasma membrane ATPase of *Saccharomyces cerevisiae*. Mol Cell Biochem *22*, 51-63.

Sheahan, J.J., Ribeiro-Neto, L., and Sussman, M.R. (1993). Cesium-insensitive mutants of *Arabidopsis thaliana*. Plant J *3*, 647-656.

Sherman, F. (1991). Getting started with yeast. Methods Enzymol 194, 3-21.

Smyth, D.R., Bowman, J.L., and Meyerowitz, E.M. (1990). Early flower development in *Arabidopsis*. Plant Cell 2, 755-767.

Stark, C., Breitkreutz, B.J., Reguly, T., Boucher, L., Breitkreutz, A., and Tyers, M. (2006). BioGRID: a general repository for interaction datasets. Nucleic Acids Res *34*, D535-539.

Steinhauser, D., Usadel, B., Luedemann, A., Thimm, O., and Kopka, J. (2004). CSB.DB: a comprehensive systems-biology database. Bioinformatics *20*, 3647-3651.

Stevens, T., Esmon, B., and Schekman, R. (1982). Early stages in the yeast secretory pathway are required for transport of carboxypeptidase Y to the vacuole. Cell *30*, 439-448.

Stevens, T.H., Rothman, J.H., Payne, G.S., and Schekman, R. (1986). Gene dosage-dependent secretion of yeast vacuolar carboxypeptidase Y. J Cell Biol *102*, 1551-1557.

Styron, C.E., Hagan, T.M., Campbell, D.R., Harvin, J., Whittenburg, N.K., Baughman, G.A., Bransford, M.E., Saunders, W.H., Williams, D.C., Woodle, C.*, et al.* (1976). Effects of temperature and salinity on growth and uptake of ^{65}Zn and ^{137}Cs for six marine algae. Journal of Marine Biological Association of the United Kingdom *56*, 13-20.

Tataruch, F., and Kiersdorf, H. (2003). Mammals as biomonitors. In Trace Metals and other Contaminants in the Environment, pp. 737-772.

Tomashek, J.J., Graham, L.A., Hutchins, M.U., Stevens, T.H., and Klionsky, D.J. (1997). V1-situated stalk subunits of the yeast vacuolar proton-translocating ATPase. J Biol Chem *272*, 26787-26793.

Tomioka, N., Uchiyama, H., and Yagi, O. (1992). Isolation and characterization of cesium-accumulating bacteria. Appl Environ Microbiol *58*, 1019-1023.

Tomioka, N., Uchiyama, H., and Yagi, O. (1994). Cesium Accumulation and Growth Characteristics of *Rhodococcus erythropolis* CS98 and *Rhodococcus sp*. Strain CS402. Appl Environ Microbiol *60*, 2227-2231.

UNSCEAR (2000). Report to the general assembly, sources and effects of ionizing radiation (New York, United Nations Scientific Committee on the Effects of Atomic Radiation).

Untergasser, A., Nijveen, H., Rao, X., Bisseling, T., Geurts, R., and Leunissen, J.A. (2007). Primer3Plus, an enhanced web interface to Primer3. Nucleic Acids Res *35*, W71-74.

Unterweger, M.P., Hoppes, D.D., and Schima, F.J. (1992). New and revised half-life measurements results. Nuclear Instruments and Methods in Physics Research Section A *312*, 349-352.

Valcke, E., and Cremers, A. (1994). Sorption-desorption dynamics of radiocaesium in organic matter soils. Sci Total Environ *157*, 275-283.

Vandenhove, H., Cremers, A., Smolders, E., and Van Hees, M. (2005). Effect of K and bentonite additions on Cs-transfer to ryegrass. J Environ Radioact *81*, 233-253.

Venema, K., Belver, A., Marín-Manzano, M.C., Rodriguez-Rosales, M.P., and Donaire, J.P. (2003). A novel intracellular K^+/H^+ antiporter related to Na^+/H^+ antiporters is important for K^+ ion homeostasis in plants. J Biol Chem *278*, 22453-22459.

Vida, T.A., and Emr, S.D. (1995). A new vital stain for visualizing vacuolar membrane dynamics and endocytosis in yeast. J Cell Biol *128*, 779-792.

Vidal, M., Camps, M., Grebenshikova, N., Sanzharova, N., Ivanov, Y., Vandecasteele, C., Shand, C., Rigol, A., Firsakova, S., Fesenko, S.*, et al.* (2001). Soil- and plant-based countermeasures to reduce ^{137}Cs and ^{90}Sr uptake by grasses in natural meadows: the REDUP project. J Environ Radioact *56*, 139-156.

Volkov, A.G., Paula, S., and Deamer, D.W. (1997). Two mechanisms of permeation of small neutral molecules and hydrated ions across phospholipid bilayers. Bioelectrochemistry and Bioenergetics *42*, 153-160.

Walker, D.J., Leigh, R.A., and Miller, A.J. (1996). Potassium homeostasis in vacuolate plant cells. Proc Natl Acad Sci U S A *93*, 10510-10514.

Wallace, A., Romney, E.M., Cha, J.W., and Chaudhry, F.M. (1977). Lithium toxicity in plants. Communications in Soil Science and Plant Analysis *8*, 773-780.

Wells, K.M., and Rao, R. (2001). The yeast Na^+/H^+ exchanger Nhx1 is an N-linked glycoprotein. Topological implications. J Biol Chem *276*, 3401-3407.

White, P.J., Bowen, H.C., Demidchik, V., Nichols, C., and Davies, J.M. (2002). Genes for calcium-permeable channels in the plasma membrane of plant root cells. Biochim Biophys Acta *1564*, 299-309.

White, P.J., and Broadley, M.R. (2000). Mechanisms of caesium uptake by plants. New Phytol *147*, 214-256.

White, P.J., Wiesel, L., and Broadley, M.R. (2010). Cation Channels and the Uptake of Radiocaesium by Plants. In Ion Channels and Plant Stress Responses, V. Demidchik, and F. Maathuis, eds. (Berlin-Heidelberg, Springer-Verlag), pp. 47-67.

Wiemken, A., and Durr, M. (1974). Characterization of amino acid pools in the vacuolar compartment of *Saccharomyces cerevisiae*. Arch Microbiol *101*, 45-57.

Winzeler, E.A., Shoemaker, D.D., Astromoff, A., Liang, H., Anderson, K., Andre, B., Bangham, R., Benito, R., Boeke, J.D., Bussey, H.*, et al.* (1999). Functional characterization of the *S. cerevisiae* genome by gene deletion and parallel analysis. Science *285*, 901-906.

Witherspoon, J.P., and Brown, G.N. (1965). Translocation of Cesium-137 from Parent Trees to Seedlings of *Liriodendron tulipifera*. Botanical Gazette *Vol. 126*, 181-185.

Wong, L.C., Ngan, H.Y., Cheung, A.N., Cheng, D.K., Ng, T.Y., and Choy, D.T. (1999). Chemoradiation and adjuvant chemotherapy in cervical cancer. J Clin Oncol *17*, 2055-2060.

Yasunari, T.J., Stohl, A., Hayano, R.S., Burkhart, J.F., Eckhardt, S., and Yasunari, T. (2011). Cesium-137 deposition and contamination of Japanese soils due to the Fukushima nuclear accident. Proc Natl Acad Sci U S A *108*, 19530-19534.

Yoshida, S., and Muramatsu, Y. (1998). Concentrations of alkali and alkaline earth elements in mushrooms and plants collected in a Japanese pine forest, and their relationship with ^{137}Cs. J Environ Radioact *41*, 183-205.

Yoshihisa, T., and Anraku, Y. (1990). A novel pathway of import of alpha-mannosidase, a marker enzyme of vacuolar membrane, in *Saccharomyces cerevisiae*. J Biol Chem *265*, 22418-22425.

Zhou, X., Arita, A., Ellen, T.P., Liu, X., Bai, J., Rooney, J.P., Kurtz, A.D., Klein, C.B., Dai, W., Begley, T.J*., et al.* (2009). A genome-wide screen in *Saccharomyces cerevisiae* reveals pathways affected by arsenic toxicity. Genomics *94*, 294-307.

Zhu, Y.G., and Smolders, E. (2000). Plant uptake of radiocaesium: a review of mechanisms, regulation and application. J Exp Bot *51*, 1635-1645.

Zimmermann, P., Laule, O., Schmitz, J., Hruz, T., Bleuler, S., and Gruissem, W. (2008). Genevestigator transcriptome meta-analysis and biomarker search using rice and barley gene expression databases. Mol Plant *1*, 851-857.

Appendices

Appendix A. Cs^+ accumulation in *S. cerevisiae*

All repetitions that were taken into account for the analysis and calculation of the yeast mutant phenotype are given in the following table. The background correction was already introduced. Using the 'correction factor' the counts per minute (CCPM) can be translated to a concentration. +D = addition of doxycycline. *sec22Δ::Sec22 (comp)* is the *Sec22* complemented yeast strain, *sec22Δ::OE_Sec22* is the *Sec22* overexpression strain and *sec22Δ::OE_AtSec22* is the *A. thaliana SEC22* complemented yeast strain.
* after background correction; background determined by measurement of 3 ml HNO_3;Background ranged between 40 and 100 CCPM. Related to 10^7 cells.
** concentration of stable CsCl in the media correlated with the activity of ^{134}Cs tracer in the media (CCPM).
Multiplying measured activity with the calculation factor results in nmol Cs^+ taken up per amount of cells analysed. *sec22Δ* samples 11 – 15 and *sec22Δ::Sec22* samples 17 – 20 were incubated with 10 times the amount of ^{134}Cs.

Caesium concentration in yeast cells
Number of cells: $2*10^7$ as determined by OD_{600} measurement.

ID	Biological replicate	Measured CCPM*	Calculation factor**	nmol/10^7 cells	conc. (mM)
Wild Type	1	202.4	0.0039	0.80	2.36
Wild Type	2	215.0	0.0039	0.85	2.51
Wild Type	3	204.5	0.0039	0.81	2.39
Wild Type	4	207.5	0.0039	0.82	2.42
Wild Type	5	208.6	0.0039	0.83	2.44
Wild Type	6	217.2	0.0039	0.86	2.54
Wild Type	7	219.2	0.0037	0.81	2.39
Wild Type	8	216.1	0.0037	0.80	2.35
Wild Type	9	297.9	0.0037	0.79	2.33
Wild Type	10	214.2	0.0026	0.79	2.31
sec22Δ	1	87.8	0.0039	0.35	1.03
sec22Δ	2	75.6	0.0039	0.30	0.88
sec22Δ	3	94.8	0.0039	0.38	1.11
sec22Δ	4	93.1	0.0039	0.37	1.09
sec22Δ	5	91.5	0.0039	0.36	1.07
sec22Δ	6	83.6	0.0039	0.33	0.98
sec22Δ	7	78.1	0.0037	0.31	0.91
sec22Δ	8	100.3	0.0037	0.37	1.09
sec22Δ	9	108.6	0.0037	0.40	1.18
sec22Δ	10	107.8	0.0037	0.40	1.17
sec22Δ	11	98.7	0.044	0.39	1.15
sec22Δ	12	82.8	0.044	0.36	1.07
sec22Δ	13	80.6	0.044	0.35	1.04
sec22Δ	14	84.5	0.044	0.37	1.09
sec22Δ	15	85.2	0.044	0.38	1.10
sec22Δ::Sec22	1	199.3	0.0039	0.79	2.33
sec22Δ::Sec22	2	200.8	0.0039	0.80	2.34
sec22Δ::Sec22	3	196.1	0.0039	0.78	2.29
sec22Δ::Sec22	4	196.3	0.0039	0.78	2.29
sec22Δ::Sec22	5	189.3	0.0039	0.75	2.21
sec22Δ::Sec22	6	186.3	0.0039	0.74	2.17
sec22Δ::Sec22	7	197.1	0.0039	0.78	2.30
sec22Δ::Sec22	8	193.8	0.0039	0.77	2.26
sec22Δ::Sec22	9	199.5	0.0039	0.79	2.33
sec22Δ::Sec22	10	185.4	0.0037	0.69	2.02
sec22Δ::Sec22	11	198.5	0.0037	0.73	2.16
sec22Δ::Sec22	12	202.0	0.0037	0.75	2.20
sec22Δ::Sec22	13	192.3	0.0037	0.71	2.09
sec22Δ::Sec22	14	193.9	0.0037	0.72	2.11
sec22Δ::Sec22	15	196.5	0.0037	0.73	2.14
sec22Δ::Sec22	16	190.7	0.0037	0.71	2.07
sec22Δ::Sec22	17	188.6	0.044	0.83	2.44

Caesium concentration in yeast cells

Number of cells: $2*10^7$ as determined by OD_{600} measurement.

ID	Biological replicate	Measured CCPM	Calculation factor	nmol/10^7 cells	conc. (mM)
sec22Δ::Sec22	18	209.5	0.044	0.92	2.71
sec22Δ::Sec22	19	194.3	0.044	0.86	2.51
sec22Δ::Sec22	20	189.3	0.044	0.83	2.45
sec22Δ::OE_Sec22	1	435.2	0.0039	1.70	4.99
sec22Δ::OE_Sec22	2	373.1	0.0039	1.46	4.28
sec22Δ::OE_Sec22	3	428.8	0.0039	1.67	4.92
sec22Δ::OE_Sec22	4	402.4	0.0039	1.57	4.62
sec22Δ::OE_Sec22	5	422.2	0.0039	1.65	4.84
sec22Δ::OE_Sec22	6	429.6	0.0037	1.59	4.68
sec22Δ::OE_Sec22	7	439.4	0.0037	1.63	4.78
sec22Δ::OE_Sec22	8	433.2	0.0037	1.60	4.71
sec22Δ::OE_Sec22	9	428.9	0.0037	1.59	4.67
sec22Δ::OE_Sec22+D	1	67.6	0.0039	0.26	0.78
sec22Δ::OE_Sec22+D	2	96.3	0.0039	0.38	1.11
sec22Δ::OE_Sec22+D	3	104.9	0.0039	0.41	1.20
sec22Δ::OE_Sec22+D	4	100.6	0.0039	0.39	1.15
sec22Δ::OE_Sec22+D	5	86.5	0.0039	0.34	0.99
sec22Δ::OE_Sec22+D	6	79.6	0.0037	0.31	0.91
sec22Δ::OE_Sec22+D	7	83.3	0.0037	0.31	0.91
sec22Δ::OE_Sec22+D	8	81.1	0.0037	0.30	0.88
sec22Δ::OE_AtSec22	1	132.4	0.0039	0.52	1.52
sec22Δ::OE_AtSec22	2	191.5	0.0039	0.75	2.20
sec22Δ::OE_AtSec22	3	157.8	0.0039	0.62	1.81
sec22Δ::OE_AtSec22	4	189.1	0.0039	0.74	2.17
sec22Δ::OE_AtSec22	5	195.4	0.0039	0.72	2.13
sec22Δ::OE_AtSec22	6	167.4	0.0039	0.62	1.82
sec22Δ::OE_AtSec22	7	188.9	0.0039	0.70	2.06
sec22Δ::OE_AtSec22	8	135.9	0.0037	0.50	1.48
sec22Δ::OE_AtSec22	9	210.8	0.0037	0.78	2.29
sec22Δ::OE_AtSec22	10	188.1	0.0037	0.70	2.05
sec22Δ::OE_AtSec22	11	207.9	0.0037	0.77	2.26
sec22Δ::OE_AtSec22+D	1	77.9	0.0039	0.30	0.89
sec22Δ::OE_AtSec22+D	2	62.9	0.0039	0.25	0.72
sec22Δ::OE_AtSec22+D	3	57.9	0.0039	0.23	0.66
sec22Δ::OE_AtSec22+D	4	71.7	0.0039	0.28	0.82
sec22Δ::OE_AtSec22+D	5	57.3	0.0039	0.22	0.66
sec22Δ::OE_AtSec22+D	6	57.6	0.0039	0.22	0.66
sec22Δ::OE_AtSec22+D	7	94.3	0.0039	0.37	1.08
sec22Δ::OE_AtSec22+D	8	102.4	0.0037	0.40	1.17
sec22Δ::OE_AtSec22+D	9	89.1	0.0037	0.35	1.02
sec22Δ::OE_AtSec22+D	10	117.1	0.0037	0.46	1.34
sec22Δ::OE_AtSec22+D	11	69.3	0.0037	0.27	0.80

Appendix B. Rb^+ accumulation in *S. cerevisiae*

All repetitions that were taken into account for the analysis and calculation of the yeast mutant phenotype are given in the following table. The background correction was already introduced. Using the 'correction factor' the counts per minute (CCPM) can be translated to a concentration. ID denotes the identity of the sample

* after background correction; background determined by measurement of 3 ml HNO_3;Background ranged between 30 and 120 CCPM. Related to $1*10^7$ cells.

** concentration of stable RbCl in the media correlated with the activity of ^{86}Rb tracer in the media (CCPM) : nmol/CCPM Rb^+.

Rubidium concentration in yeast cells

Number of cells: $2*10^7$ as determined by OD_{600} measurement.

ID	Biological replicate	Measured CCPM*	Calculation factor**	nmol/10^7 cells	conc. (mM)
Wild Type	1	681.5	0.0019	1.30	3.87
Wild Type	2	661.8	0.0019	1.26	3.76
Wild Type	3	667.3	0.0019	1.27	3.79
Wild Type	4	703.5	0.0019	1.34	3.99
Wild Type	5	705.9	0.0019	1.34	4.01
Wild Type	6	704.9	0.0019	1.34	4.00
Wild Type	7	731.1	0.0019	1.39	4.15
Wild Type	8	638.2	0.0019	1.21	3.62
Wild Type	9	664.9	0.0019	1.26	3.77
Wild Type	10	674.9	0.0019	1.28	3.83
Wild Type	11	653.9	0.0019	1.24	3.71
Wild Type	12	612.1	0.0019	1.16	3.47
*sec22*Δ	1	632.5	0.0019	1.20	3.59
*sec22*Δ	2	571.8	0.0019	1.09	3.24
*sec22*Δ	3	680.1	0.0019	1.29	3.86
*sec22*Δ	4	756.0	0.0019	1.44	4.29
*sec22*Δ	5	636.0	0.0019	1.21	3.61
*sec22*Δ	6	641.5	0.0019	1.22	3.64
*sec22*Δ	7	616.1	0.0019	1.17	3.50
*sec22*Δ	8	709.6	0.0019	1.35	4.03
*sec22*Δ	9	615.9	0.0019	1.17	3.49
*sec22*Δ	10	647.5	0.0019	1.23	3.67

Appendix C. Stable cation accumulation in *S. cerevisiae*

All repetitions that were taken into account for the analysis and calculation of the yeast mutant phenotype are given in the following table. The analysed ion is indicated in the table header. It is further indicated whether the data was derived from experiments under assay conditions or from cells grown in full media. The concentration per analysed cell number and the derived intracellular concentrations are shown. ID denotes the identity of the sample.

* determined in 5 ml 10 % HNO_3 (dissolved from filter). after background correction; background determined by measurement of 10 % HNO_3; without cells. n = 6 per setup.

** considering the number of cells per sample. the experimentally determined cell volume (34 fl) and the molar mass of the according ion (K^+, Na^+, Mg^{2+} or Ca^{2+}).

Potassium concentration in yeast cells

Cells grown under assay conditions.

Each sample contains $5*10^7$ cells on a filter. Filters were dissolved in 5 ml HNO_3 for measurement.

ID	Biological replicate	K^+ (mg/l_{sample})*	= µg K^+/$5*10^7$ cells	conc. (mmol/l_{cell})**
Wild Type	1	25.4	127.0	191.1
Wild Type	2	24.0	120.0	180.5

Potassium concentration in yeast cells (continued)
Cells grown under assay conditions.
Each sample contains $5*10^7$ cells on a filter. Filters were dissolved in 5 ml HNO_3 for measurement.

Wild Type	3	17.0	85.0	127.9
Wild Type	4	17.8	89.0	133.9
Wild Type	5	19.2	96.0	144.4
Wild Type	6	26.9	134.5	201.6
Wild Type	7	19.6	98.0	147.4
Wild Type	8	17.7	88.5	144.6
Wild Type	1	19.9	99.7	150.0
Wild Type	2	19.3	96.4	145.1
*sec22*Δ	3	21.5	107.3	161.4
*sec22*Δ	4	19.9	99.5	149.7
*sec22*Δ	5	19.8	98.8	148.6
*sec22*Δ	6	20.1	100.5	151.2
*sec22*Δ	7	21.0	104.9	157.7
*sec22*Δ	8	20.9	104.7	157.5
*sec22*Δ	9	21.0	104.8	157.8
*sec22*Δ	10	20.1	100.5	151.3
*sec22*Δ	11	19.7	98.5	148.1
*sec22*Δ	12	21.9	109.5	164.5

Potassium concentration in yeast cells
Cells grown on full medium.
Each sample contains $5*10^7$ cells on a filter. Filters were dissolved in 5 ml HNO_3 for measurement.

ID	Biological replicate	K^+ (mg/l_{sample})*	= µg $K^+/5*10^7$ cells	conc. (mmol/l_{cell})**
Wild Type	1	31.6	158	237.70
Wild Type	2	30.5	152.4	228.67
Wild Type	3	38.9	194.6	292.76
Wild Type	4	31.6	158	237.70
Wild Type	5	30.2	151	227.17
Wild Type	6	30.0	150	225.67
Wild Type	7	28.8	144	216.63
*sec22*Δ	1	29.1	145.5	218.85
*sec22*Δ	2	35.0	175	263.27
*sec22*Δ	3	30.9	154.4	232.28
*sec22*Δ	4	30.0	150	225.66
*sec22*Δ	5	32.2	161	242.21
*sec22*Δ	6	30.5	152.5	229.42
*sec22*Δ	7	29.4	147	221.15
*sec22*Δ	8	28.7	143.7	216.18
*sec22*Δ	9	28.7	143.4	215.73

Sodium concentration in yeast cells
Cells grown under assay conditions.
Each sample contains $5*10^7$ cells on a filter. Filters were dissolved in 5 ml HNO_3 for measurement.

ID	Biological replicate	Na^+ (mg/l_{sample})*	= µg $Na^+/5*10^7$ cells	conc. (mmol/l_{cell})**
Wild Type	1	11.6	0.5	0.7
Wild Type	2	11.7	0.5	0.8
Wild Type	3	16.2	0.7	1.0
Wild Type	4	15.9	0.65	0.9
Wild Type	5	13.3	0.85	1.1
Wild Type	6	17.5	0.9	1.2
Wild Type	7	18.9	0.84	1.1
Wild Type	8	17.2	0.6	0.8
*sec22*Δ	1	12.9	0.6	0.9
*sec22*Δ	2	13.3	0.5	0.7
*sec22*Δ	3	10.9	0.7	1.0
*sec22*Δ	4	15.0	0.54	0.7
*sec22*Δ	5	11.2	0.5	0.8
*sec22*Δ	6	12.0	0.6	0.9
*sec22*Δ	7	13.5	0.6	0.9
*sec22*Δ	8	13.6	0.5	0.74
*sec22*Δ	9	13.5	0.5	0.8

Sodium concentration in yeast cells

Cells grown on rich medium (= YPAD, pH = 6).
Each sample contains $5*10^7$ cells on a filter. Filters were dissolved in 5 ml HNO_3 for measurement.

ID	Biological replicate	Na^+ (mg/l_{sample})*	= µg $Na^+/5*10^7$ cells	conc. ($mmol/l_{cell}$)**
Wild Type	1	43.5	2.0	2,8
Wild Type	2	41.6	1.9	2,7
Wild Type	3	44.4	2.0	2,9
Wild Type	4	48.9	2.2	3,2
Wild Type	5	38.6	1.7	2,5
*sec22*Δ	1	40.7	1.8	2,6
*sec22*Δ	2	42.0	1.9	2,7
*sec22*Δ	3	41.6	1.9	2,7
*sec22*Δ	4	40.4	1.8	2,6

Magnesium concentration in yeast cells

Cells grown under assay conditions.
Each sample contains $5*10^7$ cells on a filter. Filters were dissolved in 5 ml HNO_3 for measurement.

ID	Biological replicate	Mg^{2+} (mg/l_{sample})*	= µg $Mg^{2+}/5*10^7$ cells	conc. ($mmol/l_{cell}$)**
Wild Type	1	0.6	2.8	9.2
Wild Type	2	0.5	2.5	8.2
Wild Type	3	0.8	3.9	12.7
Wild Type	4	0.7	3.5	11.4
Wild Type	5	0.7	3.4	11.1
Wild Type	6	0.6	3.0	10.5
Wild Type	7	0.5	2.5	8.2
Wild Type	8	0.6	2.9	9.5
*sec22*Δ	1	0.7	3.4	11.1
*sec22*Δ	2	0.5	2.6	8.6
*sec22*Δ	3	0.5	2.7	8.9
*sec22*Δ	4	0.7	3.4	11.0
*sec22*Δ	5	0.5	2.4	7.7
*sec22*Δ	6	0.4	2.0	6.4
*sec22*Δ	7	0.4	1.9	6.3
*sec22*Δ	8	0.4	1.9	6.2
*sec22*Δ	9	0.6	3.1	10.3

Calcium concentration in yeast cells

Cells grown under assay conditions.
Each sample contains $5*10^7$ cells on a filter. Filters were dissolved in 5 ml HNO_3 for measurement.

ID	Biological replicate	Ca^{2+} (mg/l_{sample})*	= µg $Ca^{2+}/5*10^7$ cells	conc. ($mmol/l_{cell}$)**
Wild Type	1	0.06	0.30	0.44
Wild Type	2	0.05	0.24	0.35
Wild Type	3	0.07	0.36	0.53
Wild Type	4	0.07	0.37	0.54
Wild Type	5	0.08	0.40	0.59
Wild Type	6	0.07	0.37	0.54
Wild Type	7	0.07	0.35	0.51
Wild Type	8	0.07	0.33	0.48
*sec22*Δ	1	0.06	0.30	0.44
*sec22*Δ	2	0.06	0.29	0.43
*sec22*Δ	3	0.07	0.35	0.51
*sec22*Δ	4	0.08	0.38	0.56
*sec22*Δ	5	0.06	0.32	0.47
*sec22*Δ	6	0.06	0.32	0.47
*sec22*Δ	7	0.07	0.37	0.54
*sec22*Δ	8	0.06	0.31	0.45
*sec22*Δ	9	0.07	0.33	0.48

Calcium concentration in yeast cells
Cells grown on full medium.
Each sample contains $5*10^7$ cells on a filter. Filters were dissolved in 5 ml HNO_3 for measurement.

ID	Biological replicate	Ca^{2+} (mg/l_{sample})*	= µg $Ca^{2+}/5*10^7$ cells	conc. ($mmol/l_{cell}$)**
Wild Type	1	0.24	1.22	1.79
Wild Type	2	0.28	1.42	2.08
Wild Type	3	0.23	1.16	1.70
Wild Type	4	0.22	1.09	1.60
Wild Type	5	0.24	1.21	1.78
*sec22*Δ	1	0.17	0.85	1.25
*sec22*Δ	2	0.22	1.09	1.60
*sec22*Δ	3	0.15	0.76	1.12
*sec22*Δ	4	0.20	0.98	1.44
*sec22*Δ	5	0.20	0.99	1.45

Appendix D. Cs^+ accumulation kinetics at 50 µM external CsCl in *S. cerevisiae* (mean)

All repetitions (n ≥ 6) were taken into account for the analysis and calculation of the yeast mutant phenotype. Time, tracer activity, the correction factor and the concentration is presented. Note that only mean values are shown. ID denotes the identity of the sample. Note that wild type and mutant are placed side by side.
* after background correction; background determined by measurement of 3 ml HNO_3; Background ranged between 20 and 100 CCPM. n = 6 per setup; related to $1*10^7$ cells.
** concentration of stable CsCl in the media correlated with the activity of ^{134}Cs tracer in the media (CCPM) : nmol/CCPM Cs^+.

Caesium kinetics in yeast cells
WILD TYPE
Cells incubated with 50 µM CsCl in 100 µl buffer volume.

Time (h)	Measured CCPM*	Calculation factor**	nmol/10^7 cells	conc. (mM)
0.25	15.82	0.0040	0.063	0.19
0.50	24.47	0.0048	0.117	0.35
0.75	28.11	0.0045	0.126	0.37
1.00	31.91	0.0044	0.140	0.41
1.25	33.33	0.0044	0.147	0.43
1.75	36.23	0.0046	0.167	0.49
2.00	39.70	0.0045	0.179	0.53
3.00	67.71	0.0045	0.305	0.90
4.00	88.90	0.0044	0.391	1.15
5.00	112.16	0.0044	0.493	1.45
6.00	143.83	0.0044	0.633	1.86
7.00	151.05	0.0045	0.680	2.00
8.00	169.49	0.0045	0.763	2.24
9.00	174.54	0.0044	0.768	2.26
10.0	179.32	0.0045	0.807	2.37
11.0	180.88	0.0045	0.814	2.39
12.0	178.19	0.0046	0.820	2.41
13.0	180.71	0.0045	0.813	2.39
14.0	190.06	0.0044	0.836	2.46
15.0	189.02	0.0044	0.832	2.45
16.0	182.73	0.0045	0.822	2.42
17.0	191.08	0.0045	0.860	2.53
18.0	188.14	0.0045	0.847	2.49

Caesium kinetics in yeast cells
***sec22*Δ**
Cells incubated with 50 µM CsCl in 100 µl buffer volume.

Time (h)	Measured CCPM	Calculation factor	nmol/10^7 cells	conc. (mM)
0.25	14.28	0.0040	0.057	0.17
0.50	19.53	0.0048	0.094	0.28
0.75	23.33	0.0045	0.105	0.31
1.00	25.59	0.0044	0.113	0.33
1.25	27.84	0.0044	0.122	0.36
1.75	31.25	0.0046	0.144	0.42
2.00	32.10	0.0045	0.144	0.42
3.00	35.39	0.0045	0.159	0.47
4.00	38.12	0.0044	0.168	0.49
5.00	45.80	0.0044	0.202	0.59
6.00	57.60	0.0044	0.253	0.75
7.00	60.58	0.0045	0.273	0.80
8.00	67.13	0.0045	0.302	0.89
9.00	61.57	0.0044	0.271	0.80
10.0	64.42	0.0045	0.290	0.85
11.0	65.32	0.0045	0.294	0.86
12.0	64.62	0.0046	0.297	0.87
13.0	66.44	0.0045	0.299	0.88
14.0	66.55	0.0044	0.293	0.86
15.0	67.80	0.0044	0.298	0.88
16.0	66.21	0.0045	0.298	0.88
17.0	67.62	0.0045	0.304	0.89
18.0	68.55	0.0045	0.308	0.91

Appendix E. Cs^+ accumulation kinetics at 200 µM external CsCl in *S. cerevisiae* (mean)

All repetitions n ≥ 6 were taken into account for the analysis and calculation of the yeast mutant phenotype. Time, tracer activity, the correction factor and the concentration is presented. Note, that only mean values are shown. ID denotes the identity of the sample. Note that wild type and mutant are placed side by side.
* after background correction; background determined by measurement of 3 ml HNO_3;Background ranged between 20 and 100 CCPM. n = 6 per setup; related to $1*10^7$ cells.
** concentration of stable CsCl in the media correlated with the activity of ^{134}Cs tracer in the media (CCPM) : nmol/CCPM Cs^+.

Caesium kinetics in yeast cells
WILD TYPE
Cells incubated with 200 µM CsCl in 200 µl buffer volume.

Time (h)	Measured CCPM*	Calculation factor**	nmol/10^7 cells	conc. (mM)
0.25	55.51	0.0045	0.25	0.76
0.50	69.07	0.0045	0.32	0.95
0.75	76.42	0.0044	0.34	1.01
1.00	75.96	0.0044	0.35	1.04
1.25	77.99	0.0046	0.36	1.07
1.75	81.17	0.0046	0.38	1.13
2.00	88.49	0.0044	0.39	1.17
3.00	106.69	0.0045	0.48	1.44
5.00	167.67	0.0045	0.75	2.24
7.00	222.26	0.0045	0.99	2.96
8.00	234.55	0.0046	1.08	3.21
9.00	234.24	0.0044	1.08	3.21
10.0	255.31	0.0046	1.17	3.50
13.0	251.64	0.0044	1.11	3.32
15.0	255.86	0.0044	1.14	3.40
18.0	256.69	0.0045	1.16	3.45

Caesium kinetics in yeast cells

***sec22*Δ**

Cells incubated with 200 µM CsCl in 200 µl buffer volume.

Time (h)	Measured CCPM	Calculation factor	nmol/10^7 cells	conc. (mM)
0.25	57.93	0.0045	0.27	0.79
0.50	68.05	0.0045	0.31	0.93
0.75	71.01	0.0044	0.31	0.93
1.00	67.62	0.0044	0.31	0.93
1.25	72.25	0.0046	0.33	0.99
1.75	74.29	0.0046	0.35	1.03
2.00	84.67	0.0044	0.38	1.12
3.00	82.39	0.0045	0.37	1.11
5.00	101.62	0.0045	0.46	1.36
7.00	127.59	0.0045	0.57	1.70
8.00	141.53	0.0046	0.65	1.94
9.00	143.20	0.0044	0.66	1.96
10.0	143.96	0.0046	0.66	1.97
13.0	143.02	0.0044	0.63	1.89
15.0	149.72	0.0044	1.99	1.11
18.0	144.33	0.0045	1.94	1.36

Appendix F. Mathematical model predictions for Michaelis Menten substitution of k_1c

parameter	wild type	mutant
$\hat{k}_1$ (=v_{max})	5.6 mM/h	9.1 mM/h
k_2	4.3/h	4.1/h
Γ	$9.3*10^8$	$9.4*10^8$
$\hat{k}_{M,1}$	0.03 mM	0.1 mM
$\hat{\tau}$	0. 8	0.5
n	3.4	4.6
thresh	4.4 h	4.9 h

a) Parameter estimations for the model replacing k_1 by MM kinetics terms. No statistical analysis was performed, as the model was further modified (see Table 5).

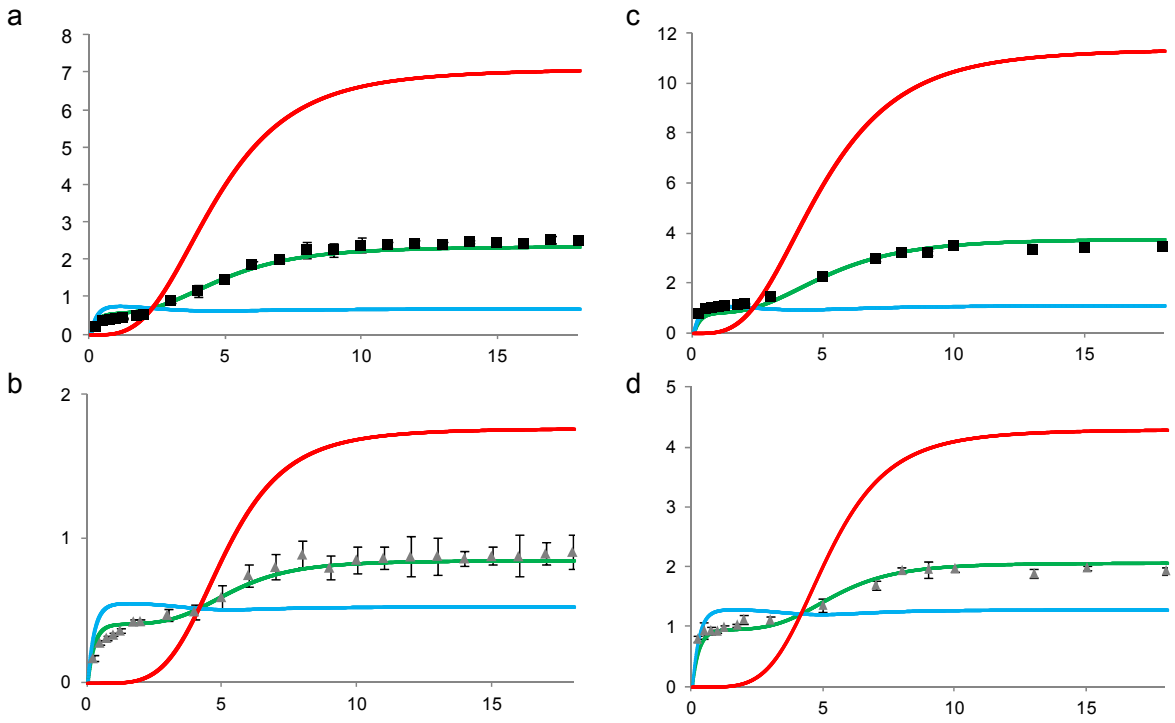

b) Model estimations for wild-type (a, c) and *sec22*Δ (b, d) Cs^+ accumulation at 50 µM (a, b) and 200 µM (c, d) external CsCl after replacing k_1 by Michaelis-Menten terms. Total intracellular concentration as measured (datapoints) and as estimated (green trajectory) are shown together with the cytoplasmic (blue) and vacuolar (red) concentration.

Appendix G. Enzymatic tests after density gradient fractionation of yeast – raw data and negative controls.

Vacuoles from yeast cells were isolated by Ficoll density gradient centrifugation (see Methods) and the purity of the obtained *fraction 3* was analyzed using marker enzymes. In addition to *fraction 3* (floating material after the second gradient), the following steps were analyzed: *control* - unfractionated spheroblast, *fraction 1* - pellet of first gradient centrifugation and *fraction 2* - pellet of second gradient centrifugation. Marker enzymes are indicated: PM ATPase for plasma membrane; NADPH cytochrome c reductase for endoplasmic reticulum; succinate dehydrogenase for mitochondria; α-mannosidase for vacuole membranes; carboxypeptidase Y for vacuole lumen; α-Mannosyltransferase for the Golgi apparatus and Catalase A for peroxisomes). The activities are indicated in mu/ml in case of the plasma membrane, ER, Golgi, mitochondrial and vacuolar markers and by the ratio of reduced H_2O_2 / ml for the peroxisomal marker. Note that in case of the negative controls, values reach background level, so that single fractions may show higher activities than control.

Raw values		**Wild type**				***sec22*Δ**			
Fraction		Control	1	2	3	Control	1	2	3
PM ATPase	Isolation 1	39.1	24.3	25.9	4.4	33.5	30.5	23.0	2.1
	Isolation 2	53.1	33.0	31.9	7.4	48.9	36.7	25.0	2.9
	Isolation 3	63.5	28.8	33.7	6.8	55.8	25.0	27.0	2.8
NADPH cytochrome c reductase	Isolation 1	132.6	84.3	42.3	3.7	134.6	74.4	39.9	6.8
	Isolation 2	169.8	101.2	62.4	7.4	173.6	106.2	66.0	9.0
	Isolation 3	157.4	97.2	59.8	4.3	170.7	101.0	55.1	7.1
Succinate dehydroge-nase	Isolation 1	42.5	25.2	14.6	1.1	40.6	24.9	21.4	1.1
	Isolation 2	58.1	36.5	25.7	1.3	50.0	32.5	25.4	1.5
	Isolation 3	43.1	28.6	26.1	2.3	46.8	31.8	25.5	1.2
α-Mannosi-dase	Isolation 1	113.5	4.1	3.0	100.1	127.0	3.8	2.8	99.3
	Isolation 2	107.6	2.9	2.7	91.3	93.5	2.9	2.7	67.5
	Isolation 3	104.0	3.3	2.4	89.1	78.4	3.1	2.3	56.2
Carboxypep-tidase Y	Isolation 1	20.6	0.4	0.3	5.8	20.2	0.2	0.2	5.2
	Isolation 2	15.7	0.4	0.3	6.2	12.3	0.3	0.1	5.7
	Isolation 3	15.7	0.1	0.1	5.6	14.1	0.3	0.1	5.4
α-Mannosyl-transferase	Isolation 1	9.1	2.0	0.5	0.1	7.7	4.1	0.5	0.1
	Isolation 2	30.0	18.2	0.5	0.1	28.7	13.3	0.4	0.1
	Isolation 3	24.2	15.7	0.5	0.0	29.7	22.1	0.4	0.1
Catalase A	Isolation 1	0.8	0.7	0.2	0.1	0.9	0.7	0.1	0.1
	Isolation 2	0.8	0.6	0.2	0.1	0.9	0.7	0.2	0.1
	Isolation 3	0.8	0.7	0.1	0.0	0.9	0.6	0.1	0.1

negative controls		**Wild type**				***sec22Δ***			
Fraction		Control	1	2	3	Control	1	2	3
PM ATPase	Isolation 1	1.6	1.8	1.3	4.0	2.7	0.9	5.0	1.4
	Isolation 2	2.7	4.0	2.3	2.1	1.4	2.2	1.4	1.9
	Isolation 3	0.5	2.2	3.6	1.9	1.6	2.1	1.1	0.9
NADPH cytochrome c reductase	Isolation 1	9.3	3.4	1.4	2.0	2.2	1.4	2.2	1.0
	Isolation 2	4.3	4.3	1.8	1.7	3.5	4.1	1.8	3.1
	Isolation 3	4.4	3.1	3.1	2.1	2.8	1.0	3.0	1.2
Succinate dehydroge-nase	Isolation 1	2.3	1.2	1.6	1.3	1.4	1.2	2.1	1.0
	Isolation 2	1.8	5.2	2.4	1.0	4.0	2.3	2.1	0.3
	Isolation 3	4.0	0.7	3.1	1.4	1.8	3.0	2.7	3.2
α-Mannosi-dase	Isolation 1	5.2	0.9	0.4	2.3	2.7	0.1	2.5	3.0
	Isolation 2	2.0	0.8	1.7	1.8	3.1	0.4	2.2	1.1
	Isolation 3	3.9	2.2	0.9	1.8	0.5	1.2	1.7	2.2
Carboxypep-tidase Y	Isolation 1	2.5	0.5	0.1	0.3	1.3	0.1	0.3	1.0
	Isolation 2	1.8	0.2	0.8	1.2	1.9	0.1	0.1	0.2
	Isolation 3	3.8	1.4	0.2	1.3	0.6	0.1	0.1	0.1
α-Mannosyl-transferase	Isolation 1	2.5	2.0	0.1	0.1	3.5	1.1	1.1	0.1
	Isolation 2	1.8	1.0	0.1	0.1	1.8	0.5	0.2	0.1
	Isolation 3	3.4	2.5	0.1	0.1	1.8	2.3	1.4	0.4
Catalase A	Isolation 1	0.0	0.5	0.0	0.1	0.1	0.1	0.1	0.0
	Isolation 2	0.1	0.1	0.1	0.0	0.1	0.1	0.1	0.0
	Isolation 3	0.1	0.1	0.1	0.0	0.1	0.0	0.1	0.1

Appendix H. Cs^+ efflux kinetics at 50 µM external CsCl in *S. cerevisiae*

All repetitions that were taken into account for the analysis and calculation of the yeast mutant phenotype are given in the following table. Cells were incubated for 13 h with tracer before washing. The cells were further incubated and analysed from this time on at 50 µM CsCl in the buffer solution. Time, tracer activity, the correction factor and the concentration are presented. ID denotes the identity of the sample. Note that wild type and mutant are placed side by side.

* after background correction; background determined by measurement of 3 ml HNO_3;Background ranged between 20 and 100 CCPM. n = 6 per setup; related to $1*10^7$ cells.

** concentration of stable CsCl in the media correlated with the activity of ^{134}Cs tracer in the media (CCPM) : nmol/CCPM Cs^+. Multiply measured activity (CCPM) with the calculation factor to achieve nmol Cs^+ taken up per amount of cells analysed.

Caesium efflux kinetics in yeast cells
WILD TYPE
Cells washed after 13 h incubation; further incubation included 50 µM CsCl in 100 µl buffer volume.

Time (h)	Measured CCPM*	Calculation factor**	nmol/10^7 cells	conc. (mM)
0.00	101.40	0.0080	0.81	2.39
0.00	99.62	0.0080	0.80	2.34
0.00	100.43	0.0080	0.80	2.36
0.00	100.00	0.0080	0.80	2.35
0.00	97.62	0.0080	0.78	2.30
0.00	99.53	0.0080	0.80	2.34
0.00	97.52	0.0080	0.78	2.29
0.00	102.64	0.0080	0.82	2.42
0.33	97.24	0.0080	0.78	2.29
0.33	97.76	0.0080	0.78	2.30
0.33	95.20	0.0080	0.76	2.24
0.33	98.25	0.0080	0.79	2.31
0.33	96.77	0.0080	0.77	2.28
0.33	95.90	0.0080	0.77	2.26
0.33	98.69	0.0080	0.79	2.32
0.33	97.20	0.0080	0.78	2.29
0.67	96.23	0.0080	0.77	2.26
0.67	95.65	0.0080	0.77	2.25
0.67	93.71	0.0080	0.75	2.20
0.67	93.84	0.0080	0.75	2.21
0.67	95.23	0.0080	0.76	2.24
0.67	97.17	0.0080	0.78	2.29
1.00	96.21	0.0080	0.77	2.26
1.00	96.19	0.0080	0.77	2.26
1.00	96.75	0.0080	0.77	2.28
1.00	93.05	0.0080	0.74	2.19
1.00	95.86	0.0080	0.77	2.26
1.00	96.29	0.0080	0.77	2.27
1.00	95.36	0.0080	0.76	2.24
1.00	96.30	0.0080	0.77	2.27
2.00	90.49	0.0080	0.72	2.13
2.00	92.39	0.0080	0.74	2.17
2.00	90.41	0.0080	0.72	2.13
2.00	89.06	0.0080	0.71	2.10
2.00	91.53	0.0080	0.73	2.15
2.00	92.03	0.0080	0.74	2.17
2.00	91.68	0.0080	0.73	2.16
2.00	91.10	0.0080	0.73	2.14
3.00	85.65	0.0080	0.69	2.02
3.00	86.31	0.0080	0.69	2.03
3.00	87.64	0.0080	0.70	2.06
3.00	84.73	0.0080	0.68	1.99
3.00	86.91	0.0080	0.70	2.04
3.00	86.28	0.0080	0.69	2.03
3.00	88.06	0.0080	0.70	2.07
3.00	90.47	0.0080	0.72	2.13

Caesium efflux kinetics in yeast cells

***sec22*Δ**

Cells washed after 13 h incubation; further incubation included 50 µM CsCl in 100 µl buffer volume.

Time (h)	Measured CCPM	Correction factor	nmol/10^7 cells	conc. (mM)
0.00	43.78	0.0080	0.35	1.03
0.00	42.29	0.0080	0.34	1.00
0.00	41.86	0.0080	0.33	0.98
0.00	42.05	0.0080	0.34	0.99
0.00	41.51	0.0080	0.33	0.98
0.00	42.83	0.0080	0.34	1.01
0.00	43.72	0.0080	0.35	1.03
0.00	42.16	0.0080	0.34	0.99
0.33	41.02	0.0080	0.33	0.97
0.33	39.49	0.0080	0.32	0.93
0.33	39.01	0.0080	0.31	0.92
0.33	40.75	0.0080	0.33	0.96
0.33	40.26	0.0080	0.32	0.95
0.33	39.29	0.0080	0.31	0.92
0.33	39.81	0.0080	0.32	0.94
0.33	40.05	0.0080	0.32	0.94
0.67	35.48	0.0080	0.28	0.83
0.67	37.87	0.0080	0.30	0.89
0.67	38.29	0.0080	0.31	0.90
0.67	38.17	0.0080	0.31	0.90
0.67	37.78	0.0080	0.30	0.89
0.67	39.21	0.0080	0.31	0.92
1.00	38.92	0.0080	0.31	0.92
1.00	38.81	0.0080	0.31	0.91
1.00	32.58	0.0080	0.26	0.77
1.00	34.97	0.0080	0.28	0.82
1.00	35.40	0.0080	0.28	0.83
1.00	35.28	0.0080	0.28	0.83
1.00	34.88	0.0080	0.28	0.82
1.00	36.31	0.0080	0.29	0.85
2.00	36.02	0.0080	0.29	0.85
2.00	35.91	0.0080	0.29	0.84
2.00	31.66	0.0080	0.25	0.75
2.00	32.12	0.0080	0.26	0.76
2.00	31.40	0.0080	0.25	0.74
2.00	30.93	0.0080	0.25	0.73
2.00	31.32	0.0080	0.25	0.74
2.00	31.56	0.0080	0.25	0.74
3.00	31.73	0.0080	0.25	0.75
3.00	27.11	0.0080	0.22	0.64
3.00	28.40	0.0080	0.23	0.67
3.00	28.02	0.0080	0.22	0.66
3.00	27.87	0.0080	0.22	0.66
3.00	27.60	0.0080	0.22	0.65
3.00	27.53	0.0080	0.22	0.65
3.00	27.01	0.0080	0.22	0.64

Appendix I. Cs^+ accumulation in *A. thaliana* shoot and root.

Concentration was determined by translating the counts per minute (CCPM) of ^{134}Cs tracer to a concentration/fresh weight. The correction factor for this was derived from the measured activity in the defined buffer (i.e. nutrient) solution. Different lines are indicated. *sec22-3::SEC22* is the *A. thaliana SEC22* complemented plant line. CCPM values are after background correction; background determined by measurement of 3 ml HNO_3; Background ranged between 50 and 100 CCPM. n = 6 per setup.
*Replicates with similar numbers were grown in the same hydroponic growth box for direct comparison;complete setup was repeted twice (not shown).
** concentration of stable CsCl in the media correlated with the activity of ^{134}Cs tracer in the media (CCPM) : nmol/CCPM Cs^+. Multiplying measured activity (CCPM) with the calculation factor results in nmol Cs^+ taken up per amount of cells analysed.

Caesium concentration in *Arabidopsis thaliana*
Shoot material
Number of cells: $2*10^7$ as determined by OD_{600} measurement.

ID	Biological replicate*	CCPM/g(fwt.)	Number of plants	Fresh weight (g)	Calculation factor**	nmol/g (fwt)
Wild Type	1	3456.44	8.00	0.73	0.0312	107.78
Wild Type	2	3657.56	8.00	0.78	0.0304	111.22
Wild Type	3	3648.75	7.00	0.64	0.0297	108.21
Wild Type	4	3928.40	8.00	0.75	0.0294	115.48
Wild Type	5	3379.29	8.00	0.70	0.0308	103.92
Wild Type	6	3448.23	9.00	0.79	0.0294	101.27
Wild Type	7	3781.53	8.00	0.72	0.0311	117.52
sec22-3	1	1445.26	8.00	0.76	0.0312	45.07
sec22-3	2	1701.64	8.00	0.73	0.0304	51.74
sec22-3	3	2045.78	7.00	0.63	0.0297	60.67
sec22-3	4	1984.66	8.00	0.73	0.0294	58.34
sec22-3	5	1948.24	8.00	0.68	0.0308	59.91
sec22-3	6	1868.07	9.00	0.83	0.0294	54.86
sec22-3	7	1949.13	8.00	0.75	0.0311	60.57

Caesium concentration in *Arabidopsis thaliana*
Root material
Number of cells: $2*10^7$ as determined by OD_{600} measurement.

ID	Biological replicate	CCPM/g(fwt.)	Number of plants	Fresh weight (g)	Calculation factor	nmol/g (fwt)
Wild Type	1	1119.72	8.00	0.36	0.0312	34.92
Wild Type	2	1630.33	8.00	0.30	0.0304	49.58
Wild Type	3	1471.82	7.00	0.22	0.0297	43.65
Wild Type	4	1318.62	8.00	0.29	0.0294	38.76
Wild Type	5	1457.50	8.00	0.28	0.0308	44.82
Wild Type	6	1509.71	9.00	0.34	0.0294	44.34
Wild Type	7	1252.40	8.00	0.25	0.0311	38.92
sec22-3	1	886.15	8.00	0.39	0.0312	27.63
sec22-3	2	1275.71	8.00	0.28	0.0304	38.79
sec22-3	3	1091.67	7.00	0.21	0.0297	32.37
sec22-3	4	1567.67	8.00	0.30	0.0294	46.09
sec22-3	5	948.50	8.00	0.30	0.0308	29.17
sec22-3	6	1072.50	9.00	0.32	0.0294	31.50
sec22-3	7	1112.08	8.00	0.24	0.0311	34.56

Caesium concentration in *Arabidopsis thaliana*
Shoot material
Number of cells: $2*10^7$ as determined by OD_{600} measurement.

ID	Biological replicate	CCPM/g(fwt.)	Number of plants	Fresh weight (g)	Calculation factor	nmol/g (fwt)
Wild Type	1	2764.49	8.00	0.78	0.0392	108.32
Wild Type	2	2951.47	8.00	0.75	0.0382	112.70
Wild Type	3	2614.43	9.00	0.88	0.0392	102.44
Wild Type	4	3021.50	8.00	0.80	0.0303	91.54
Wild Type	5	3467.00	7.00	0.70	0.0299	103.78
sec22-3::SEC22	1	3202.89	8.00	0.74	0.0392	125.50
sec22-3::SEC22	2	2934.03	8.00	0.77	0.0382	112.03
sec22-3::SEC22	3	3076.75	9.00	0.80	0.0392	120.56
sec22-3::SEC22	4	3417.40	8.00	0.77	0.0303	103.53
sec22-3::SEC22	5	3615.22	7.00	0.69	0.0299	108.22

Caesium concentration in *Arabidopsis thaliana*
Root material
Number of cells: $2*10^7$ as determined by OD_{600} measurement.

ID	Biological replicate	CCPM/g(fwt.)	Number of plants	Fresh weight (g)	Calculation factor	nmol/g (fwt)
Wild Type	1	1061.29	8.00	0.31	0.0392	41.58
Wild Type	2	1404.67	8.00	0.30	0.0382	53.63
Wild Type	3	1308.57	9.00	0.35	0.0392	51.27
Wild Type	4	1235.16	8.00	0.31	0.0303	37.42
Wild Type	5	1043.45	7.00	0.29	0.0299	31.23
sec22-3::SEC22	1	1327.00	8.00	0.30	0.0392	52.00
sec22-3::SEC22	2	1108.44	8.00	0.32	0.0382	42.32
sec22-3::SEC22	3	1325.10	9.00	0.31	0.0392	51.92
sec22-3::SEC22	4	1562.50	8.00	0.28	0.0303	47.34
sec22-3::SEC22	5	1340.65	7.00	0.31	0.0299	40.13

Appendix J. Rb^+ accumulation in *A. thaliana* shoot and root.

Concentration was determined by translating the counts per minute (CCPM) of ^{86}Rb tracer to a concentration/fresh weight. The correction factor for this was derived from the measured activity in the defined buffer (i.e. nutrient) solution. CCPM values are after background correction; background determined by measurement of 3 ml HNO_3; Background ranged between 50 and 100 CCPM. n = 6 per setup.
*Replicates with similar numbers were grown in the same hydroponic growth box for direct comparison;complete setup was repeted twice (not shown).
** concentration of stable RbCl in the media correlated with the activity of ^{86}Rb tracer in the media (CCPM) : nmol/CCPM Rb^+.

Rubidium concentration in *Arabidopsis thaliana*
Shoot material
Number of cells: $2*10^7$ as determined by OD_{600} measurement.

ID	Biological replicate*	CCPM/g(fwt.)	Number of plants	Fresh weight (g)	Calculation factor***	nmol/g (fwt)
Wild Type	1	2335.62	10.00	1.63	0.0669	156.17
Wild Type	2	2222.13	10.00	1.31	0.0671	149.00
Wild Type	3	2385.40	10.00	1.47	0.0669	159.50
Wild Type	4	2356.16	9.00	0.70	0.0673	158.60
Wild Type	5	2300.41	8.00	0.73	0.0721	165.96
sec22-3	1	2864.71	10.00	1.40	0.0669	191.64
sec22-3	2	2338.49	11.00	1.46	0.0671	156.94
sec22-3	3	2213.46	10.00	1.33	0.0669	148.08
sec22-3	4	2806.30	9.00	1.19	0.0673	188.86
sec22-3	5	2703.28	8.00	0.70	0.0721	194.90
sec22-3	6	2384.64	8.00	0.84	0.0621	148.08
sec22-3	7	2763.40	9.00	1.03	0.0741	197.30
sec22-3	8	2134.46	8.00	0.96	0.0730	155.82
sec22-3	9	2799.58	9.00	1.23	0.0691	193.54
sec22-3	10	2037.41	8.00	1.35	0.0747	152.20

Rubidium concentration in *Arabidopsis thaliana*
Root material
Number of cells: $2*10^7$ as determined by OD_{600} measurement.

ID	Biological replicate	CCPM/g(fwt.)	Number of plants	Fresh weight (g)	Calculation factor	nmol/g (fwt)
Wild Type	1	701.63	10.00	0.65	0.0669	46.91
Wild Type	2	877.02	10.00	0.50	0.0671	58.81
Wild Type	3	763.59	10.00	0.57	0.0669	51.06
Wild Type	4	773.85	9.00	0.39	0.0673	52.09
Wild Type	5	764.25	8.00	0.40	0.0721	55.14
sec22-3	1	813.70	10.00	0.53	0.0669	54.41
sec22-3	2	772.56	11.00	0.50	0.0671	51.80
sec22-3	3	863.48	10.00	0.57	0.0669	57.74
sec22-3	4	743.80	9.00	0.48	0.0673	50.07
sec22-3	5	648.50	8.00	0.33	0.0721	46.79

Appendix K. Cation accumulation in *A. thaliana* shoot (and root) – stable ions.

Concentration was determined by mass spectrometrical determination in dried plant material.

* considering the molar mass of the according element/ion (K^+. Na^+. Mg^{2+}. Ca^{2+}).

Potassium concentration in *Arabidopsis thaliana*
Shoot
Material was dried. freeze-dried and grinded to powder. before measurement.

ID	Biological replicate	K^+ (mg/g_{sample})*	conc. (mmol/g)*
Wild Type	1	50.00	1.28
Wild Type	2	34.50	0.88
Wild Type	3	49.90	1.28
Wild Type	4	64.00	1.64
Wild Type	5	54.10	1.38
sec22-3	1	52.40	1.34
sec22-3	2	49.70	1.27
sec22-3	3	49.65	1.27
sec22-3	4	58.15	1.49
sec22-3	5	56.20	1.44
sec22-3	6	49.96	1.28

Potassium concentration in *Arabidopsis thaliana*
Root
Material was dried. freeze-dried and grinded to powder. before measurement.

ID	Biological replicate	K^+ (mg/g_{sample})	conc. (mmol/g)*
Wild Type	1	2.40	0.61
Wild Type	2	2.20	0.56
Wild Type	3	3.20	0.82
Wild Type	4	1.90	0.49
Wild Type	5	2.50	0.64
sec22-3	1	2.78	0.71
sec22-3	2	1.76	0.45
sec22-3	3	2.43	0.62
sec22-3	4	2.56	0.65
sec22-3	5	3.25	0.83
sec22-3	6	2.40	0.61

Sodium concentration in *Arabidopsis thaliana*

Shoot
Material was dried. freeze-dried and grinded to powder. before measurement.

ID	Biological replicate	Na^+ (mg/g_{sample})	conc. (mmol/g)*
Wild Type	1	0.46	0.20
Wild Type	2	0.30	0.13
Wild Type	3	0.53	0.23
Wild Type	4	0.54	0.24
Wild Type	5	0.47	0.21
sec22-3	1	0.50	0.22
sec22-3	2	0.41	0.18
sec22-3	3	0.43	0.18
sec22-3	4	0.46	0.20
sec22-3	5	0.48	0.21
sec22-3	6	0.42	0.18

Calcium concentration in *Arabidopsis thaliana*
Shoot
Material was dried. freeze-dried and grinded to powder. before measurement.

ID	Biological replicate	Ca^{2+} (mg/g_{sample})	conc. (mmol/g)*
Wild Type	1	0.60	0.15
Wild Type	2	0.52	0.13
Wild Type	3	0.61	0.15
Wild Type	4	0.58	0.14
Wild Type	5	0.66	0.16
sec22-3	1	0.61	0.15
sec22-3	2	0.56	0.14
sec22-3	3	0.59	0.15
sec22-3	4	0.69	0.17
sec22-3	5	0.62	0.15
sec22-3	6	0.57	0.14

Magnesium concentration in *Arabidopsis thaliana*
Shoot
Material was dried. freeze-dried and grinded to powder. before measurement.

ID	Biological replicate	Mg^{2+} (mg/g_{sample})	conc. (mmol/g)*
Wild Type	1	0.73	0.30
Wild Type	2	0.68	0.28
Wild Type	3	0.65	0.27
Wild Type	4	0.88	0.36
Wild Type	5	0.80	0.33
sec22-3	1	0.78	0.32
sec22-3	2	0.63	0.26
sec22-3	3	0.73	0.30
sec22-3	4	0.76	0.31
sec22-3	5	0.71	0.29
sec22-3	6	0.62	0.26

Acknowledgements

This work is dedicated to Doris Giselle Arǵueta Baires (1982 – 2012) – never forgotten.

This project was supported by the German Federal Ministry of Education and Research (BMBF) with the contract 02NUK002B.The contents are solely the responsibility of the authors.

The author would like to thank supervisor PD Dr. Anton R. Schäffner for the major contribution to the work and permanent direction – the work would have looked different without his universal knowledge and understanding ability.

Further supervision was given by Dr. Ulrike Kanter, with whom I went through the initial phase of my work. She gave me the trust to take on the project and lead me in the right direction.

I wish to thank following persons:

Prof. Dr. Karl-Peter Hopfner and the members of the examination committee (Prof. Dr. Förstemann, Prof. Dr. Martin and Prof. Dr. Cramer) for reviewing this work and spending time on this unusual subject. Special thanks go to Prof. Dr. Durner for his permanent support and to Dr. Katja Lammens of the Gene Center, Munich, who put a lot of energy into advising me, even though my work was far out of scope of her own work.

Dr. Sabine Heuck was of extraordinary importance for this thesis as she was giving me insight into her work and a lot of advice when I started.

Prof. Dr. Johannes Müller, TU München, Dr. Burkhard Hense and Dr. Weibo Li spent many hours of practical help and nerve-wrecking mathematical modeling.

Dr. Hagen Scherb for advising me on many statistical analyses of this work.

Sincere thanks to Dr. Jochen Tschiersch, and Prof. Dr. Peter Jacob, as well as Oliver Meisenberg and Wolfgang Schultz who offered me all possible assistance when I needed it. Especially the introduction to safe working with radioactive substances was essential for this work.

Monika Röhmuß and Birgit Geist must be highlighted as they contributed time and work on different parts of the project and followed me along the way – also in moral questions.

Many thanks go to Dr. Günther Bahnweg and Mrs. Millers, together with Dr. Vera Höllriegel, who gave me important advice for language corrections.

Acknowledgements further go to Elisabeth Becker (TUM), who contributed an important part during her practical course.

Besides the planning, experiments and evaluation, this thesis would not have been possible without the moral help of my family – it is good to know that there is a backup when needed.

Without Dr. Veronica v. Saint Paul, this work would never have been finished, as her advice and role model was amazingly inspiring. Furthermore, I would probably still be sitting somewhere on a mountain if it was not for her.

Dr. Ruohe Yin was equally pushing, even though his ambition was sometimes scary.

The author wishes to thank the group of Dr. Anton R. Schäffner, namedly Birgit Geist, who makes it all possible, Wei Zhang, Malay Das, Chen Liu, Jin Ming and Jin Zhao, as well as the BIOP, the working groups of Corina Vlot, Christian Lindermayr and Jörg Durner, in unity with EUS.

Thanks also go to Alexandra Dangel, Clara Steinhauser, Finni Wittek, Heiko Breitenbach and Christian Holzmeister for discussing and sometimes helping me to forget about my troubles. Gitto Kurutukulangaracoola, Andi Fröhlich and Frank Gaupels supported me during the hard times of the PHD studies.

The ISS working group Radioökologie, especially naming Stefanie , Alexandra Dieter, Kerstin Hürkamp, Stefanie Tafelmeier, Stefanie Gierl, Sabine Sickinger, Taeko Shinonaga, Rainer Lindner, Peter Feistenauer, Wang Jin, Bi Lei, Felix Bernauer, and Wolfgang Schultz, who kept up my morals when the direction of my work was becoming unclear.

The author would like to acknowledge the chief secretaries of two institutes, Anita Pedone (ISS) and Karoline Stoll (BIOP) for their help.

I would like to thank the CEOs of the Helmholtz Zentrum München.

Finally, I wish to thank Dr. Eckermann and Frau Irger who know what they did for me and what cannot be repaid.